Investigation of prion protein turnover in neuronal activity-dependent processes

Dissertation

Zur Erlangung des Doktorgrades der Naturwissenschaften vorgelegt im Fachbereich Chemie der Fakultät für Mathematik, Informatik und Naturwissenschaften der Universität Hamburg

Vorgelegt von
Michaela Mischak

Hamburg
2022

This work was done from 2019 until 2022 at the Institute of Molecular Neurogenetics in the Center for Molecular Neurobiology Hamburg at Universitätsklinikum Hamburg-Eppendorf (UKE) in the research group of Dr. Frank Heisler.

Gutachter:

Dr. Frank Heisler

Prof. Hartmut Schlüter

Prüfungskommissionsmitglieder:

Dr. Frank Heisler
Prof. Hartmut Schlüter
Prof. Matthias Kneussel
Prof. Christian Betzel
Prof. Kay Grünewald

Disputationstermin: 25.11.2022

I. Table of contents

II. Abbreviations

Aβo	β-amyloid oligomers
AC	adenylate cyclase
ACSF	artificial cerebrospinal fluid without Magnesium
AD	Alzheimer's disease
ADAM10	a-disintegrin-and-metalloproteinase 10
ADP	adenosine diphosphate
AMPA	α-amino-3-hydroxy-5-methyl-4-isoazolepropionic acid
ANOVA	analysis of varience
APP	amyloid precursor protein
ATP	adenosine triphosphate
BDNF	brain-derived neurotrophic factor
Bic	bicuculline
BSA	Bovine serum albumin
CA	cornu ammonis
Ca^{2+}	calcium ions
$CaCl_2$	Calcium chloride
CNQX	Cyanquixaline
CaM	calmodulin (calcium-modulated protein)
CaMKII	calmodulin-dependent protein kinase II
cAMP	cyclic adenosine monophosphate
cLTD	chemically induced LTD
cLTP	chemically induced LTP
Cat. no.	catalogue number
CI	confidence interval
Cl^-	chloride ions
CNS	central nervous system
CREB	cAMP response element binding protein
Ctrl	control
DG	dentate gyrus
DIV	days *in vitro*

DMEM	Dulbecco's Modified Eagle *Medium*
DMSO	Dimethyl sulfoxide
DNA	deoxyribonucleic acid
DTT	Dithiothreitol
E15.5	embryonic day 15
ECFP	enhanced cyan fluorescent protein
E. coli	*Escherichia coli*
EPSP	excitatory postsynaptic potential
ER	endoplasmic reticulum
ESCRT	endosomal sorting complex required for transport
F-actin	filamentous actin
FCS	Fetal calf serum
GABA	γ-aminobutyric acid
$GABA_A$	ionotropic GABA receptors
$GABA_B$	metabotropic GABA receptors
G-actin	globular actin monomers
GDI	GDP dissociation inhibitor
GDF	GDI displacement factors
GDP	guanosine diphosphate
GPI	glycosylphosphatidylinositol
GRIP1	glutamate receptor interacting protein 1
GTP	guanosine triphosphate
HBSS	Hank’s balanced salt solution
HCl	Hydrochloric acid
HEPES	4-(2-hydroxyethyl)-1-piperazineethanesulfonic acid
hiPSC	human induced pluripotent stem cell
HRP	horseradish peroxidase
htau	human tau
ICC	immunocytochemistry
IgG	immunoglobulin G
ILV	intraluminal vesicles
IP	immunoprecipitation

IPSP	inhibitory postsynaptic potential
JIP1	JNK-interacting protein 1
JNK	c-Jun-amino-terminal kinase-interacting protein
K^+	potassium ions
KCl	potassium chloride
KO	knock out
KOH	potassium hydroxide
Lamp1	lysosomal-associated membrane protein 1
LTD	long-term depression
LTP	long-term potentiation
mGluR5	metabotropic glutamate receptor 5
MAP	MT associated proteins
MECP2	methyl CpG binding protein
Mg^{2+}	magnesium ions
mRFP	monomeric red fluorescent protein
MT	microtubules
MTOC	microtubule-organizing centers
MVB	multivesicular bodies
Na^+	sodium ions
$Na_2HPO_4 \cdot 2H_2O$	disodium hydrogen phosphate
NaH_2PO_4	sodium dihydrogen phosphate
NaOH	sodium hydroxide
N-Cad	N-cadherin
NMDA	N-methyl-D-aspartic acid
nSMase	neutral sphingomyelinase
pCREB	phosphorylated CREB
PAGE	polyacrylamide gel electrophoresis
PBS	phosphate buffered saline
PFA	paraformaldehyde
PKA	protein kinase A
PKC	protein kinase C
PMSF	Phenylmethylsulfonyl fluoride

PNS	peripheral nervous system
PP	protein phosphatases
PrP^{C}	cellular prion protein
PrP^{Sc}	misfolded prion protein scrapie form
PSD	postsynaptic density
PSD95	postsynaptic density protein-95
PTM	posttranslational modifications
PVDF	Polyvinylidene difluoride
RILP	Rab-interacting lysosomal protein
ROI	region of interest
RS-MCPG	(RS)-α-methyl-4-carboxyphenylglycine
RT	room temperature
SDC	spinning disc confocal
SDS	sodium dodecyl sulfate
SEM	standard error of the mean
SNARE	soluble N-ethylmaleimide-sensitive factor attachment protein receptors
TBST	tris-buffered saline with tween
TEMED	Tetramethylethylenediamine
TIR	total internal reflection
TIRF	total internal reflection fluorescence
tris	tris(hydroxymethyl)aminomethane
TSE	transmissible spongiform encephalopathies
TSG101	tumor susceptibility gene 101
TTX	tetrodotoxin
VGAT	vesicular GABA transporter
v_{max}	maximum velocity
v_{mean}	average velocity without pauses
v_{net}	general velocity
WT	wild type
YFP	yellow fluorescent protein

III. Zusammenfassung

Das zelluläre Prion Protein (PrP^C) wird im hohen Maße im Gehirn und den Nervenzellen exprimiert. Es ist bekannt für seine Rolle in der übertragbaren spongiformen Enzephalopathie und es wird vermutet, dass es auch in anderen neurodegenerativen Erkrankungen wie der Alzheimer Erkrankung eine Rolle spielt. Obwohl die Struktur von PrP^C und seine Fehlfaltung, sowie der Mechanismus der Krankheitsentstehung umfangreich untersucht wurden, ist seine physiologische Rolle auf zellulärer Ebene größtenteils ungeklärt. In dieser Arbeit wurde die Rolle von PrP^C an der Synapse und in neuronalen Aktivitätsprozessen untersucht.

Zuerst wurde die Lokalisierung von PrP^C an verschiedenen Synapsentypen in kultivierten murinen Neuronen des Hippocampus untersucht. Aus diesen Untersuchungen ergab sich, dass PrP^C sowohl an exzitatorischen und inhibitorischen Synapsen lokalisiert ist. Im Anschluss an die Beobachtung, dass PrP^C an der Plasmamembran der exzitatorischen Synapse angereichert ist, wurde dessen vesikulärer Transport und Verteilung zwischen neuronalen Subdomänen nach der Induktion von synaptischer Plastizität analysiert. Ein mäßiger Effekt konnte nach der chemischen Indizierung von Langzeit Depression (cLTD) auf den aktiven Transport von PrP^C und dessen Lokalisation an der Synapse und in endolysosomalen Kompartimenten beobachtet werden. Des Weiteren wurde der aktive Transport von PrP^C nach der Überexpression von humanen Tau Protein untersucht, da dieses eine synaptotoxische Rolle bei der Alzheimer Erkrankung spielt, allerdings konnten keine Effekte beobachtet werden. Aufgrund der hohen Konzentration von PrP^C auf Exosomen sollte die Wirkung von neuronaler Aktivität auf die Ausschüttung von Exosomen untersucht werden, jedoch konnte unter den gewählten Konditionen kein Einfluss auf diese nachgewiesen werden. Hinsichtlich einer potentiell physiologischen Rolle von PrP^C an Synapsen konnten die zwei synaptischen Zelladhäsions-moleküle N-Cadherin und Neuroligin-2 als neue Interaktionspartner von PrP^C mittels Immunpräzipitation aus Mausgehirnen identifiziert werden. Zudem konnte durch Lebendzell-Mikroskopie gezeigt werden, dass hohe Anteile an PrP^C und N-Cadherin in denselben Vesikeln transportiert werden. Um die Wirkung von PrP^C auf die endolysosomale Lokalisierung von N-Cadherin zu untersuchen, wurde PrP^C in kultivierten Neuronen des Hippocampus überexprimiert und die N-Cadherin Lokalisation mittels Immunzytochemie erforscht. PrP^C verstärkte dabei die gezielte Lokalisation von N-Cadherin in endolysosomalen Kompartimenten.

Zusammengenommen zeigen diese Ergebnisse, dass die Lokalisierung und der aktive Transport von PrP^C teilweise durch synaptische Plastizität modifiziert werden und dass PrP^C die Entfernung von synaptischen Zelladhäsionsmolekülen wie N-Cadherin und dessen Lokalisierung in endolysosomale Kompartimente unterstützt. Die zuvor diskutierte Rolle von PrP^C bei Prozessen der Zelladhäsion konnte durch die Entdeckung zweier Zelladhäsions-moleküle als neue PrP^C Interaktionspartner in dieser Arbeit weiter gestärkt werden.

IV. Abstract

The cellular prion protein (PrP^C) is highly expressed in the brain and neurons. It is well known for its role in transmissible spongiform encephalopathies and is suggested to be involved in the pathophysiology of other neurodegenerative diseases including Alzheimer's disease (AD). Although PrP^C structure, misfolding, and mechanisms of pathogenesis have been extensively studied, its physiological functions on a cellular level largely remain elusive. In this thesis, the role of PrP^C at the synapse and in neuronal activity processes was investigated.

Initially, PrP^C localization to different types of synapses was analyzed in cultured murine hippocampal neurons. The analysis revealed that PrP^C localized at both excitatory and inhibitory synapses. Following the observation that PrP^C is enriched at the plasma membrane of excitatory synapses, the localization of PrP^C to neuronal subdomains and its vesicle trafficking in response to different chemical stimulation protocols were analyzed. A moderate effect of chemically induced long-term depression (cLTD) could be observed on the active transport of PrP^C and its concentration at synaptic regions and endolysosomal compartments., Further, PrP^C active transport was investigated following the overexpression of human tau, because of its potentially synaptotoxic role in AD, but no effects were observed. Since PrP^C is abundant on exosomes, the impact of neuronal activity on exosome release was investigated in this project. However, no significant changes could be observed under the selected conditions. With respect to a potential physiological role of PrP^C at synapses, the synaptic cell adhesion molecules Neuroligin-2 and N-cadherin were identified as novel PrP^C interaction partners in co-immunoprecipitation experiments from mouse brains. Furthermore, neuronal live imaging revealed high portions of PrP^C and N-Cadherin to undergo cotransport within the same vesicles. To investigate a potential effect of PrP^C on N-cadherin targeting to endolysosomal compartments, PrP^C was overexpressed in dissociated hippocampal neurons and N-cadherin localization was investigated by immunocytochemistry. Functionally, PrP^C facilitated the targeting of N-Cadherin to endolysosomes.

Together the data suggest that PrP^C synaptic localization and vesicle trafficking are modified during synaptic plasticity and that PrP^C might assist in the removal of synaptic cell adhesion proteins such as N-cadherin and in their targeting toward endolysosomal compartments. The previously discussed role for PrP^C in cellular adhesion is further supported through the discovery of two cell adhesion molecules as novel PrP^C interaction partners in this work.

1. Introduction

1.1 The brain and neurodegenerative diseases

The ability to learn and to form memories are some of the key aspects of life. The brain is a highly complex organ in which these processes occur. Together with the spinal cord, they form the central nervous system (CNS). As the name suggests, the CNS is the center for information processing, receiving signals from the peripheral nervous system (PNS) that connects the CNS with the whole body. In the CNS, external signals are translated into sensations, perceptions, emotions, memories, and speech. These processes mainly take place in the brain (Bear et al. 2016).

The brain is subdivided into the cerebral cortex, cerebellum, midbrain, and brain stem. These regions all serve different functions in the brain. For example, the brain stem is important for vital functions, whereas the cerebral cortex is the cognitive center of the organism. They can be further subdivided into different subregions based on their functional and anatomical aspects (Bear et al. 2016). Despite this high complexity, the development and architecture of the brain are conserved among mammals, as shown in figure 1.1 (Defelipe 2011).

Within the cerebral cortex, learning and memory are processed in the hippocampus (Shrager et al. 2007). In the 1950s a patient underwent bilateral hippocampal resections due to untreatable epilepsy. This patient could not recall recent autobiographical memories, while childhood memories were still preserved. This suggested a role of the hippocampus in memory encoding (SCOVILLE and MILNER 1957). Humans and other mammals have two hippocampi, due to the symmetric structure of the cerebral cortex (Bear et al. 2016). The hippocampus comprises two sheets folded in on each other, the dentate gyrus (DG) and the cornu ammonis (CA). The CA is divided into several different regions, but this work only focuses on the regions CA1 and CA3. The hippocampus receives input from the entorhinal cortex into the DG, which is first relayed to CA3 and then further to CA1 along Schaffer collaterals. From the CA1 the signals are forwarded to other regions of the brain. Such local neural circuits and their interconnections, which lead to large scale brain networks, represent the main functional units of the brain and form the basis for learning and memories (Cammalleri et al. 2019).

On the cellular level, the brain consists of glial cells and neurons. Glial cells have a supportive function to the neurons. Neurons are the main cellular unit that transmit signals through complex brain networks. Glial cells meanwhile include astrocytes,

microglia, oligodendrocytes, and Schwann cells. Astrocytes supply neurons with energy and regulate signal transmission between neurons. Oligodendrocytes ensure the fast propagation of these signals in the CNS, while Schwann cells have the same function in the PNS. Microglia are the immune cells of the CNS and are activated during inflammation (Bear et al. 2016).

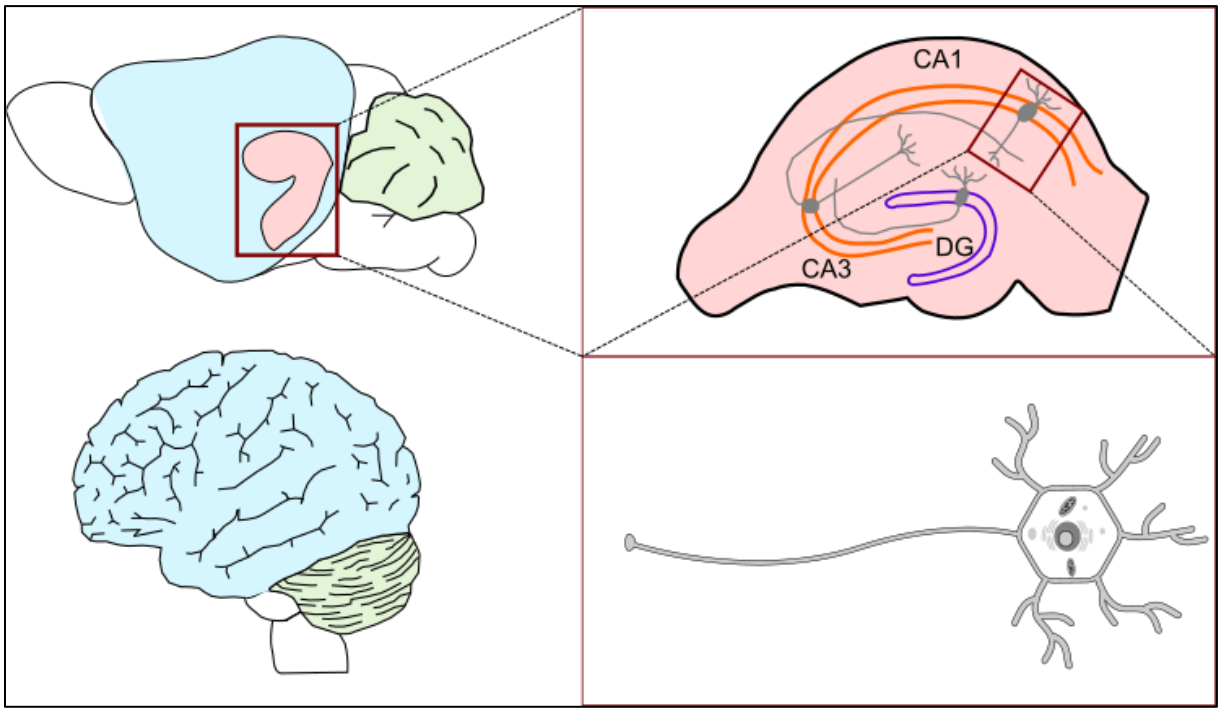

Figure 1.1: The architecture of the brain and neurons as a functional cellular unit. On the left, the human (lower) and mouse brains (upper) are shown. The brain consists of the cerebral cortex (blue), cerebellum (green), and medulla (white), which connects the brain with the spinal cord (Miterko et al. 2018). In the mouse brain the area of the hippocampus is highlighted by a red box and depicted in more detail on the right (adapted from: (Cammalleri et al. 2019)). The hippocampus consists of two cell layers folded over each other, the dentate gyrus (DG) and cornu ammonis (CA). The DG receives input from the entorhinal cortex (not shown) through the prefrontal pathway. Mossy fiber axons connect the DG to cells from CA3, which forward the signal to CA1. Signals are then passed on to other brain regions (Cammalleri et al. 2019). Here, the red box highlights the functional unit of this circuit, the neuron, which is depicted below the hippocampus. Neurons are highly polarized and specialized cells and are explained in greater detail in chapter 1.2.

Damage to neurons or the connections between neurons, the synapses, can lead to loss of function, cell death, and ultimately, degeneration of brain tissue. This process is called neurodegeneration and is observed in neurodegenerative diseases such as Alzheimer's disease (AD), Parkinson's disease, multiple sclerosis, and prion diseases. These diseases are characterized by the progressive degeneration of the structure and function of the PNS and CNS (Bear et al. 2016). Although these diseases can show

different symptoms caused by a variety of distinct pathophysiological changes, some share similarities including the deposition of atypical protein aggregates that are thought to lead to cell death (Rubinsztein 2006; Bredesen et al. 2006).

1.2 Neurons and synaptic transmission

Within the brain, neurons receive, transform, and transmit signals. For this purpose, they are highly polarized cells, consisting of a cell soma from which originate long protrusions called neurites. The soma contains the typical components of a eukaryotic cell such as the nucleus, Golgi apparatus, and endoplasmic reticulum (ER) (Bear et al. 2016). Neurites are responsible for the characteristic morphology and function of neurons, and they interconnect neurons in complex networks. The neurites can be divided into dendrites and axons. Dendrites are highly branched extensions from the soma that connect the neuron to other neurons via synaptic contacts. These connections are called synapses and they are important for the transfer of signals between neurons. Dendrites play a critical role in integrating and propagating these signals toward the soma, where they are processed and transmitted along the axon to other neurons. Axons are typically thinner and longer than dendrites and are less branched. Only at the far end do axons commonly divide into branches. A schematic neuron is shown in figure 1.2. Each individual neuron is in contact with many other neurons, leading to a highly complex network (Bear et al. 2016).

Information is passed as electrical signals in neurons. The generation of electrical signals relies on changes in the membrane potential of neurons (Bear et al. 2016). During quiescence, the cells are at resting potential. This electrical potential across the plasma membrane is due to an unequal distribution of ions between the extracellular and intracellular space, leading to a difference in electrical charge between the inside and outside of the plasma membrane, which is called the membrane potential. Sodium (Na^+), calcium (Ca^{2+}), and chloride (Cl^-) ions are concentrated on the outside of the neuron, whereas potassium ions (K^+) and negatively charged molecules such as amino acids are concentrated on the inside, leading to electrochemical gradients. The resting potential is maintained by ion pumps that pump ions against their concentration gradient and by the selective permeability of the plasma membrane for ions that pass through ion channels along their concentration gradients. A change in the membrane potential above a certain threshold can lead to the generation of an action potential. This signal is propagated along the axon and transmitted to another neuron via the synapse (Alberts 2015). The synapse can be divided into the pre- and postsynaptic

sites. The presynaptic site is the axonal bouton or terminal, where the axon of one cell is in contact with the postsynaptic site of a dendrite or the soma of a second neuron. Within the nervous system, two different types of synapses can be distinguished. At the electrical synapse, the electrical signal is directly transferred through gap junctions. Most synapses are chemical synapses, as shown in figure 1.2. Here electrical impulses are converted into chemical signals (Bear et al. 2016).

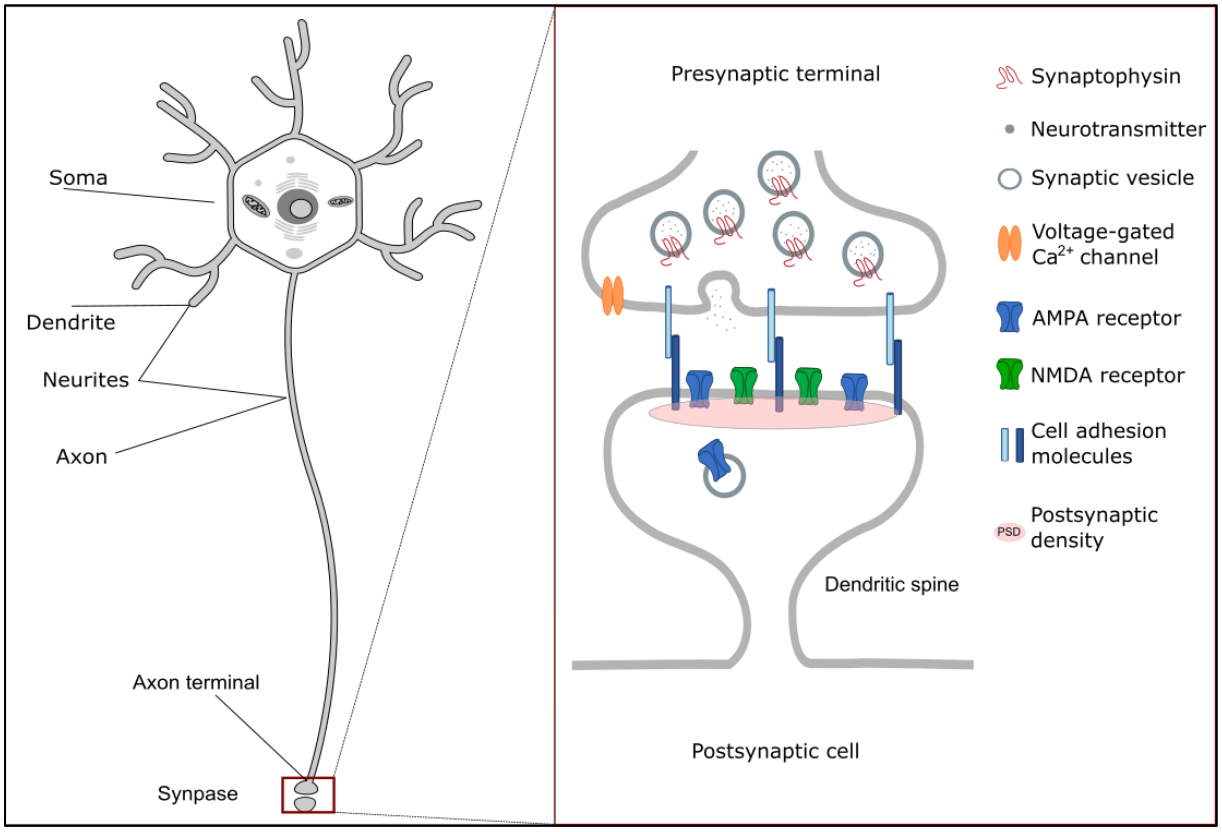

Figure 1.2: Neuronal morphology and the chemical synapse. A schematic representation of a neuron is shown on the left. The neuron consists of soma and protrusions called neurites. The neurites can be divided into dendrites that receive signals from other neurons and propagate them toward the soma, and into axons that transfer the signals to other neurons via the axon terminal and the synapse. The synapse is shown enlarged on the right. It is composed of the presynaptic terminal (at the axon), the postsynaptic compartment (located at a dendritic spine), and the synaptic cleft localized between the two compartments. The active zone of the presynaptic terminal contains synaptic vesicles filled with neurotransmitters. If an action potential reaches the axon terminal, voltage-gated ion channels in the presynaptic membrane open, causing an influx of calcium ions. This leads to the fusion of synaptic vesicles with the presynaptic membrane and the release of neurotransmitters into the synaptic cleft. The neurotransmitters bind to neurotransmitter receptors such as ligand-gated ion channels that are present in the postsynaptic membrane. Their activation in turn leads to an ion influx and a change in the membrane potential at the postsynaptic compartment. The postsynaptic density (PSD) is a multi-protein assembly that organizes the anchoring of neurotransmitter receptors, cell adhesion molecules, and

signaling molecules at the postsynaptic membrane. Neuronal cell adhesion molecules physically mediate the contact between pre- and postsynaptic compartments (Alberts 2015; Bear et al. 2016).

At the chemical synapse, neurotransmitters are released from synaptic vesicles into the synaptic cleft. When an action potential reaches the presynaptic terminal, voltage-gated Ca^{2+} channels open. A rise in presynaptic Ca^{2+} levels leads to docking and fusion of synaptic vesicles at the presynaptic membrane and consequently to the release of neurotransmitters into the synaptic cleft. The neurotransmitters can then bind to neurotransmitter receptors at the postsynaptic terminal. The receptors can be metabotropic or ionotropic receptors. Metabotropic receptors are G-protein-coupled receptors that can initiate several metabolic steps to modulate the activity of the neurons through signaling cascades. Ionotropic receptors are ligand-gated ion channels that open upon ligand binding, allowing ions to pass the membrane, which can lead to changes in the membrane potential. There is a large variety of synapses, defined by the neurotransmitter that is released. The most prominent neurotransmitters in the mammalian brain are glutamate and γ-aminobutyric acid (GABA) (Bear et al. 2016).

Of the many types of synapses of a neuron, some tend to excite while other others inhibit the postsynaptic neuron. While inhibitory postsynaptic sites mainly localize to the soma and dendritic shafts, excitatory synapses are frequently located at dendritic spines, a specialized, small membranous protrusion of dendrites. The main difference between these two types of synapses is the neurotransmitter released from the presynaptic cell and the corresponding postsynaptic receptors.

At inhibitory synapses, GABA is the most common neurotransmitter. Upon release, it binds to GABA receptors. There are two types of GABA receptors. $GABA_A$ are ligand-gated Cl^- channels, while $GABA_B$ receptors are metabotropic receptors. When GABA binds to $GABA_A$ receptors, they become permeable for Cl^-. This leads to a decrease in the membrane potential (hyperpolarization), also referred to as inhibitory postsynaptic potential (IPSP). It can inhibit the generation of an action potential in the postsynaptic cell (Bear et al. 2016). In contrast, glutamate is the main excitatory neurotransmitter in the brain. There are different types of ionotropic glutamate receptors, differentiated by their function and binding antagonists (Bear et al. 2016). The α-amino-3-hydroxy-5-methyl-4-isoazolepropionic acid (AMPA) receptors are tetramers composed of the subunits GluA1 to GluA4, each containing a ligand-binding site. Receptors containing the GluA2 subunits are impermeable for Ca^{2+}, which is important for synaptic plasticity,

as is explained later (Hollmann et al. 1991). N-Methyl-D-aspartic acid (NMDA) receptors are another type of voltage-gated ionotropic glutamate receptors. In addition to ligand-binding, they also need the membrane to be depolarized to release a magnesium ion (Mg^{2+}) which blocks the channel and allows the pore to open (Mayer et al. 1984). Activation of NMDA receptors leads to an influx in Ca^{2+}, which is crucial for synaptic plasticity (MacDermott et al. 1986). Glutamate binding to AMPA or NMDA receptors induces an influx of positively charged ions, depolarizing the membrane, and leading to an excitatory postsynaptic potential (EPSP). After depolarization, other voltage-gated ion channels, which are typically potassium channels, open, leading to efflux of potassium ions and repolarization of the membrane potential. The EPSPs and IPSPs are passively conveyed along the dendrite toward the soma, where they converge. Multiple EPSPs are needed to induce the firing of an action potential, while IPSPs reduce the membrane potential and therefore the probability of the firing of an action potential (Bear et al. 2016; Alberts 2015). From the soma, the action potential is propagated along the axon toward the axon terminal to transmit the signal to other cells. This process is expedited by the myelin sheath created by compaction of the oligodendroglia plasma membrane around CNS axons. The myelin sheath does not wrap around the neuron continuously but is separated by nodes of Ranvier, where voltage-gated Na^+ channels are concentrated. In saltatory conduction, the action potential leaps from node to node, accelerating the transmission (Bear et al. 2016).

1.3 Synaptic plasticity

The synaptic connections between neurons are not static but undergo constant structural remodeling and functional changes based on neuronal activity. This process, known as synaptic plasticity, occurs over both short and long-time scales. In short-term plasticity the synaptic efficacy changes in response to presynaptic spiking for a few milliseconds or at most a few seconds (Fioravante and Regehr 2011; Bear et al. 2016). Long-term plasticity, which lasts for minutes to hours, is widely considered to be crucial for learning and memory formation (Bear et al. 2016).

A phenomenon called long-term potentiation (LTP) describes the persistent increase in synaptic strength following the repetitive high-frequent depolarization of the postsynaptic membrane, as shown in figure 1.3.

Activation of AMPA receptors by glutamate leads to an influx in positively charged ions, such as Na^+, and raises the membrane potential. If glutamate also binds to NMDA receptors while the membrane is depolarized, NMDA receptors open, leading to an

increased influx of Ca^{2+} in particular. This causes activation of Ca^{2+}-dependent kinases, such as the Calcium/Calmodulin dependent kinase II (CaMKII) and protein kinase C (PKC) (MacDermott et al. 1986). They in turn mediate an increase in the sensitivity of postsynaptic membrane-localized AMPA receptors and in the recruitment of additional receptors from extra-synaptic sites and internal stores to the postsynaptic membrane. These processes can cause an immediate and strong increase in synaptic strength. Ca^{2+} signaling also facilitates the synthesis of cyclic adenosine monophosphate (cAMP), which activates protein kinase A (PKA) and consequently causes phosphorylation and activation of the CREB. Activated CREB can modify the expression of several genes, which is considered to be important for the persistence of LTP. Furthermore, LTP is characterized by increases in the size of the dendritic spine, the PSD, and the corresponding presynaptic terminal. This increase in size is at least partially due to rearrangements of the actin cytoskeleton. In contrast to LTP, less frequent synaptic stimulation leads to an internalization of AMPA receptors, as well as to weakening and shrinking of the synapse. This process, called long-term depression (LTD), is influenced by low Ca^{2+} influx and the activation of phosphatases. Dysfunction of these processes might also play a role in the development and progression of neurodegenerative diseases, such as in AD, where LTP is impaired (Bear et al. 2016).

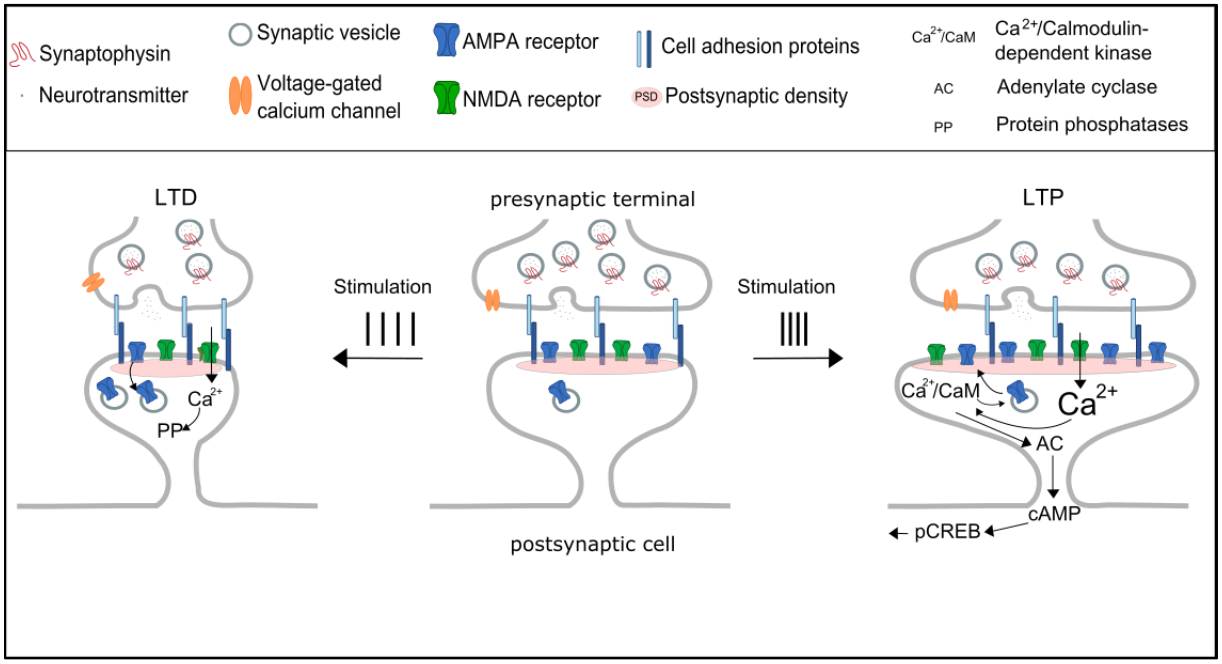

Figure 1.3: Synaptic plasticity. According to the type of stimulation the synapse receives, it can undergo long-term depression (LTD, left) or long-term potentiation (LTP, right). If the synapse is stimulated at a high frequency, the postsynaptic membrane gets depolarized, dislodging the Mg^{2+} at NMDA receptors, which leads to a high influx in Ca^{2+}. Calcium ions can activate calmodulin, which in turn activates kinases such as calmodulin-dependent protein kinase II (CaMKII). CaMKII can phosphorylate AMPA receptors,

making them more sensitive, and it can activate adenylate cyclase (AC). It also mediates the recruitment of additional AMPA receptors from extra-synaptic or internal stores into the postsynaptic membrane, thereby immediately increasing synaptic strength. Meanwhile, AC produces cAMP, an important second messenger that activates the cAMP response element binding protein (CREB). CREB is a transcription factor that modulates gene expression in the nucleus, important for the late stages of LTP. If the synapse is stimulated less frequently it is weakly depolarized, this leads to a moderate rise in Ca^{2+} and to LTD. It is accompanied by the activation of phosphatases such as protein phosphatase 1 (PP). They dephosphorylate AMPA receptors and CREB, leading to an internalization of AMPA receptors and the shrinking of the synapse (Bear et al. 2016).

Activity-dependent synaptic plasticity in LTP and LTD creates a positive feedback that when uncompensated can lead to network instability (Lee and Kirkwood 2019). Homeostatic plasticity, meanwhile, operates to compensate for prolonged activity changes to maintain the stability and functionality of the neuronal networks (Desai 2003).

While LTP and LTD change synaptic strength in a synapse-specific manner, homeostatic plasticity regulates the total synaptic strength of a neuron (Turrigiano et al. 1998). In response to changes in neuronal activity, neurons can regulate intrinsic excitability, neurotransmitter release, or neurotransmitter receptor abundance (O'Brien et al. 1998; Murthy et al. 2001; Thiagarajan et al. 2005; Bacci et al. 2001). Synaptic scaling is a proposed mechanism, by which the neurons balance synaptic plasticity by modulating the activity of the synapse (Desai 2003). Prolonged activity deprivation leads to an upscaling of excitatory synapses, while increased activity downscales them to maintain an overall average firing rate (Lee and Kirkwood 2019). Homeostatic and synaptic plasticity are similar in their molecular mechanisms and probably converge to regulate common effectors at the synapse. Prolonged neuronal inactivity or sustained overexcitation, induced by either blockade of neuronal firing or blocking inhibitory synaptic transmission, accordingly scale up or down AMPA receptors, important players in synaptic plasticity (Turrigiano et al. 1998; Lissin et al. 1998; O'Brien et al. 1998). Suppression of activity leads to an increased number of available synaptic vesicles at the active zone of the presynaptic terminal and enhanced vesicle recycling (Moulder et al. 2006; Murthy et al. 2001; Bacci et al. 2001; Thiagarajan et al. 2005). Persistent elevation of network activity meanwhile leads to a decrease in presynaptic vesicle release and changes in glutamate content in synaptic vesicles (Moulder et al. 2004; Gois et al. 2005; Wilson et al. 2005; Moulder et al. 2006; Branco et al. 2008).

These mechanisms are important in a constantly changing network to maintain functional stability.

1.4 Neuronal transport

Neurons are highly polarized cells, with axons that can reach up to one meter in length in the human spinal cord. Most protein synthesis and degradation take place in the soma of the neuron (Bear et al. 2016). Membrane proteins such as neurotransmitter receptors need to be processed and transported in the secretory pathway from the endoplasmic reticulum (ER) to the Golgi apparatus, before being transported to the plasma membrane (Alberts 2015). Rapid turnover of synaptic molecules is critical for synapse formation and function, which makes active transport extremely important to maintain metabolic balance (Hirokawa et al. 2010; Chevalier-Larsen and Holzbaur 2006). Membrane organelles, protein complexes, nucleic acids, signaling molecules, and vesicular and cytoskeletal components need to be transported to and from the soma along the neurites along molecular tracks provided by the cytoskeleton and by motor proteins. Microtubules (MTs) and actin filaments (F-actin) provide the tracks for transport, while the motor proteins of the kinesin, dynein, or myosin family transport cargo along the cytoskeleton in adenosine triphosphate (ATP)-dependent manner. The structure of motor proteins roughly consists of a tail region that binds to the cargo, a stalk domain, and a head domain that binds to the cytoskeleton and harbors ATPase activity. They either bind to F-actin (myosin), or MTs (dynein, kinesin) (Bear et al. 2016). While there are thousands of different cargos, there are only a few different motor proteins with different functions. Adaptor proteins form transport complexes with cargo and motor proteins. Many adaptor proteins can bind to different cargo vesicles and motor proteins. They can be regulated by kinases and G proteins and in turn, regulate opposing kinesin and dynein motors. This allows the specific transport of vesicles to their correct destination and rapid response to the local environment (Fu and Holzbaur 2014). Figure 1.4 shows the components of active transport in neurons. Transport along MTs is responsible for long-distance neuronal trafficking (Fu and Holzbaur 2014). MTs are polymers consisting of α- and β-tubulin dimers, polymerized to polarized protofilaments that assemble in parallel orientation to form a hollow tube, the MT. The α- and β-tubulins form dimers that can then polymerize in a GTP-dependent manner into MTs (Bear et al. 2016). MTs are formed by nucleation at microtubule-organizing centers (MTOCs) containing γ-tubulin.

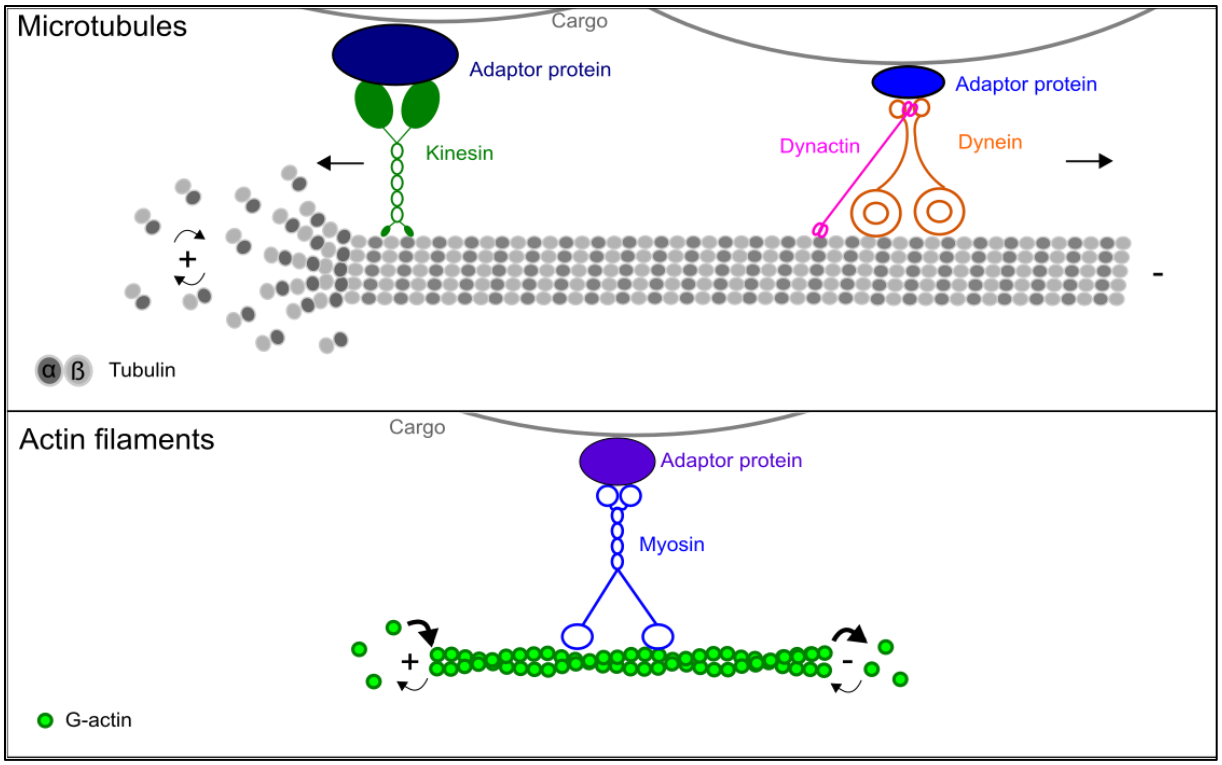

Figure 1.4: Neuronal transport. This figure shows the two components of the cytoskeleton required for motor protein dependent transport, including possible transport complex assemblies. Microtubules (grey) are composed of α- and β-tubulins that form dimers, which can polymerize into protofilaments that laterally associate in a guanosine triphosphate (GTP)-dependent manner to form a hollow tube. GTP-bound dimers of tubulin can be added to the microtubules. When bound to MTs, GTP can be hydrolyzed to guanosine diphosphate (GDP). This makes the MT less stable and when GDP-bound tubulins are exposed at the end of the MT, they dissociate, leading to shrinkage, making the structure dynamic. Most kinesins (dark green) transport their cargo along MTs toward the dynamic plus-end, while the dynein/dynactin (orange/pink) complex transports cargo toward the stabilized minus end. Adaptor proteins (dark blue and medium blue) can mediate cargo-binding to motor proteins, motor velocities, and cargo-targeting (Fu and Holzbaur 2014). F-actin (green) is composed of globular actin (G-actin), polymerizing to a two-stranded helical structure with two distinct ends in an ATP-dependent manner. New ATP-bound G-actin is added at the plus-end where the filament grows. ATP is then hydrolyzed to adenosine diphosphate (ADP). ADP-bound G-actin detaches at the minus-end, where F-actin shrinks. Myosins are motor proteins that transport cargos along F-actin. They also have a preferred transport direction. Only myosin VI transports cargo toward the minus end (Alberts 2015). Myosins also bind adaptor proteins (purple) that regulate their cargo binding and release, as well as motor activity (Fu and Holzbaur 2014).

Together with other proteins the γ-tubulins form a ring complex, from where α/β-tubulin dimers polymerize into MTs. The ring serves as a cap at the minus-end of the MT while it assembles (Desai and Mitchison 1997). The MT has a fast-growing plus-end with β-tubulin facing outwards and a more stable minus-end with α-tubulin at the end (Bear et al. 2016). In axons, MTs are oriented with their minus-end toward the soma, in

dendrites, there is a mixed orientation. Over time, GTP is hydrolyzed to GDP. GDP-bound tubulin dimers at the tip of the MT will disassociate. While growing, GTP-bound tubulin is added to the MT to form a cap, but when GTP hydrolysis is faster than polymerization, the MT begins to depolymerize and shrink. This switch from growth to shrinkage is called a catastrophe. GTP-bound tubulin can be added to the depolymerizing end to rescue it from further shrinkage (Mitchison and Kirschner 1984). This dynamic instability is important in developing neurons for normal neurite outgrowth. In mature neurons, the MTs become less dynamic due to their interaction with MT-associated proteins (MAP) such as tau that stabilize the MTs in axons (Chevalier-Larsen and Holzbaur 2006). At the plus-end of the MT, plus-end-tracking proteins can regulate MT growth by stabilizing or catalyzing the addition of GTP-tubulins, while at the minus-end, minus-end binding proteins stabilize MTs (Hendershott and Vale 2014). MAPs do not only stabilize MTs. Some, such as catastrophin, destabilize MTs, while others, such as katanin, can sever them (Alberts 2015). Additionally, posttranslational modifications (PTM) of MTs can regulate MT stability or the activities of MT-associated motor proteins. (Hammond et al. 2010; Sirajuddin et al. 2014). MTs in dendrites differ fundamentally from MTs in axons in their PTMs and MT binding proteins (Aiken and Holzbaur 2021).

In neurons the proteome of motor proteins is more complex than in most other cell types, indicating an enhanced importance of regulated and specific intracellular transport, likely due to their highly polarized morphology and function (Kuta et al. 2010; Silverman et al. 2010). Conventional kinesin holoenzymes (kinesin-1) are heterotetramers composed of two heavy chains and two light chains. The heavy chains contain the globular ATPase motor domain at the N-terminus and associate with the light chains via the C-terminus. The light chain can bind different cargos. Cargo-binding results in kinesin unfolding from its inactive state and the activation of the motor domain (Chevalier-Larsen and Holzbaur 2006). The motor domain in the heavy chain has a binding site for the MT and one for ATP. ATP binding, hydrolysis, and ADP release change the conformation of the motor domain leading the kinesin to move along MTs in a highly processive manner (Chevalier-Larsen and Holzbaur 2006). Most kinesins move in the plus-end direction of MTs and regulate the targeting of cargo to axons or dendrites (Nakata and Hirokawa 2003). Cytoplasmic dynein 1 is the major motor protein responsible for driving MT minus-end directed transport in neurons. It is a large and complex molecule, assembled from many protein subunits. In contrast to the

variety of different kinesin heavy chains found, there is only one dynein heavy chain, which is responsible for MT-based transport in neurons (Roberts et al. 2013). The holoenzyme of this dynein is formed by two identical heavy chains, containing the ATPase motor domain, two intermediate chains, two light intermediate chains, and light chains associated with the heavy chains to form a cargo-binding domain. While the motor domain is encoded only by a single gene, there is more variety for the other subunits and accessory proteins binding to the dynein complex, which gives it further diversity (Kuta et al. 2010). The dynactin complex mediates cargo-binding to dynein (Gill et al. 1991). Due to MT organization in axons, dynein relies on kinesin-1 for axon terminal localization, as it cannot enter the axon due to its minus-end polarity (Twelvetrees et al. 2016).

The motor proteins usually do not bind cargo directly but via adaptor proteins. Adaptor proteins interact with membrane-associated cargo receptors, components of kinesin and dynein motor complexes, as well as signaling proteins such as kinases or GTPases (Fu and Holzbaur 2014). They regulate directionality as well as the targeting to different compartments in the cell. While some adaptor proteins such as the c-Jun-amino-terminal kinase-interacting protein 1 (JIP1) bind to kinesin light chains, others, such as the glutamate receptor-interacting protein (GRIP1), bind to the C-terminus of the kinesin heavy chain (Chevalier-Larsen and Holzbaur 2006). The targeting of cargo toward the dendrite or the axon can be influenced by the way the adaptor proteins are bound to kinesins (Hirokawa and Takemura 2004). GRIP1, for example, is essential for kinesin-1 mediated transport of AMPA receptors and N-cadherin in dendrites (Setou et al. 2002; Heisler et al. 2014). PTMs such as phosphorylation regulate the binding and release of cargo to adaptors and adaptor binding to motor proteins (Park et al. 2017). Also, neuronal activity influences motor-cargo interactions. In postsynaptic regions, kinesins can be phosphorylated by CaMKII, disrupting adaptor protein and kinesin binding and leading to cargo uncoupling (Guillaud et al. 2008). Other examples of Ca^{2+} signaling that can regulate cargo loading or unloading are summarized in Aiken and Holzbaur from 2021.

Opposing motor proteins can bind simultaneously to transport vesicles. There are different models to explain how transport is regulated. The simplest model is an unregulated tug-of-war that can be observed for endolysosomal transport (Hendricks et al. 2010). Other models suggest a coordinated regulation of the different motor types so that only a single motor is active at any time (Welte 2004; Fu and Holzbaur 2014).

There is strong evidence that adaptor proteins regulate the activities of opposing motors (Fu and Holzbaur 2014). Cargo-loading and unloading is a complex interplay between PTMs of motor proteins as well as adaptor proteins, specific adaptor and cargo interactions, MAP decoration, and MT organization. Further investigations are needed to investigate presynaptic and postsynaptic cargo delivery, as well as cargo binding to adaptors and motor proteins (Aiken and Holzbaur 2021).

F-actin is concentrated beneath the plasma membrane, especially in presynaptic terminals and postsynaptic sites (Halpain et al. 1998; Matus et al. 1982; Bridgman 2004). It is also important in axonal growth cones and developing dendrites (Matus 2000; Pak et al. 2008; Hotulainen and Hoogenraad 2010). A high concentration of F-actin can also be found in the axon initial segment (Huang and Rasband 2016). F-actin is composed of G-actin monomers that polymerize in an ATP-dependent manner to a two-stranded helical structure with two distinct ends, termed barbed plus-end and pointed minus-end. At steady-state conditions, ATP-bound G-actin is added to the plus-end while ADP-bound G-actin disassociates from the minus-end leading to treadmilling. (Pollard and Cooper 2009). Cofilin binds ADP-actin filaments and accelerates disassembly, while profilin binds ATP-bound G-actin monomers and accelerates F-actin elongation (Alberts 2015). F-actin acts as a scaffold to dock vesicles and coordinate neurotransmitter release and recycling in the pre- and postsynaptic regions (Sankaranarayanan et al. 2003; Cingolani and Goda 2008). It supports submembrane receptor trafficking and influences the diffusion rate of receptors within the plasma membrane (Kneussel and Loebrich 2007; Cingolani and Goda 2008). It has also been described as anchoring neurotransmitter receptors in the postsynaptic region (Allison et al. 1998). Actin dynamics are important for synaptic plasticity (Fischer et al. 2000). Reorganization and enhanced polymerization of F-actin are required for spine growth during LTP (Matsuzaki et al. 2004; Cingolani and Goda 2008; Honkura et al. 2008; Hotulainen and Hoogenraad 2010). Ca^{2+} signaling regulates F-actin remodeling, cargo transport, and motor activity (Oertner and Matus 2005; Hou et al. 2015; Mikhaylova et al. 2018). Actin plays an essential role in Ca^{2+}-mediated presynaptic vesicle release and recycling (Chanaday et al. 2019). Myosins are a superfamily of motor proteins associated with F-actin (Bear et al. 2016). They consist of a head containing the ATPase motor domain, a stalk region, and a cargo-binding tail domain (Harrington and Rodgers 1984). Generally, myosins move toward the plus-end of F-actin, except myosin VI, which moves toward the minus-end

(Sweeney and Houdusse 2010). They play significant roles in cell movement, membrane trafficking, and anchoring, signal transduction, and in other areas (Hirokawa et al. 2010). Myosins coordinate short-distance trafficking, delivery, retention, and release of presynaptic cargos in neurons (Nirschl et al. 2017). They have been shown to mediate the anchoring of certain cargos at the spine neck in postsynaptic regions (Ligon and Steward 2000; Sung et al. 2008; Wagner et al. 2011; Goo et al. 2017). This anchoring is activity-dependent (Chang et al. 2006; Redondo and Morris 2011; Goo et al. 2017). Myosin light chains are Ca^{2+} sensing proteins, in the case of myosin V and VI, calmodulin binds the neck region of the heavy chain (Krementsov et al. 2004; Bahloul et al. 2004). Myosin V is important for AMPA receptor transport toward the synaptic membrane, while myosin VI is important for AMPA receptor internalization, both are critical for synaptic plasticity (Correia et al. 2008; Wang et al. 2008). Myosin V transports ER compartments into dendritic spines which is important for Ca^{2+} release in LTD (Dekker-Ohno et al. 1996; Miyata et al. 2000). Myosin VI regulates Golgi complex integrity, F-actin dynamics, and cell migration, and acts as a load-dependent anchor (Altman et al. 2004; Kneussel and Wagner 2013; Tumbarello et al. 2013). It regulates vesicular trafficking and endocytosis of neurotransmitter receptors, such as AMPA receptors, at synaptic spines (Heisler et al. 2011; Morris et al. 2002; Osterweil et al. 2005; Buss et al. 2001). Myosins also bind and are regulated by adaptor proteins. GRIP1 directly interacts with AMPA receptors and myosin VI (Huganir and Nicoll 2013; Lv et al. 2015).

1.5 Endosomal turnover in neurons

Neurons with their elaborate axonal and dendritic branching have a huge surface area. The trafficking of intracellular membranes needs to be tightly regulated to sustain neuronal polarity and function and to maintain the metabolic balance. One important player in this regulation is the family of Rab proteins, which consists of small GTPases. Active GTP-bound Rab proteins regulate the secretory and endolysosomal pathways (Alberts 2015). The nucleotide-bound state influences the localization and activity of Rab proteins. They are posttranslationally modified by geranylgeranyl lipid groups, with which they can directly bind membranes. In their GDP-bound state, Rab proteins associate with GDP dissociation inhibitor (GDI) in the cytosol. GDIs deliver the GDP-bound Rab proteins to specific membrane compartments, where they interact with GDI displacement factors (GDFs). GDFs promote Rab protein release from GDIs, while guanine nucleotide exchange factors activate Rabs by catalyzing GDP to GTP

exchange. After activation, Rab proteins can bind to membranes and Rab effectors, which mediate vesicle transport, membrane tethering, and membrane fusion. Rab effectors can be motor proteins, tethering proteins, soluble N-ethylmaleimide-sensitive factor attachment protein receptors (SNARE) proteins, kinases, phosphatases, adaptor proteins, and others. The secretory and endolysosomal pathways are depicted in figure 1.5.

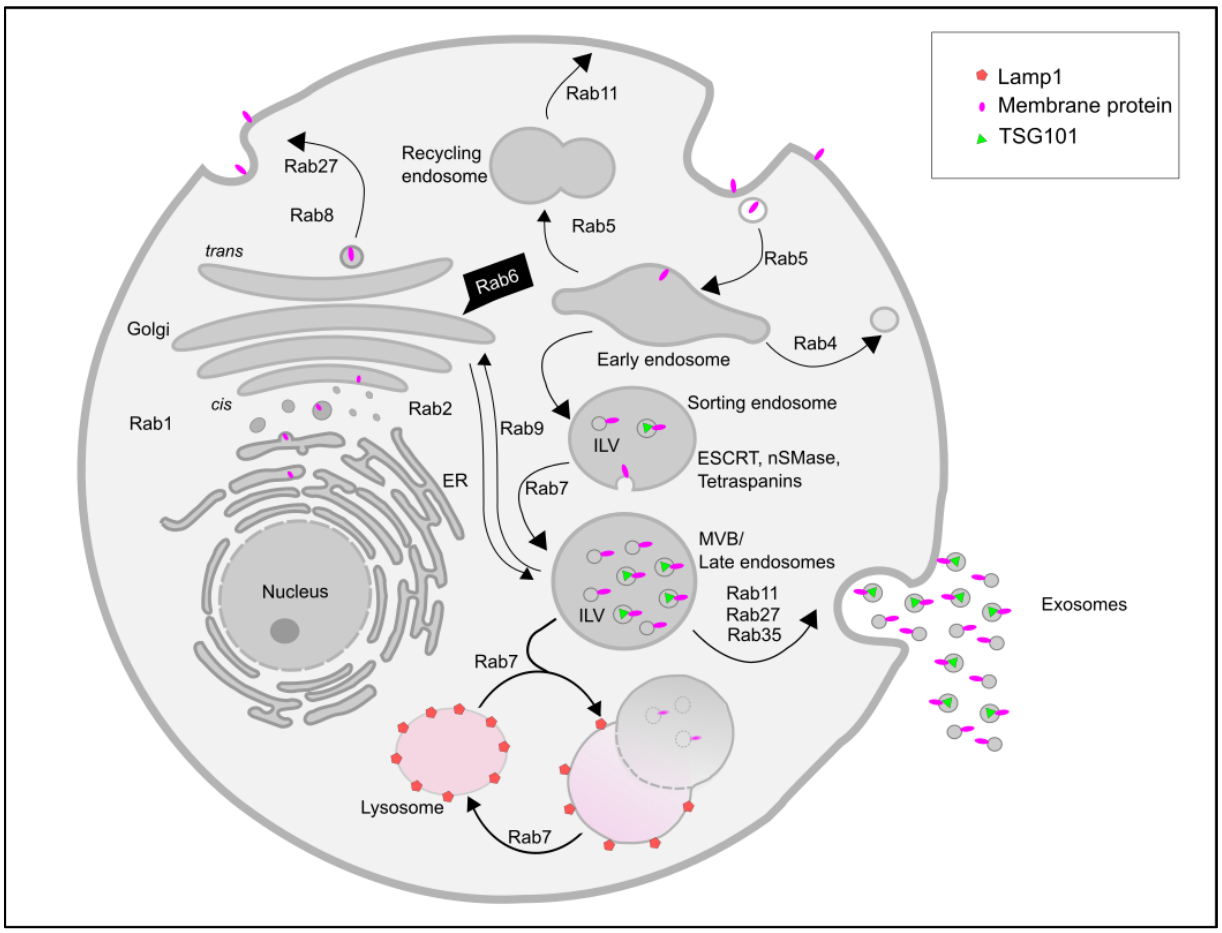

Figure 1.5: Secretory and endolysosomal pathway (adapted from: (Alenquer and Amorim 2015; Cullen and Steinberg 2018; Martinez-Arroyo et al. 2021)). Membrane and secreted proteins are synthesized in the ER. They are transported to the *cis*-Golgi. Transport between Golgi and ER is regulated by Rab1 and Rab2. In the Golgi, proteins are transported toward the *trans*-Golgi in a Rab6-dependent manner. From the Golgi, the transport of protein vesicles to the plasma membrane is regulated by Rab8 and Rab27. Endocytosed proteins are transported in vesicles to early endosomes in a Rab5-dependent manner. Rab11 mediates slow endocytic recycling through the recycling endosome, while Rab4 mediates fast recycling directly to the plasma membrane. In sorting endosomes, intraluminal vesicles (ILVs) are formed by inward budding of the endosome membrane. The endosomal sorting complex required for transport (ESCRT) machinery, lipid metabolism by neutral sphingomyelinase (nSMase), and tetraspanins organize the formation of ILVs. This leads to the formation of multivesicular bodies (MVB) and late endosomes. Rab9 mediates trafficking between late endosomes and the trans-Golgi network. MVBs can either fuse with the lysosome in a Rab7-dependent manner or with the membrane

to release ILVs as exosomes in a Rab11, Rab27, or Rab35-dependent manner (Colombo et al. 2013; Martinez-Arroyo et al. 2021).

In the secretory pathway, membrane-associated and secreted proteins are trafficked by intracellular membrane transport from one membrane-enclosed compartment to another (Alberts 2015). They are synthesized at ribosomes attached to the rough ER. During their synthesis, they are translocated into the ER lumen, where they are glycosylated and folded. Misfolded proteins are sorted to the cytosol by ER-associated degradation, where they are degraded. Correctly folded proteins are packaged into transport vesicles and transported along MTs to the Golgi apparatus, where they fuse to form the *cis*-Golgi network. Rab1 and 2 regulate vesicular trafficking between the ER and the Golgi complex. In the *cis*-Golgi, proteins can be further glycosylated and other PTMs can be added. Proteins and lipids move along the Golgi stacks from *cis*- to *trans*-Golgi networks by Rab6-dependent intra-Golgi vesicle transport. In the *trans*-Golgi network, the finished proteins are packaged into transport vesicles and dispatched to their specific destination (Alberts 2015). From the Golgi, proteins such as AMPA receptors can be transported in vesicles directly to the plasma membrane via Rab8- or Rab27-regulated trafficking (Gerges et al. 2004; Brown et al. 2007; Gu et al. 2016; Quevedo et al. 2019). Adapter proteins such as GRIP1 are also important for AMPA receptor delivery to the synapse, as well as for pooling AMPA receptors in the cytoplasm (Setou et al. 2002; Heisler et al. 2014). It controls endosomal sorting toward recycling endosomes and membrane targeting (Daw et al. 2000; Braithwaite et al. 2002; Tan et al. 2020).

AMPA receptor turnover is essential for synaptic plasticity, so Rabs play an important role because they regulate AMPA receptor transport in the endocytic and secretory pathways. Endocytic vesicles fuse with early endosomes, the primary sorting compartment, in a Rab5-mediated manner (Alberts 2015; Guo et al. 2016). The endocytosed cargo can either be directly recycled, sorted in recycling endosomes, or mature into multivesicular bodies (MVB). Rab4 and 11 mediate the fast or slow recycling of endocytosed AMPA receptors and other proteins from sorting or recycling endosomes, respectively (Zhen and Stenmark 2015). MVBs are formed by invagination of the membrane into the endosomal lumen, which leads to the formation of intraluminal vesicles (ILVs) (Alberts 2015). In the endosomal sorting complex required for transport (ESCRT)-dependent pathway, cytosolic ESCRT proteins such

as the tumor susceptibility gene 101 (TSG101) mediate the sorting process of mono-ubiquitylated proteins (Colombo et al. 2013).

However, other pathways can also be involved in forming ILVs, such as the ceramide-dependent pathway, involving the neutral sphingomyelinase (nSMase), or tetraspanins (Ghossoub et al. 2014; Trajkovic et al. 2008). MVBs can fuse with late endosomes which can fuse with lysosomes to form endolysosomes. Most proteins will be degraded in lysosomes in this pathway. MVBs can, however, also fuse with the plasma membrane to release their content into the extracellular space as exosomes (Alberts 2015). Rab11, Rab27, and Rab35 have been shown to promote Ca^{2+}-dependent fusion of MVBs with the plasma membrane (Savina et al. 2005; Colombo et al. 2014; Hsu et al. 2010; Ostrowski et al. 2010). Each stage of endosome maturation is connected to the *trans*-Golgi by vesicular transport. Rab9 connects the late endosomes to the *trans*-Golgi network, which is important in recycling transmembrane proteins. Lysosomes are recruited by the Rab7 binding Rab-interacting lysosomal protein (RILP) to late endosomes in an MT-dependent manner. Lysosomal proteins such as lysosome-associated membrane protein 1 (Lamp1) are transported in clathrin-coated transport vesicles to endosomes, where they are sorted into lysosomes. These lysosomal proteins are only activated in lysosomes due to the low pH in the lysosome. In autophagy, organelles become surrounded by a double membrane to form autophagosomes. Nonselective autophagy can occur in starvation conditions. Here, a bulk portion of cytoplasm is sequestered into autophagosomes. In selective autophagy, only specific cargos are surrounded by autophagosomes that contain very little cytosol. This strategy is used to degrade worn-out organelles or invading microbes. The autophagosomes then fuse with the lysosome, where their cargo is degraded (Alberts 2015).

1.6 Exosomes

Exosomes are small extracellular vesicles that are released following the fusion of MVBs with the plasma membrane (Colombo et al. 2014). They are 50 to 150 nm in size and can be released by different cell types and are found in all types of body fluids (Raposo and Stoorvogel 2013). Exosomes are characterized by the pathway by which they are released into the extracellular space, which is shown in the scheme from figure 1.5. The first step in exosome biogenesis is the invagination of the plasma membrane, giving rise to early endosomes (Colombo et al. 2014). In early endosomes, ILVs can be formed by inward budding of the endosomal membrane. Different mechanisms can

lead to the formation of ILVs. The best-described mechanism is the ubiquitin-dependent ESCRT pathway composed of approximately 30 different proteins, including TSG101 (Katzmann et al. 2001). Tetraspanin CD63 participates in the sorting of cargo to ILVs and is enriched in exosomes (van Niel et al. 2011). Finally, two mechanisms depending on lipid metabolisms can also lead to the biogenesis of ILVs. These mechanisms are hydrolysis of sphingomyelin to ceramide by nSMase and generation of phosphatidic acid from phosphatidylcholine by phospholipase D2 (Ghossoub et al. 2014; Trajkovic et al. 2008). Rab and SNARE proteins mediate MBV fusion to the plasma membrane to release exosomes in a Ca^{2+}-dependent manner (Savina et al. 2003; Pegtel and Gould 2019). Exosomes can carry proteins, nucleic acids (including RNA), lipids, and lipid modifications, according to their cell type of origin. Proteins carried by exosomes include cell surface receptors, cell adhesion molecules, tetraspanins, integrins, and other transmembrane proteins (Simpson et al. 2008). Their content varies with the cell of origin and physiological as well as pathological conditions. Exosomes are enriched with regulators of endosomal trafficking and sorting, such as Alix, TSG101, and tetraspanin proteins (Zöller 2009; van Niel et al. 2011; Rana et al. 2012). The genetic material found in exosomes could be translated by, or regulate the gene expression of recipient cells (Kosaka et al. 2010; Montecalvo et al. 2012). Due to the molecular load they carry, exosomes are involved in cellular communication (Lee et al. 2012; Samanta et al. 2018).

In the brain, exosomes can be secreted by neurons, neuronal stem cells, and glial cells, and they can be found in the cerebral spinal fluid (Fauré et al. 2006; Kang et al. 2008; Vella et al. 2016; Guescini et al. 2010; Lachenal et al. 2011). Neuronal exosomes can contain AMPA receptors, the cellular prion protein (PrP^C), and the cell adhesion molecule L1CAM (Fauré et al. 2006; Lachenal et al. 2011; An et al. 2013). Specific exosome functions might vary depending on their origin and content. For example, exosomes released by glial cells can promote neurite growth and neuronal survival (Wang et al. 2011). Exosomes also play a role in synaptic pruning, the immune response, and in the formation of the myelin sheath (Bakhti et al. 2011; Fröhlich et al. 2014; Yáñez-Mó et al. 2015; Bahrini et al. 2015). Hippocampal neuronal stem cells can release exosomes that protect synapses against amyloid-beta oligomers (Aβo) and restore LTP and memory in wild type (WT) mice injected with Aβo (Micci et al. 2019). In stroke, exosomes can mediate angiogenesis and improve neurogenesis and non-coding RNAs in exosomes of stroke patients show significant changes in composition

compared to healthy controls (Li et al. 2018; Lu et al. 2018; Nozohouri et al. 2020). In contrast to the reported beneficial effects, exosomes can also transfer disease-associated proteins or RNAs to propagate pathology, for example in neurodegenerative diseases (Edgar 2016; Hill 2019). This makes exosomes interesting to use as biomarkers to diagnose diseases such as stroke and predict the course of disease (Zhang et al. 2021; Alvarez-Erviti et al. 2011). Their ability to cross the blood-brain barrier makes exosomes interesting for treating diseases such as stroke (Chen and Chopp 2018).

Exosome secretion from neurons can be stimulated by depolarization, for example after stimulation with neurotransmitters (Fauré et al. 2006; Lachenal et al. 2011; Goldie et al. 2014). This suggests that activity-dependent exosome release may alter the efficiency of synaptic transmission. Enhanced AMPA receptor-containing exosome release could be a mechanism of synaptic scaling following extensive synaptic activation (Turrigiano 2008). MVBs are present in dendritic shafts and some spines, indicating that exosomes could be released near synapses (Cooney et al. 2002). The stimulation of LTP could lead to the release of exosomes, transferring newly synthesized synaptic proteins and synaptic RNAs to presynaptic terminals, where they could contribute to synaptic plasticity (Smalheiser 2007). Upon release, exosomes can be taken up by different recipient cells. Exosomes can bind to target cells through ligand-receptor interaction or adhesion molecules (Clayton et al. 2004). Neuronal exosomes can be internalized by other neurons and by glia cells (Bahrini et al. 2015; Chivet et al. 2014). The exosomes can be internalized by recipient cells through several mechanisms including phagocytosis, endocytosis, and membrane fusion (Raposo and Stoorvogel 2013). Interestingly, endocytosed exosomes that are taken up can be re-secreted from MVBs together with the cells' own exosomes (Polanco et al. 2018). Together with the fact that the release of exosomes can be triggered by synaptic activity, this may point to a role of exosomes in cell communication during neuronal activity changes.

1.7 The cellular prion protein

The "prion" was first discovered in 1982 as a "novel proteinaceous infectious particle causing scrapie" (Prusiner 1982). This finding led to the identification of PrP^{C}, a ubiquitous cell surface protein, highly expressed in the PNS and CNS, especially in neurons (Bendheim et al. 1992). It is attached to membranes by a posttranslationally added glycosylphosphatidylinositol (GPI) anchor (Biasini et al. 2012).

PRNP is the human gene encoding PrP^C (Hsiao et al. 1991). PrP^C is best known for its misfolding in neurodegenerative diseases known as transmissible spongiform encephalopathies (TSEs) or prion diseases, such as Creutzfeldt-Jacob disease in humans, scrapie in sheep, or bovine spongiform encephalopathy in cattle. They are a group of rare degenerative disorders characterized by late-onset accumulation of misfolded protein aggregates of PrP^{Sc} and by progressive neurodegeneration (Prusiner 1982; Aguzzi and Polymenidou 2004). Vacuoles form within the neurons, which leads to cell death and loss of tissue, giving the tissue a sponge-like appearance (Masters et al. 1976). TSEs can occur in a sporadic, inherited, or acquired form. Sporadic TSE occurs due to spontaneous misfolding of PrP^C to PrP^{Sc} within the brain, familial TSEs have a genetic disposition predisposing individuals to develop TSE, and acquired TSEs stem from the introduction of infectious material from an external source (Whitechurch et al. 2017). So far, TSEs are the only disorders described that are transmitted by naturally occurring infectious protein misfolding (Kraus et al. 2013). In prion diseases, PrP^C undergoes misfolding to produce the abnormal PrP^{Sc}, named after the scrapie form of the disease. PrP^C expression is essential for disease transmission and development (Büeler et al. 1993; Sailer 1994). Abnormal PrP^{Sc} differs from PrP^C structurally. It is enriched in β-sheets while PrP^C has a higher content in α-helices (Pan et al. 1993). The misfolded PrP^{Sc} is mostly insoluble in non-ionic detergents and cannot be completely digested by proteinase K, while the opposite is true for PrP^C (Meyer et al. 1986). The conversion of PrP^C to PrP^{Sc} is facilitated by PrP^{Sc} acting as a template to assist PrP^C misfolding. Misfolded proteins can act as a seed for further polymerization producing fibrils that further form amyloid plaques (Soto et al. 2006). PrP^{Sc} may spread between cells to propagate the disease (Whitechurch et al. 2017). All prion diseases are currently incurable and fatal (Aguzzi et al. 2008).

PrP^C is conserved in mammals and birds, which suggests that it has some vital functional role (Sarnataro et al. 2017). It has been reported that PrP^C plays a role in neurite outgrowth, cell adhesion, neuroprotection from oxidative stress, apoptosis-related to ER stress, copper ion binding, synaptic plasticity, and sleep (Schmitt-Ulms et al. 2001; Martins et al. 2002; Kanaani et al. 2005; Linden et al. 2008; Bounhar et al. 2001; Roucou et al. 2005; Vassallo and Herms 2003; Brown et al. 1997; Laurén et al. 2009). A scheme of PrP^C protein structure is shown in figure 1.7.

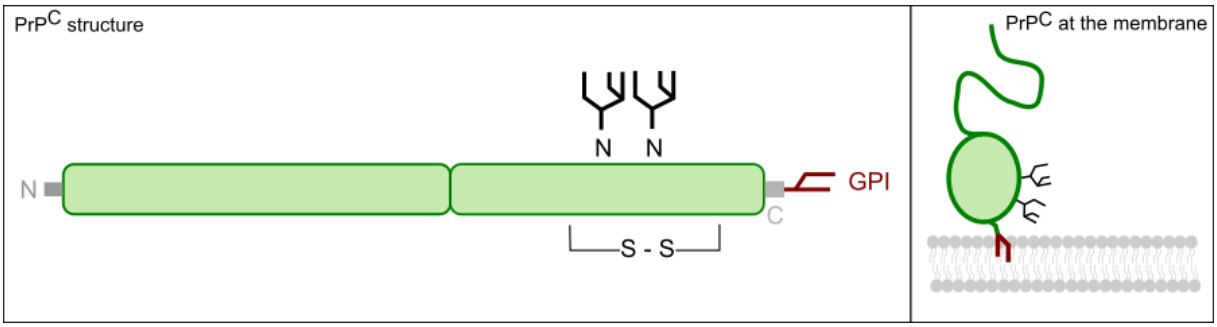

Figure 1.6: The cellular prion protein (PrP^C). PrP^C contains a GPI anchor at the C-terminus, which has a globular structure, a disulfide bond, and two N-glycosylation sites (Biasini et al. 2012). The N-terminus is intrinsically unstructured (Viles et al. 1999). The GPI anchor is a PTM at the C-terminus of the PrP^C that attaches the protein to membranes (Brown and Rose 1992; McConville and Ferguson 1993).

The GPI anchor is attached to the C-terminus of PrP^C, which has a globular structure containing three α-helices, two short β-strands, and two N-glycosylation sites (Biasini et al. 2012). This region misfolds into the β-sheet-rich pathogenic form of PrP^{Sc} in prion diseases (Pan et al. 1993). The N-terminus is intrinsically unstructured and contains an octarepeat region that can bind positively charged ions (Viles et al. 1999). PrP^C is a membrane-anchored protein that follows the secretory pathway toward the plasma membrane, where it can interact with cell adhesion and signaling proteins (Biasini et al. 2012; Aguzzi and Lakkaraju 2016; Kuffer et al. 2016). The GPI anchor is a PTM that is attached to the C-terminus of the protein in the ER, and which mediates a preferential localization of the protein to cholesterol-rich, detergent-resistant lipid rafts within the plasma membrane (Brown and Rose 1992; McConville and Ferguson 1993). PrP^C is constantly internalized and can be endocytosed by clathrin-, lipid raft-, caveolin-, and metal-dependent pathways (Taylor et al. 2005; Taylor and Hooper 2006; Peters et al. 2003; Prado et al. 2004; Vorberg 2019; Aguzzi et al. 2008). After internalization, PrP^C is transported to early endosomes. Early endosomes either recycle PrP^C back to the plasma membrane or mature to MVBs, from where PrP^C can either be degraded in lysosomes or excreted on exosomes (Borchelt et al. 1990; Campana et al. 2005; MacDermott et al. 1986; Mays and Soto 2016). The membrane of exosomes is enriched in lipid rafts, where GPI-anchored proteins such as PrP^C are abundant (Ikonen 2001; Gassart et al. 2003; Vella et al. 2008).

In neurons, PrP^C has been suggested to localize to the pre- and postsynaptic compartments (Herms et al. 1999; Moya et al. 2000). While the mechanisms of prion pathogenesis, as well as its replication and structural properties, are increasingly well-understood, there is ambiguous evidence regarding its physiological role in the

nervous system. Data generated by using PrP^C knock-out (KO) mice revealed a variety of conflicting observations on the behavioral level with respect to learning and memory (Curtis et al. 2003; Criado et al. 2005; Maglio et al. 2006; Caiati et al. 2013; Kishimoto et al. 2020; Matamoros-Angles et al. 2022). At the level of synaptic function, different studies similarly either reported enhanced or reduced LTP in PrP^C KO mice, whereas most observed an impairment in GABAergic transmission (Collinge et al. 1994; Rangel et al. 2009). These discrepancies in part might be due to genetic artifacts that were recently reported for different PrP^C KO models (Castle and Gill 2017). However, in prion diseases, synapses undergo progressive degeneration, which might indicate a physiological involvement of PrP^C in maintaining synaptic structure and regulating synaptic plasticity (Šišková et al. 2013). In general, PrP^C has also been suggested to mediate neuroprotective functions in neurons, such as against oxidative stress or the protection against kainate-induced excitotoxicity (Brown et al. 1999; White et al. 1999; Carulla et al. 2015). In contrast to this view of neuroprotective roles for PrP^C, there is evidence that PrP^C might represent an important player in sensing extracellular toxic species, and linking them to postsynaptic signaling pathways that are detrimental to synaptic function and cell viability (Roucou et al. 2005; Zhang et al. 2019). For instance, these synaptotoxic effects have been observed following the high-affinity binding of Aβo to cell surface PrP^C (Lauren et al. 2009). Aβo are one of the most noticeable aggregates that are found in the brains of AD patients and they are considered to be toxic to neurons (Grundke-Iqbal et al. 1986; Lambert et al. 1998; Shrestha et al. 2006; Snyder et al. 2005; Shankar et al. 2007). On the molecular level Aβo binding to PrP^C leads to PrP^C association with metabotropic glutamate receptor 5 (mGluR5), thereby inducing a signal cascade that activates the fyn kinase. Fyn kinase can phosphorylate the NR2B subunits of NMDA receptors, thereby destabilizing dendritic spine structure and causing suppression of LTP (Um et al. 2013; Lauren et al. 2009; Brody and Strittmatter 2018). The other most noticeable type of aggregates found in AD brains are intracellular neurofibrillary tangles consisting of hyperphosphorylated tau protein (Grundke-Iqbal et al. 1986). The fyn kinase also phosphorylates tau, connecting the two main characteristics of AD (Lee et al. 2004). It was also recently shown that extracellular soluble forms of tau can disrupt LTP and that this impairment is mediated by PrP^C (Ondrejcak et al. 2018; Ondrejcak et al. 2019). α-Synuclein aggregates in Parkinson's disease were also observed to bind to PrP^C and induce toxic signaling cascades (Ferreira et al. 2017). However, these findings are disputed (La Vitola et al.

2019). In prion disease, PrP^{Sc} binding to PrP^{C} similarly induces a stepwise synaptotoxic signaling cascade. Here, PrP^{Sc} binding triggers the activation of NMDA receptors, Ca^{2+} influx, stimulation of the mitogen-activated protein kinase pathway, and several downstream kinases, which leads to a collapse of the actin cytoskeleton within dendritic spines (Fang et al. 2018). These findings hint at a critical role of PrP^{C} in synaptotoxic signaling in neurodegenerative diseases.

However, besides the good knowledge of prion pathogenesis, its replication, PrP^{C} structural properties, and the increasing evidence of both neuroprotective and synaptotoxic roles of PrP^{C}, there are conflicting data at the behavioral and electrophysiological level concerning its natural physiological function. Unfortunately, PrP^{C} molecular function at the cellular level and especially in neurons under physiological conditions is far from being understood.

1.8 Aim of this study

PrP^{C} plays a role in multiple neurodegenerative diseases such as TSE, AD, and Parkinson's disease (Prusiner 1982; Um et al. 2012; Ferreira et al. 2017). While its folding and conversion in prion diseases have been extensively investigated, PrP^{C} function in the healthy brain remains elusive (Zhu and Aguzzi 2021). Mice not expressing PrP^{C} showed deficiencies in spatial learning and memory (Criado et al. 2005). Multiple functions have been attributed to PrP^{C}, including roles for neuroprotection, cell adhesion, metal ion homeostasis, and transduction of toxic signals from misfolded proteins such as PrP^{Sc}, Aβo, and α-synuclein (Kanaani et al. 2005; Linden et al. 2008; Bounhar et al. 2001; Roucou et al. 2005; Vassallo and Herms 2003; Brown et al. 1997; Laurén et al. 2009; Westergard et al. 2007; Um et al. 2012; Ferreira et al. 2017). Electrophysiological and behavioral data suggest a possible role for PrP^{C} in synaptic plasticity, but the molecular role of PrP^{C} at the synapse still needs to be further illuminated (Collinge et al. 1994; Curtis et al. 2003; Criado et al. 2005; Maglio et al. 2006; Rangel et al. 2009; Caiati et al. 2013; Kishimoto et al. 2020; Matamoros-Angles et al. 2022). The objective was to elucidate the role of PrP^{C} at the synapse, in neuronal activity processes, and the effects they have on endolysosomal PrP^{C} targeting.

First, PrP^{C} localization at different types of synapses was explored. To this end, primary hippocampal neurons were immunochemically stained for synaptic markers and PrP^{C}. To investigate the effect of synaptic plasticity on PrP^{C}, published chemical LTD (cLTD) and LTP (cLTP) protocols were used in dissociated hippocampal neurons.

Localization at the synapse and in endolysosomal compartments was probed for by immunocytochemistry, while transport parameters were examined using YFP-PrP^C expression and time-lapse microscopy. Since interaction partners can help to elucidate the function of proteins, immunoprecipitations were used to find new synaptic interaction partners of PrP^C. Two neuronal cell adhesion molecules of either excitatory or inhibitory synapses as well as an adaptor protein were identified to be novel interaction partners of PrP^C. The cotransport of these interaction partners was investigated by neuronal live imaging. To investigate whether PrP^C impacts the endolysosomal targeting of one novel interaction partner, its subcellular localization was examined by immunocytochemistry in neurons.

The results of this thesis should lead to a better understanding of PrP^C function at the synapse. Since PrP^C has a functional role in multiple untreatable neurodegenerative diseases, the findings of this thesis could help to better understand these diseases and therefore aid in the development of potential treatments.

2. Materials & Methods

2.1 Chemical reagents

Table 1: chemical reagents

Reagent	Cat. No.	Manufacturer
Acrylamide/Bis-acrylamide 40%	A2917	Sigma Aldrich, Germany
Ammonium persulfate (APS)	9592.1	Carl Roth GmbH and Co. KG, Germany
Ampicillin sodium salt (Amp)	K029.1	Carl Roth GmbH and Co. KG, Germany
Bicuculline (Bic)	0109	Tocris Bioscience, UK
BlueStar prestained protein marker	NWP04	NIPPON Genetics EUROPE GmbH, Germany
Bovine serum albumin (BSA)	A7030	Sigma Aldrich, Germany
BSA IgG-free	3737.2	Carl Roth GmbH and Co. KG, Germany
Calcium chloride ($CaCl_2$)	C4901	Carl Roth GmbH and Co. KG, Germany
Cyanquixaline (CNQX)	C127	Sigma Aldrich, Germany
Dimethyl sulfoxide (DMSO)	D2650	Sigma Aldrich, Germany
Disodium hydrogen phosphate ($Na_2HPO_4 \cdot 2H_2O$)	4984.1	Carl Roth GmbH and Co. KG, Germany
Dithiothreitol (DTT)	6908.2	Carl Roth GmbH and Co. KG, Germany
Fetal calf serum (FCS)	10500064	Thermo Fisher Scientific, MA, USA
Forskolin	1099	Bio-Tech, UK
Ethylen glycol bis(2-aminoethyether)-N N N'N'-tetraacetic acid (EGTA)	3054.2	Carl Roth GmbH and Co. KG, Germany
Ethanol	9065.4	Carl Roth GmbH and Co. KG, Germany
4-(2-hydroxyethyl)-1-piperazineethanesulfonic acid (HEPES)	9105.4	Carl Roth GmbH and Co. KG, Germany
Sodium dihydrogen phosphate (NaH_2PO_4)	A0324246 149	Merck Millipore, MA, USA
D-Glucose	6780.2	Carl Roth GmbH and Co. KG, Germany
Glycine	3908.3	Carl Roth GmbH and Co. KG, Germany

Glycerol	3783.1	Carl Roth GmbH and Co. KG, Germany
GW4869	D1692	Sigma Aldrich, Germany
Hank's balanced salt solution (HBSS)	14170088	Thermo Fisher Scientific, MA, USA
Hydrochloric acid (HCl)	4625.1	Carl Roth GmbH and Co. KG, Germany
Immobilon Wester HRP substrate	WBKLS0500	Merck Millipore, MA, USA
Immobilon-P membrane PVDF 0.45 µm	IPVH00010	Merck Millipore, MA, USA
Kanamycin A	T832.3	Carl Roth GmbH and Co. KG, Germany
LB-Agar	22700025	Thermo Fisher Scientific, MA, USA
LB broth base	12780052	Thermo Fisher Scientific, MA, USA
Lipofectamine 2000	11668019	Thermo Fisher Scientific, MA, USA
Magnesium chloride ($MgCl_2$)	KK36.1	Carl Roth GmbH and Co. KG, Germany
Magnesium sulfite ($MgSO_4$)	0261.1	Carl Roth GmbH and Co. KG, Germany
(RS)-α-methyl-4-carboxyphenylglycine ((RS)-MCPG)	0336	Bio-Tech, UK
Methanol	P717.1	Carl Roth GmbH and Co. KG, Germany
Milk powder	T145.3	Carl Roth GmbH and Co. KG, Germany
Potassium dihydrogen phosphate (KH_2PO_4)	3904.2	Carl Roth GmbH and Co. KG, Germany
N-methyl-D-aspartate (NMDA)	M3262	Sigma Aldrich, Germany
Optimem	11058021	Thermo Fisher Scientific, MA, USA
Paraformaldehyde (PFA)	0335.3	Carl Roth GmbH and Co. KG, Germany
Phenylmethylsulfonyl fluoride (PMSF)	6367.1	Carl Roth GmbH and Co. KG, Germany
Poly-L-lysine	P7887	Sigma Aldrich, Germany
Potassium chloride (KCl)	HN02.3	Carl Roth GmbH and Co. KG, Germany
Potassium hydroxide (KOH)	6751.1	Carl Roth GmbH and Co. KG, Germany

Isopropanol	6752.2	Carl Roth GmbH and Co. KG, Germany
Protease inhibitor	4693116001	Sigma Aldrich, Germany
Rolipram	0905	Bio-Tech
Rabbit immunoglobulin (IgG)	02-6102	Thermo Fisher Scientific, MA, USA
Sodium chloride (NaCl)	P029.3	Carl Roth GmbH and Co. KG, Germany
Sodium dodecyl sulfate (SDS)	L4509	Sigma Aldrich, Germany
Sodium hydroxide (NaOH)	6771.3	Carl Roth GmbH and Co. KG, Germany
Sucrose	4661.1	Carl Roth GmbH and Co. KG, Germany
Tetrodotoxin citrate (TTX)	120055	Abcam, UK
Tryptone	T7293	Sigma Aldrich, Germany
Tetramethylethylenediamine (TEMED)	T9821	Sigma Aldrich, Germany
Tris(hydroxymethyl)aminomethane (tris)	5429.2	Carl Roth GmbH and Co. KG, Germany
Triton X100	3051.2	Carl Roth GmbH and Co. KG, Germany
Tween 20	9127.2	Carl Roth GmbH and Co. KG, Germany
Yeast extract	2363.2	Carl Roth GmbH and Co. KG, Germany

2.2 Cell culture

Table 2: Reagents used in cell culture

Reagent	Cat. no	Manufacturer
Dulbecco's Modified Eagle *Medium (DMEM)* GlutaMAX	61965026	Thermo Fisher Scientific, MA, USA
50 U/ml penicillin and 50 μg/ml streptomycin	15140122	Thermo Fisher Scientific, MA, USA
PNGM-A bulletkit for P0 mice or rats	CC-4461	Lonza Bioscience, NC, USA
Trypsin (0.05%)	14025050	Thermo Fisher Scientific, MA, USA

2.3 Antibodies

Table 3: Primary antibodies

Target	Species	Manufacturer	Cat. No.	Dilution
Gephyrin	mouse	Synaptic systems, Germany	147111	1:300 (ICC)
GRIP1	mouse	BD Biosciences, NJ, USA	611319	1:2000 (WB)
GRIP1	rabbit	Upstate Biotechnology, NY,USA	06-986	5 µg (IP)
Lamp1	rat	BD Biosciences, NJ, USA	553792	1:100 (ICC)
N-Cadherin	mouse	BD Biosciences, NJ, USA	61921	1:500 (ICC) 1:3000 (WB)
N-Cadherin	rabbit	Proteintech, IL, USA	22018-1-AP	1:100 (ICC) 5 µg (IP)
Neuroligin 2	rabbit	Synaptic systems, Germany	129 203	1:200 (ICC) 2 µg (IP)
Prion protein	mouse	Cayman	189775	1:100 (ICC)
Prion protein	rabbit	Proteintech, IL, USA	12555-1-AP	1:100 (ICC) 2 µg (IP)
Prion protein	mouse	(Polymenidou et al. 2008)	POM2	1:100 (ICC) 1:1000 (WB)
PSD95	mouse	Thermo Fisher Scientific, MA, USA	51-6900	1:100 (ICC)
synaptophysin	guinea pig	Synaptic systems, Germany	101004	1:2000 (ICC) 1:1000 (WB)
TSG101	mouse	Genetex Inc., CA, USA	GTX70255	1:250 (ICC) 1:1000 (WB)
VGAT	guinea pig	Synaptic systems, Germany	131 004	1:500 (ICC)

Table 4: secondary antibodies

Target	company	Cat. No.	dilution
α-mouse-HRP-conjugated	Jackson ImmunoResearch, UK	715-036-151	1:10,000 (WB)
α-rabbit-HRP-conjugated	Jackson ImmunoResearch, UK	711-036-152	1:10,000 (WB)
α-guinea pig-HRP-conjugated	Jackson ImmunoResearch, UK	706-036-148	1:10,000 (WB)
α-guinea pig-Cy3	Jackson ImmunoResearch, UK	706-165-148	1:500 (ICC)
α-mouse-Cy3	Jackson ImmunoResearch, UK	715-165-150	1:500 (ICC)
α-mouse-405	Abcam, UK	ab175658	1:500 (ICC)
α-rabbit-Cy5	Jackson ImmunoResearch, UK	711-175-152	1:500 (ICC)
α-rat-488	Jackson ImmunoResearch, UK	712-546-153	1:500 (ICC)
α-rat-Cy3	Jackson ImmunoResearch, UK	712-166-150	1:500 (ICC)
Acti-stain 488 phalloidin	Cytoskeleton Inc., CO, USA	PHDG1-A	1:400 (ICC)

2.4 Commercial kits

Table 5: Kits used

Name	Purpose	Cat. No.	Manufacturer
BCA Pierce	Measuring protein concentration	23227	Thermo Fisher Scientific, MA, USA
Cytotox assay	Measuring cell death	J2380	Promega Corporation, WI, USA
NucleoBond	Isolating DNA from Bacteria	740420.50	Macherey-Nagel, Germany

2.5 Plasmids

Table 6: Plasmids

Plasmid	Source
ECFP-htau	Gift from Mandelkow lab (Goldsbury et al. 2006)
ECFP	Takara Bio, Japan
mRFP-GRIP1	(Heisler et al. 2014)
mRFP-N-cadherin	(Heisler et al. 2014)
mRFP	Takara Bio, Japan
YFP-PrP^C	Gift from Goldstein lab (Encalada et al. 2011)
YFP	Takara Bio, Japan

2.6 Instruments

Bacteria incubator: WB 22 K Mytron, Germany

Bacteria incubator: W 560 K, Mytron, Germany

Centrifuge: 5430R, Eppendorf, Germany

Centrifuge: 5804R, Eppendorf, Germany

Centrifuge: Beckman Coulter Avanti J-26 XP, Beckman Coulter, CA, USA

Cell culture hood: SteriGRAD Class II TypA/B3 (Baker Company, FL, USA); SAFE 2020 (Thermo Fisher Scientific, MA, USA)

Cell incubator: HERAcell 150/150i, Thermo Fisher Scientific, MA, USA

Chemiluminescence detection system: INTAS Chemo Cam 3.2, INTAS, Germany

Confocal microscope: Olympus Fluoview FV1000 confocal laser scanning microscope (Olympus, Germany).

Epifluorescence microscope: Zeiss, Germany

Homogenization potter: Sartorius, Germany

Microscope: Stemi 2000, Zeiss, Germany

Nanosight LM14C: (Malvern Instruments, UK) with a 532 nm laser and a CMOS camera (Hamamatsu Photonics, Japan)

Nanoquant Infinite M200pro: TECAN, Switzerland

Platform shaker: innova 2300, Eppendorf, Germany

pH meter: SevenEasy, Mettler-Toledo, Germany

Power supplies: Power Pac 200 (BioRad, Germany)

Semidry blotter: Novex Semidry, Thermo Fisher Scientific, MA, USA

Spinning disk microscopy: Nikon ECLIPSE T*i* with spinning disk confocal technology equipped with two CCD EM cameras, Visitron, Germany

Thermomixer: Eppendorf, Germany

Ultracentrifuge: Optima L-100 XP Ultracentrifuge with Sw40Ti rotor (Beckman Coulter, CA, USA)

2.7 Buffers & solutions

The water used to prepare the solutions was purified by a Milli-Q-System (Millipore, Germany) to the degree "*aqua bidest*" purity. The pH was adjusted using NaOH, KOH, or HCl. For sterilization, the solutions were autoclaved at 121 °C at 2.1 bar for 20 min or sterile filtered through a 0.22 µm pore size filter (Millipore, Germany).

Artificial cerebrospinal fluid without Magnesium (ACSF-Mg^{2+}) (pH 7.3) (Induction of chemical LTP (cLTP) or LTD (cLTD))
120 mM NaCl, 26 mM $NaHCO_4$, 1 mM NaH_2PO_4, 2.5 mM KCl, 2.5 mM $CaCl_2$, and 10 mM D-glucose saturated with 95%O_2-5%CO_2

ACSF +Mg^{2+} (pH 7.3) (Induction of cLTP or cLTD)

120 mM NaCl, 26 mM $NaHCO_4$, 1 mM NaH_2PO_4, 2.5 mM KCl, 1.3 mM magnesium sulfite $MgSO_4$, 2.5 mM $CaCl_2$, and 10 mM D-glucose saturated with 95%O_2-5%CO_2

Blotting buffer (pH 8.3) (western blot)

39 mM glycine, 48 mM tris, 0.037 % (w/v) SDS, 20% (v/v) methanol

HBS (pH 7.05) (transfection)

280 mM NaCl,10 mM KCl, 1,5 mM $Na_2HPO_4 \cdot 2H_2O$, 12 mM glucose, 50 mM HEPES

HEPES buffer for time-lapse (pH 7.4) (neuronal transfection)

135 mM NaCl, 5 mM KCl, 2 mM $MgCl_2$, 10 mM HEPES, 15 mM D-glucose, in water

IP buffer (pH 7.5) (immunoprecipitation)

50 mM tris, 5 mM $MgCl_2$, 150 mM NaCl

IMAC buffer (pH 7.2) (immunoprecipitation)

20 mM HEPES, 100 mM KCl, 5 mM EGTA, 5 mM $MgCl_2$

LB medium (pH 7.5) (plasmid re-amplification)

0.1% (w/v) tryptone, 0.05% (w/v) yeast extract, 0.05% (w/v) NaCl

LB agar (plasmid re-amplification)

1.5% (w/v) LB agar (autoclaved), 100 mg/L ampicillin or 50 mg/L kanamycin

4 x loading buffer with urea (pH 8.8) (SDS-PAGE)

250 mM tris, 400 mM DTT, 8% (w/v) SDS, 20% (v/v) glycerol, 8 M urea, bromophenol blue

N2a medium (cell culture)

Dulbecco's Modified Eagle *Medium* GlutaMAX, 10% FCS, 1% penicillin/streptomycin

PFA with sucrose (immunocytochemistry)

4% (w/v) PFA, 4% (w/v) sucrose in PBS

Phosphate buffered saline (PBS) (immunocytochemistry, cell culture, immunoprecipitation)
1.37 M NaCl, 27 mM KCl, 100 mM Na_2HPO_4, 180 mM KH_2PO_4

SDS PAGE running buffer (pH 8.3) (SDS PAGE)

50 mM tris, 384 mM glycine, 0.2% (w/v) SDS in water

SOC medium (plasmid re-amplification)

0.5% Yeast Extract, 2% Tryptone, 10 mM NaCl, 10 mM $MgCl_2$, 10 mM $MgSO_4$, 20 mM Glucose, 2.5 mM KCl

Stripping buffer (pH 2) (western blot)

25 mM glycine, 1% (w/v) SDS, HCl to adjust pH, in water

Tris-buffered saline with tween (TBST) (pH 7.2) (western blot)

1 mM tris, 1.5 M NaCl, 0.5% (v/v) Tween 20

2.8 Programs

Table 7: Programs used in the thesis

Name	Manufacturer	Purpose
MetaMorph® imaging series 7.7	Molecular Devices (CA, USA)	Analyzing images
Fiji	ImageJ (NIH, MD, USA)	Analyzing videos
Visiview	Visitron (Germany)	Live-cell image acquisition
Sigmaplot	Systat Software Inc. (Germany)	Statistical analysis

2.9 Methods

2.9.1 Culture of dissociated hippocampal neurons

Prior to the preparation, 12 mm sterile glass coverslips (P231.1, Carl Roth GmbH and Co. KG, Germany, Germany) or glass-bottom dishes (D35-14-1.5-N, CA, USA) were

coated with 50 mg/L poly-L-lysine in PBS overnight at 37 °C. The next day, the dishes were washed 3 times with sterile water and primary hippocampal medium (PNGM-A bulletkit for P0 mice or rats, Lonza Bioscience, NC, USA) was added. Primary hippocampal neurons were prepared from mouse embryos on embryonic day 15 (E15.5). The embryos were dissected, and the hippocampi were isolated in cold HBSS under the microscope (Stemi 2000, Zeiss, Germany). The hippocampi were collected and incubated with 0.05% trypsin (Thermo Fisher Scientific, MA, USA) for 5 min at 37 °C. The trypsin was removed, and the cells were washed with HEPES buffer and resuspended in HBSS and dissociated using a fire-polished glass Pasteur pipette. The cell density was calculated using a Neubauer counting chamber (Paul Marienfeld GmbH & Co. KG, Germany), and the cells were plated according to the requirements of the experiment. The hippocampal neurons were stored at 37 °C with 5% CO_2 in a cell incubator (HERAcell 150, Thermo Fisher Scientific, MA, USA) for up to 21 days.

2.9.2 Culture of Neuro-2a cells

Neuro-2a (N2a) cells were maintained in DMEM medium with 10% FCS and 1% penicillin-streptomycin (50 U/mL) at 37 °C with 5% CO_2. To maintain the cells, they were split 2 times a week. To split the N2a cells, they were washed once with PBS and incubated 5 min at 37 °C with 0.05% trypsin. After 5 min the medium was added, the cells resuspended and transferred to new plates with fresh medium in appropriate dilution.

2.9.3 Brain lysates

Wild type (WT) mice were sacrificed according to the German Animal Welfare Act (TierSchG) and the brains were isolated and transferred to ice-cold IMAC buffer (20 mM HEPES, 100 mM KCl, 5 mM EGTA, 5 mM $MgCl_2$, pH 7.2) containing protease inhibitor, 5 mM PMSF, and 1 mM DTT. The brains were homogenized in a homogenization potter (Sartorius, Germany) at 900 rpm for 9 strokes, followed by 30 min on ice with 1% TritonX-100. The lysate was centrifuged (5430R, Eppendorf, Germany) at 1,000 xg for 10 min at 4°C. The supernatant (S1) was transferred into a new tube and used straight away or frozen in liquid nitrogen and stored at -80 °C.

2.9.4 N2a lysates

To lyse N2a cells, they were first washed with PBS. Then ice-cold IMAC buffer (20 mM HEPES, 100 mM KCl, 5 mM EGTA, 5 mM $MgCl_2$, pH 7.2) containing 1% Triton X-100,

protease inhibitor, 5 mM PMSF, and 1 mM DTT was added, and the cells were scraped off the plate and transferred into a tube. The tube was incubated on ice for 30 min, then centrifuged (5430R, Eppendorf, Germany) at 1,000 xg for 10 min at 4 °C. The supernatant was transferred to a fresh tube and the pellet discarded. The lysate was either used instantly or stored at -80 °C.

2.9.5 Sodium dodecyl sulfate polyacrylamide gel electrophoresis

To separate proteins by size and later analyze them by western blot a sodium dodecyl sulfate (SDS) polyacrylamide gel electrophoresis (PAGE) was used. The gels to separate the proteins were casted between two glass plates according to manufacturer's guidelines (Biorad, Germany), first the 12% separation and then the 4% stacking gel, as presented in table 8.

Table 8: Polyacrylamide gels for SDS PAGE

Components	**4% stacking gel [mL]**	**12% separation gel [mL]**
Water	5.7	17.2
Acrylamide/Bis-acrylamide	1.0	12
Tris buffer (pH 8.8)	--	10
Tris buffer (pH 6.8)	1.0	--
10% SDS (w/v)	0.08	0.4
APS	0.08	0.4
TEMED	0.008	0.016

A comb was inserted into the stacking gel to provide pockets to load the samples. After polymerization, the gels were placed in an electrophoresis chamber (Mini-Protean III Systems, Biorad, Germany) SDS PAGE running buffer (50 mM tris, 384 mM glycine, 0.2% (w/v) SDS in water) was added. The samples were mixed with 4x loading buffer with urea (250 mM tris, 400 mM DTT, 8% (w/v) SDS, 20% (v/v) glycerol, 8 M urea, bromophenol blue) and heated to 70 °C for 10 min. Then the samples were loaded together with a protein marker (BlueStar prestained protein marker, NIPPON Genetics EUROPE GmbH, Germany) and run with 90 V for 10 min and then at 120 V until the bromophenol blue front had reached the bottom of the glass plate.

2.9.6 Western blot (WB)

To analyze the proteins that were separated by size in the SDS-PAGE, a semi-dry western blot was used. The PVDF membrane (Millipore, Germany), previously activated in methanol and washed with water, was saturated with the blotting buffer (39 mM glycine, 48 mM tris, 0.037 % (w/v) SDS, 20% (v/v) methanol). Membrane and gel from the SDS-PAGE were flanked by filter papers also saturated in blotting buffer. A current of 80 mA per membrane was applied for 2 h to transfer the proteins onto the PVDF membrane. The proteins were subsequently analyzed using immunoblotting.
To avoid unspecific binding of the antibodies, the membrane was blocked in 5% milk or 3% IgG-free BSA in TBST (1 mM tris, 1.5 M NaCl, 0.5% (v/v) Tween 20, pH 7.2) at RT for 1 h or overnight at 4 °C, following incubation with the primary antibody (see table 3) overnight in 5% milk or 3% IgG-free BSA in TBST. Afterwards, the membrane was washed 4 times with TBST, incubated 1 h at RT with the appropriate HRP coupled secondary antibody (see table 4), and washed again 4 times. To visualize the specific protein bands the membrane was incubated with immobilon Wester HRP substrate (Merck, Millipore, Germany) and recorded by a chemiluminescence detection system (INTAS Chemo Cam 3.2, INTAS, Germany).

2.9.7 Immunoprecipitation

Immunoprecipitation (IP) was used to identify new interaction partners. Brains from adult mice or N2a cells were collected and lysed as described. Magnetic Dynabeads Protein A (Thermo Fisher Scientific, MA, USA) were washed three times with PBS and then coupled to antibodies (see table 3) at 4 °C for 2 h. As a control, the beads were coupled with IgG from the species that the antibodies were produced in. The beads were washed three times with IMAC buffer (20 mM HEPES, 100 mM KCl, 5 mM EGTA, 5 mM $MgCl_2$, pH 7.2) and the lysate was added overnight at 4 °C. The beads were washed extensively 6 times with IP buffer (50 mM tris, 5 mM $MgCl_2$, 150 mM NaCl, pH 7.5) containing 1% Triton X-100, followed by one wash with sterile water. To remove all supernatant, the beads were centrifuged at full speed in an Eppendorf centrifuge (5430R, Eppendorf, Germany) for 30 s. After removing all supernatant, the beads were resuspended in 48 µL sterile water and 12 µL 4x loading buffer with urea (250 mM tris, 400 mM DTT, 8% (w/v) SDS, 20% (v/v) glycerol, 8 M urea, bromophenol blue) and subsequently heated to 70 °C for 10 min to elute the proteins from the beads. The samples were analyzed by SDS-PAGE and western blotting.

2.9.8 Immunocytochemistry (ICC)

Primary hippocampal neurons were grown on glass coverslips and used on varying days of *in vitro* (DIV) to investigate protein localization and colocalization. The cells were either stimulated first with chemical induction protocols as described later or fixed straight away with 4% PFA with 4% sucrose in PBS (1.37 M NaCl, 27 mM KCl, 100 mM Na_2HPO_4, 180 mM KH_2PO_4) for 8 min at room temperature (RT). Subsequently, the cells were washed three times with PBS and permeabilized for 3 min using 0.25% Triton-X100 in PBS. After washing the cells again with PBS, they were blocked with 1% BSA in PBS for 1 h at RT to avoid unspecific binding of primary antibodies. The primary antibodies (see table 3) were added in 1% BSA in PBS and the cells incubated overnight at 4 °C. Afterwards, the cells were washed three times with PBS and incubated with the appropriate secondary antibody (see table 4) in 1% BSA in PBS for 1 h at RT in the dark. Then the cells were washed three times in PBS and once with filtered water to get rid of the salts, the coverslips were mounted onto glass slides using Aqua Poly Mount (Polysciences, PA, USA). The cells were imaged using the Olympus Fluoview FV1000 confocal laser scanning microscope (Olympus, Germany). Image analysis of immunofluorescent images was performed using the MetaMorph® imaging series 7.7 software with “Integrated Morphometry Analysis” and “Measure Colocalization” (Molecular Devices, CA, USA).

2.9.8.1 Surface staining

To visualize PrP^C at the plasma membrane surface staining in DIV dissociated hippocampal neurons was performed with the help of Ines Wieser. The neurons were first stimulated, as described below, and then incubated under non-permeabilizing conditions with the POM2 antibody against PrP^C in HEPES buffer for time-lapse (135 mM NaCl, 5 mM KCl, 2 mM $MgCl_2$, 10 mM HEPES, 15 mM D-glucose, in water) for 2 h at 4 °C. After washing, the neurons were fixed and permeabilized as described above.

2.9.9 Chemical induction of cLTP or cLTD

Primary hippocampal neurons were grown on glass coverslips and or in glass bottom dishes and at DIV14 the neurons were stimulated to induce cLTP or cLTD. To stimulated cLTP, a published protocol by Otmakhov *et al*. was used.

The cells were incubated with ACSF-Mg (120 mM NaCl, 26 mM $NaHCO_4$, 1 mM NaH_2PO_4, 2.5 mM KCl, 1.3 mM $MgSO_4$, 2.5 mM $CaCl_2$, and 10 mM D-glucose saturated with 95%O_2-5%CO_2) containing 50 µM forskolin and 0.1 µM rolipram for 10 min at 37 °C and 5% CO_2, then the cells were recovered in conditioned medium for 20 min at 37°C. To induce cLTD, the protocol published by Bhattacharyya in 2009 was used (Bhattacharyya et al. 2009). The cells were incubated with conditioned medium containing 1 µM TTX and 10 µM CNQX, after 5min, 100 µM NMDA were added for another 5 min, after which the medium was removed, and the cells were recovered for 20 min in conditioned medium with 1 µM TTX and 10 µM CNQX. Subsequently, the cells were analyzed by time-lapse microscopy or ICC.

2.9.10 Exosome isolation with stimulation

For exosome isolation from stimulated neurons, the method adapted from Heisler et al. 2018 was used.

DIV12 hippocampal neurons were incubated with either 1 µM TTX, 50 µM Bic or water as control. After 48 h of stimulation, the medium of the cells was collected, samples were taken for subsequent cytotoxicity assays (Promega Corporation, WI, USA). To remove cell debris, the supernatant was first centrifuged at 1,000 xg for 10 min, then at 7,500 xg for 15 min (Beckman Coulter Avanti J-26 XP, Beckman Coulter, CA, USA), while cooling at 4 °C, and passed through a 0.22 µm filter. Finally, the supernatant was centrifuged at 100,000 xg for 70 min at 4 °C in an Optima L-100 XP Ultracentrifuge using a Sw40Ti rotor (Beckman Coulter, CA, USA). The supernatant was removed completely and the pellet containing the exosomes was resuspended in conditioned medium from dissociated hippocampal neurons at DIV14, the same preparation as the neurons from which the exosomes were isolated. The exosomes were quantified and characterized using the Nanosight LM14C (Malvern Instruments, UK) with a 532 nm laser and a CMOS camera (Hamamatsu Photonics, Japan). Five videos were made of 60 s length each, to calculate average exosome size and concentration. The exosomes were directly added to neurons of the same preparation (DIV14) for 6 days.

2.9.11 Plasmid re-amplification

For plasmid amplification, DH5α competent *Escherichia coli* (E. coli) were transformed with different expression vectors, adapted from Inoue *et al.* 1990.

Briefly, 100 ng plasmid DNA were added to 50 µL of DH5α cells and incubated 30 min on ice. After 45 s heat shock at 42 °C, the bacteria were transferred to ice for 2 min,

500 µL SOC medium were added. The bacteria were allowed to grow for 45 min at 37 °C while shaking. After the incubation, 100 µL of bacteria solution were plated onto agar plates, containing the appropriate antibiotic (ampicillin or kanamycin) and bacteria were grown overnight at 37 °C in an incubator (WB 22 K Mytron, Germany).
The next day, a clone was selected and transferred to 100 mL LB medium containing the appropriate antibiotic and grown overnight at 37 °C in an incubator (W 560 K, Mytron, Germany) with a platform shaker (innova 2300, Eppendorf, Germany). To isolate the DNA, the NucleoBond™ Xtra Midi (Macherey-Nagel, Germany) kit was used according to the manufacturers' guidelines. The plasmid was resuspended in water and the DNA concentration was determined by a nanodrop spectrophotometer Nanoquant Infinite M200pro (TECAN, Switzerland). To assess the purity of the DNA the absorbance was measured at 260 and 280 nm and the A260/A280 ratio was calculated. Only DNA with a ratio between 1.8 and 2 was used.

2.9.12 Transfection of neurons

Dissociated hippocampal neurons grown in glass-bottom dishes or on glass coverslips were transfected at DIV10 using calcium phosphate, a method adapted from Kohrman *et al.* 1999 (Köhrmann et al. 1999). Briefly, for one 12 mm dish, 1 - 9 µg plasmid DNA were mixed with 6.25 µL calcium chloride and filled with water to 25 µL, the solution was added dropwise to 25 µL 2x HBS while vortexing and incubated at RT for 20 min. The conditioned medium was removed from the neurons until only 500 µL remained to cover the cells. The conditioned media was stored at 37 °C for further use. The transfection mix was added dropwise to the neurons in 0.5 mL medium and the cells were incubated at 37 °C for 140 min, then washed with warm HEPES for time-lapse-buffer, and the conditioned media was added to the neurons again. They were stored at 37 °C and 5% CO_2 for 24 or 48 h and then analyzed by ICC or by time-lapse microscopy (Visitron, Germany).

2.9.13 Transfection of N2a

The cells were transfected when they were roughly 70% confluent using lipofectamine 2000, according to manufacturers' guidelines. Briefly, for one 6-well well, 1 - 9 µg plasmid DNA were mixed with 25 µL optimem, the solution was added to 25 µL containing 6 µL lipofectamine 2000 and incubated for 20 min at RT. The dish was placed at 37 °C and 5% CO_2 for 24 h and then the cells were checked for transfection

efficiency using an epifluorescence microscope (Zeiss, Germany) and imaged using time-laps microscopy.

2.9.14 Time-lapse video microscopy

Live cell imaging was conducted with a spinning disc confocal (SDC) microscope (Visitron, Germany) at 37 °C and 5% CO_2 with a CCD camera (Hamamatsu, EM-CCD, Digital camera C9100). Videos were acquired at an inverted microscope (Nikon Instruments, Amsterdam, Netherlands) combined with Spinning Disc (Yokogawa, Amersfoort, Netherlands) Live Cell Confocal technology (Visitron Systems Puchheim, Germany) with the Visiview software (Visitron Systems, Germany). Dissociated hippocampal neurons were imaged using the 60x objective, while N2a were recorded with a 100X objective. N2a cells were also imaged by total internal reflection fluorescence (TIRF) microscope. Whenever light encounters the interface of two transparent media with different refractive indices at a critical angle, it will be completely reflected. The phenomenon is called total internal reflection (TIR). An evanescent field occurs. The energy of the evanescent field decreases exponentially with distance to the interface so that only fluorescent molecules close to the interface, like membrane-associated proteins, are excited (Fish 2009). To investigate the velocity of moving particles in N2a cells, the videos taken in SDC setting were analyzed using the TrackMate plug in from Fiji (ImageJ, NIH, MD, USA). The velocities of moving particles in dissociated hippocampal neurons were analyzed by generating kymographs. Kymographs are generated by drawing a line type region of interest (ROI) where particle movement is detected. Kymographs represent dynamic processes as spatial position over time in one still image. The signals visible in the kymograph result from fluorescent particles moving along the ROI. The particles can be stationary, resulting in vertical lines in kymograph or moving causing the lines to have a slope. The slopes of individual particle trajectories were used to calculate the velocity using a macro by Fiji (ImageJ, NIH, MD, USA) to “read velocities from tsp”. Stationary particles were defined as object moving slower than 0.095 µm/s, as previously described (Encalada et al. 2011). The velocities of the moving particles were further divided into overall velocities (v_{net}), segmental velocities without pauses (v_{mean}), and maximum segmental velocities (v_{max}) were determined. The segmental velocities higher than 0.095 µm/s were added together to establish v_{mean}, the velocity when the particle was actively transported.

2.9.15 Statistical analysis

All statistical analysis was performed by SigmaPlot (version 14.0). Normality was tested with Shapiro-Wilk test and equal variance was tested by the Brown-Forsythe test. Normally distributed data with equal variance were analyzed using the Student's t-test or, when more than two conditions were compared, the analysis of variance (ANOVA) was performed. Welch's t-test was performed with normally distributed data with unequal variance. If the data was not normally distributed the Mann-Whitney rank sum test was used for two conditions, while the Kruskal-Wallis one way ANOVA on ranks with Dunn's method for multiple comparisons was used for three or more conditions. The data are represented with their median and the standard error of the mean (SEM). The data is usually presented in a box-and-whiskers plot. The box extends from the 25^{th} to the 75^{th} percentile, while the whiskers are drawn from the smallest to the largest value to represent all data points. In the text, the median value is given with the standard error of the mean. Data where no more than five data points were available were presented in a scatter dot plot, with the whiskers extending to the 95% confidence interval (CI).

3. Results

3.1 PrP^C localizes to the excitatory and inhibitory synapse

It has been shown by electron micrographs and confocal microscopy that PrP^C in principle can localize to the synapse in brain slices (Salès et al. 1998; Herms et al. 1999). Here, the localization of PrP^C to filopodia and different types of synapses, and its plasma membrane distribution were explored for the first time in dissociated hippocampal neurons.

Dendritic spines are defined as F-actin-rich protrusions forming the postsynaptic part of most excitatory synapses (Matus et al. 1982; Halpain et al. 1998). They connect to presynaptic sites where F-actin is also abundant. The presynaptic terminal contains synaptophysin, a synaptic vesicle protein (Wiedenmann and Franke 1985). Here, F-actin hotspots co-labeled with synaptophysin were defined to be excitatory synapses, while F-actin hotspots without synaptophysin were protrusions. First, immunocytochemical surface staining was used to label PrP^C only attached to the plasma membrane. Living DIV14 neurons were incubated with the antibody directed against PrP^C, as described in the methods (chapter 2.9.8.1). Subsequently, the cells were permeabilized and co-labeled for synaptophysin and F-actin. The fluorescent signals were visualized by using confocal laser scanning microscopy. A representative image of the surface staining is shown in figure 3.1A. A high colocalization of PrP^C fluorescent intensity to F-actin, and to synaptophysin fluorescent intensities was observed. Figure 3.1B shows a dendritic section from figure 3.1A at higher magnification. At this magnification, it was apparent that PrP^C intensity is enriched at F-actin hotspots co-labeled for synaptophysin. To assess the intensity of PrP^C at the surface of the synaptic membrane as compared to extrasynaptic sections of the membrane, a line scan analysis was performed. Line scans show the fluorescence intensity values along a linear ROI. An example of a line scan is shown in figure 3.1C. The intensities of the channels were plotted with the distance of the ROI. The PrP^C intensity maximum approximately coincided with the F-actin intensity maximum as well as the synaptophysin intensity, although the curve of synaptophysin intensity was slightly shifted to the left compared to F-actin and PrP^C intensities. Regions, where synaptophysin and F-actin fluorescence intensities were high, were used to generate line scans at synaptic regions. Regions of low intensities for synaptophysin and F-actin were considered to represent extrasynaptic sites.

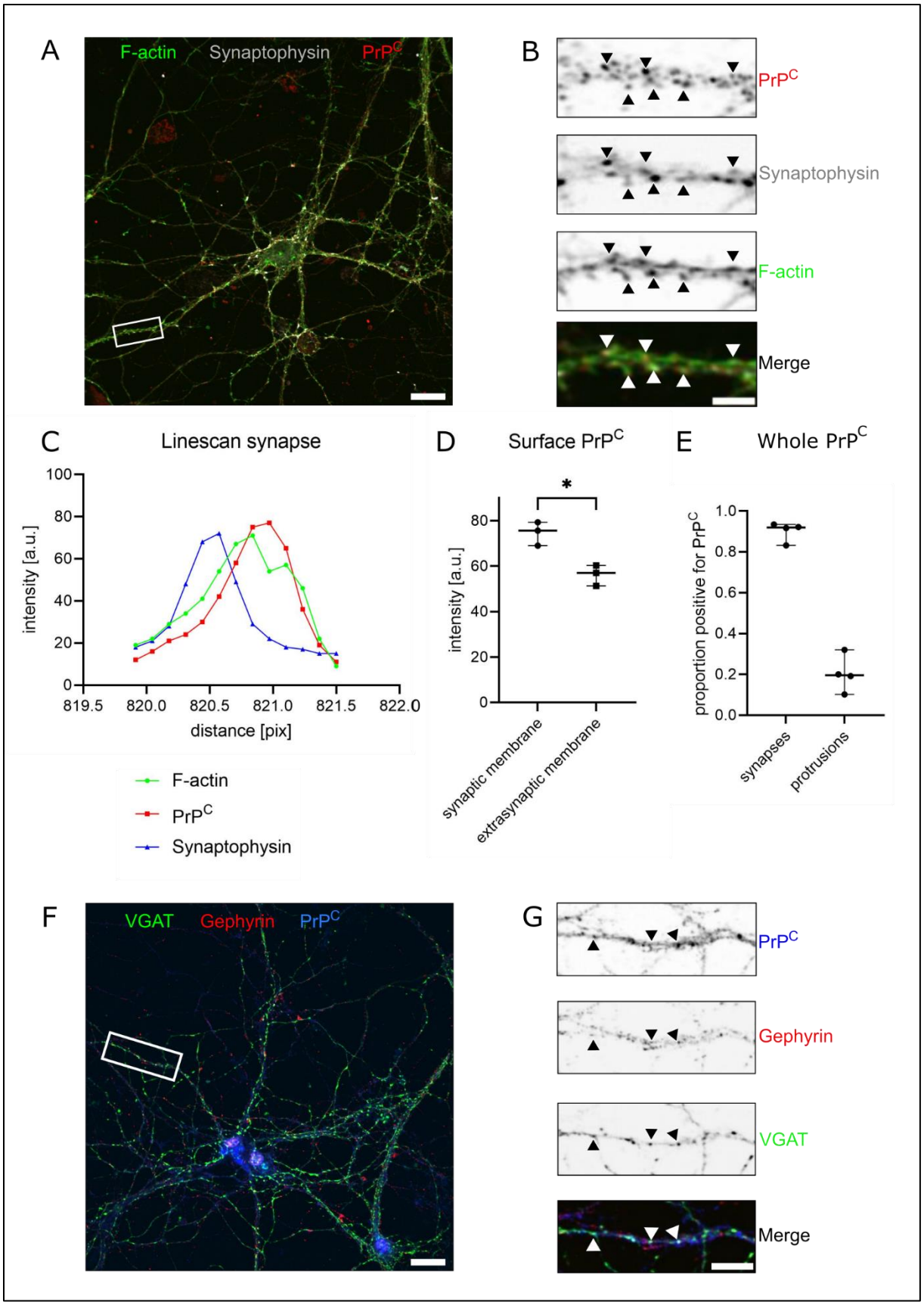

Figure 3.1: PrP^C localizes to excitatory and inhibitory synapses. (**A**) Dissociated hippocampal mouse neurons were stained for surface PrP^C, synaptophysin, and F-actin at DIV14. Colocalization of surface PrP^C with F-actin and synaptophysin is shown. The scale bar represents 20 µm. (**B**) A dendrite section

from (A), as indicated by the white box, is shown at higher magnification. Inverted greyscale images are shown individually for each channel and at the bottom, the merge is shown with a scale bar representing 5 µm. The arrowheads indicate colocalization of synaptophysin, F-actin, and PrP^C at synapses. (**C**) A representative line scan across a synaptic region shows the fluorescence intensity profiles of PrP^C, F-actin, and synaptophysin signals. The fluorescent intensity maxima of PrP^C and F-actin roughly coincide, while the intensity maximum of synaptophysin is slightly shifted. (**D**) Quantitative analysis of PrP^C maximum intensity values obtained from line scan analysis across synaptic and extrasynaptic membrane regions are shown. PrP^C intensities are higher at synaptic (74.67 ± 3.02) compared to extrasynaptic sites (56.22 ± 2.63). The dot plot shows individual data points and the median, the error bars represent the 95% confidence interval (CI). The statistical analysis was performed by heteroscedastic, unpaired, two-tailed t-test (n= 3 independent experiments). (**E**) Quantitative analysis reveals the proportion of synapses (0.920 ± 0.02) or protrusions (0.196 ± 0.04) positive for PrP^C signals. The individual points per experiment were plotted with the median shown by a line and the error bars representing 95% CI (n= 3 independent experiments). (**F**) Immunofluorescence staining of DIV14 mouse dissociated hippocampal neurons for VGAT, gephyrin, and PrP^C. The scale bar represents 20 µm. (**G**) A section of a dendrite from (F), as indicated by the white box, is shown at higher magnification. Inverted greyscale images are shown individually for each channel and at the bottom, the merge is shown with a scale bar representing 5 µm. The arrowheads indicate the colocalization of VGAT, gephyrin, and PrP^C signals at inhibitory synapses.

The maximum intensity values for PrP^C were plotted for extrasynaptic and synaptic regions in figure 3.1D. At synaptic regions, the maximum intensity of PrP^C was increased by about 25% compared to the extrasynaptic membrane. To investigate the distribution of PrP^C within the neurons DIV14 dissociated hippocampal neurons were immunochemically stained for whole PrP^C. Additionally, the neurons were immunochemically stained for F-actin and synaptophysin. Colocalization of F-actin and synaptophysin was defined as a synapse, while F-actin without synaptophysin was defined as a protrusion without synaptic contacts. These images were used to quantify the proportion of synapses or protrusions positive for PrP^C fluorescence. The results are shown in figure 3.1E. While over 90% of synapses were labeled for whole PrP^C, only about 20% of protrusions contained PrP^C fluorescence.

So far, PrP^C has not been described at inhibitory synapses in dissociated hippocampal neurons. However, $GABA_A$ receptor-mediated fast inhibition is weakened in PrP^C KO mice, indicating that PrP^C might play a role at the inhibitory synapse (Collinge et al. 1994). To investigate whether PrP^C localizes to inhibitory synapses, DIV14 dissociated hippocampal neurons were fluorescently labeled with antibodies directed against gephyrin, vesicular GABA transporter (VGAT), and whole PrP^C. Fluorescent signals

were visualized by confocal laser scanning microscopy. Gephyrin is a scaffold protein at inhibitory synapses important for anchoring inhibitory neurotransmitter receptors at the postsynaptic compartment. VGAT is a synaptic vesicle component present at the presynaptic site of inhibitory synapses (Kneussel et al. 1999). Here, the colocalization of VGAT and gephyrin was defined as an inhibitory synapse. A representative image is shown in figure 3.1F. Fluorescence labeled PrP^C co-localized with gephyrin and VGAT. Figure 3.1G shows a magnification of the dendritic portion of the neuron. PrP^C fluorescence can be seen at gephyrin and VGAT labeled spots, indicating that PrP^C is localized at inhibitory synapses.

Together, these results reveal that PrP^C is present at the vast majority of excitatory synaptic sites and enriched at the synaptic membrane. The co-staining of PrP^C with inhibitory synaptic markers showed that PrP^C also is frequently present at inhibitory synapses.

3.2 Synaptic plasticity affects PrP^C dynamics and localization

Synaptic plasticity is the ability of synapses to become stronger or weaker in an activity-dependent manner. It is thought to be an important foundation of learning and memory (Bear et al. 2016). Multiple PrP^C KO mouse models showed impairments in synaptic plasticity. Although the findings are disputed, most studies showed a reduction in excitatory glutamatergic transmission, late afterhyperpolarization, LTP, and impaired hippocampal-dependent spatial learning in mice lacking PrP^C (Maglio et al. 2006; Maglio et al. 2004; Lledo et al. 1996; Carleton et al. 2001; Collinge et al. 1994; Colling et al. 1996; Mallucci et al. 2002; Criado et al. 2005). This indicates that PrP^C might have a role in synaptic plasticity, but its cellular role in synaptic plasticity has barely been investigated.

3.2.1 Localization of PrP^C in synaptic plasticity conditions

Since this work showed that PrP^C is enriched at excitatory synapses and it has been shown that lack of PrP^C does impair synaptic plasticity, the impact of synaptic plasticity on PrP^C localization to the synapse was to be explored (Maglio et al. 2006; Maglio et al. 2004; Lledo et al. 1996; Carleton et al. 2001; Collinge et al. 1994; Colling et al. 1996; Mallucci et al. 2002; Criado et al. 2005).

Enrichment of PrP^C at excitatory synapses was shown in this work by the colocalization of immunochemically labeled F-actin, presynaptic synaptophysin, and postsynaptic postsynaptic density protein-95 (PSD95) (defined as a synapse). PSD95 is a scaffold protein at excitatory synapses, anchoring excitatory neurotransmitter receptors at the postsynaptic compartment (Hunt et al. 1996; Kornau et al. 1995; Chen et al. 2000). To investigate PrP^C localization in synaptic plasticity conditions, DIV14 dissociated hippocampal neurons were stimulated as described or left untreated as control. Established protocols were used to chemically induce synaptic plasticity in dissociated hippocampal neurons (Otmakhov et al. 2004; Bhattacharyya et al. 2009). Forskolin and rolipram were used to induce cLTP by increasing cAMP production (Otmakhov et al. 2004). For cLTD, synaptic transmission was blocked by administrating TTX and NMDA (Bhattacharyya et al. 2009). After the stimulation, the neurons were allowed to recover in the conditioned medium for 20 min, before fixation and immunocytochemical staining for PSD95, synaptophysin, F-actin, and PrP^C. Subsequently, confocal laser scanning microscopy was utilized to detect the respective signals. Representative images of dendrites are shown in figure 3.2A. The arrows show colocalization of PrP^C, synaptophysin, PSD95, and F-actin, at synaptic sites. ROIs were created at points positive for synaptophysin, PSD95, and F-actin signals, defined in this work as synapses. These ROIs were used to measure the fluorescence intensity of labeled PrP^C at synapses. The results are shown in figure 3.2B. No significant changes in PrP^C fluorescence intensity at synapses were observed between the control and cLTP conditions. However, after cLTD induction PrP^C intensity was reduced by over 25% compared to the control condition. Staining for whole PrP^C showed changes in the PrP^C signal in these conditions but did not allow to differentiate between intracellular PrP^C and PrP^C on the spine membrane. Thus, to ascertain whether the changes in intensity were due to changes in PrP^C at the spine surface membrane, immunofluorescent surface staining of PrP^C was performed. First, the cells were treated according to the described protocols above. To immunofluorescently label PrP^C only at the membrane, living DIV14 dissociated hippocampal neurons were incubated with an antibody directed against PrP^C for 2 h at 4°C. Subsequently, the cells were fixed and co-labeled for synaptophysin and F-actin. Representative images of dendrites from these cells at different conditions are shown in figure 3.2C, while the quantitative analysis is shown in figure 3.2D. A significant decrease in plasma membrane PrP^C intensity by approximately 25% was observed at synaptic regions in cLTD compared to control

conditions, while no significant changes in PrP^C intensity were observed after cLTP induction compared to control conditions.

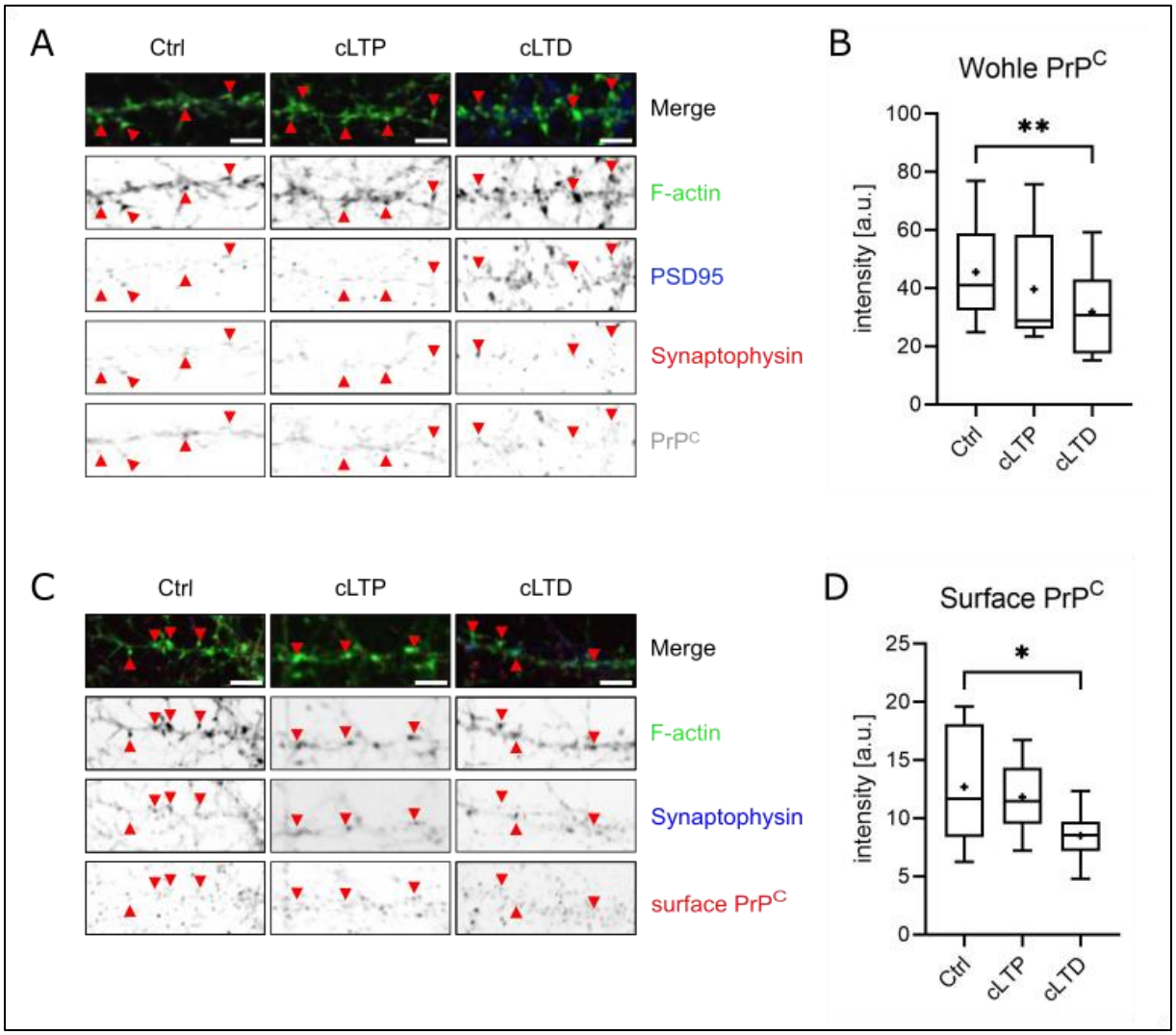

Figure 3.2: PrP^C localization at the synapse under synaptic plasticity conditions. (**A**) Representative images of dendrites from DIV14 dissociated hippocampal mouse neurons in control (ctrl), cLTP, and cLTD conditions. Inverted greyscale images of individual channels are shown below. The arrowheads indicate regions where PSD95, F-actin, and synaptophysin colocalize with PrP^C. The scale bars represent 5 µm. (**B**) Synaptic regions positive for F-actin, synaptophysin, and PSD95 are analyzed for PrP^C fluorescence intensity in ctrl, cLTP, and cLTD conditions. A box-and-whisker plot is shown, with the line representing the median, and the cross representing the mean. The median of PrP^C intensity is reduced at synaptic regions with induced cLTD (30.695 ± 2.752) compared to ctrl conditions (40.946 ± 2.897), while no significant changes are observed after cLTP induction (28.786 ± 3.306). A Kruskal-Wallis one way ANOVA on ranks with Dunn's Post Hoc test was used to assess statistical significance (*$p < 0.05$, **$p < 0.01$), (n= 30 cells (ctrl), 28 cells (cLTP), 26 cells (cLTD); from 3 independent experiments). (**C**) DIV14 dissociated hippocampal mouse neurons were chemically treated to induce cLTP or cLTD or untreated as ctrl, subjected to live immunostaining for surface PrP^C, then fixed and stained for synaptophysin and F-actin. The merge is shown atop, and the scale bars represent 5 µm.

Inverted greyscale images of individual channels are shown below. Arrowheads mark spots where F-actin and synaptophysin colocalize with PrP^C. (**D**) The intensity of plasma membrane (surface) PrP^C fluorescence at synaptic regions, defined here by F-actin and synaptophysin colocalization, was quantified in ctrl, cLTP, and cLTD conditions. The box-and-whisker plot shows the median (line) and the mean (cross). The median of surface PrP^C intensity is reduced at synaptic regions with induced cLTD (8.555 ± 0.481) compared to ctrl conditions (11.656 ± 1.497), while no significant changes were observed after the induction of cLTP (11.456 ± 0.751). A Kruskal-Wallis one way ANOVA on ranks with Dunn's Post Hoc test was performed as statistical analysis (*$p < 0.05$), (n= 11 cells (ctrl), 14 (cLTP), 17 (cLTD); 3 independent experiments).

These results showed that PrP^C localization at the synapse is moderately affected by the induction of cLTD. This indicates that a redistribution of PrP^C occurs upon cLTD stimulation.

3.2.2 Effects of synaptic plasticity on PrP^C transport

Active transport is important for the redistribution of synaptic proteins during synaptic plasticity (Collingridge et al. 2004). The reduction of PrP^C at synaptic regions after cLTD induction compared to control conditions might be due to internalization of PrP^C. Since whole PrP^C and membrane PrP^C intensity were reduced, it was hypothesized that PrP^C was transported in vesicles to other compartments in the neurons. In order to examine the intracellular trafficking of PrP^C in transport vesicles, a previously characterized PrP^C fusion protein with yellow fluorescent protein (YFP) YFP-PrP^C was used in live-cell imaging experiments (Heisler et al. 2018).

Dissociated hippocampal neurons were transfected at DIV12 with a plasmid encoding YFP-PrP^C. After two days the cells were treated to chemically induce synaptic plasticity using the same protocols that were used to measure PrP^C intensity at synapses. The active intracellular transport of YFP-PrP^C positive particles was visualized with an SDC time-lapse microscope. One representative frame taken from a video resulting from time-lapse microscopy is shown in figure 3.3A. The red arrow indicates an ROI, which was used to generate a kymograph from the entire video. The kymograph is shown in figure 3.3B. Kymographs are used to graphically display dynamic processes as spatial position over time in one still image. The signals that are visible in the kymograph result from YFP-PrP^C fluorescence including individual particle trajectories of YFP-PrP^C containing vesicles that can either be stationary (vertical lines in the kymograph) or moving (lines with a slope). The slopes of individual particle trajectories were used to calculate the velocity of YFP-PrP^C vesicles.

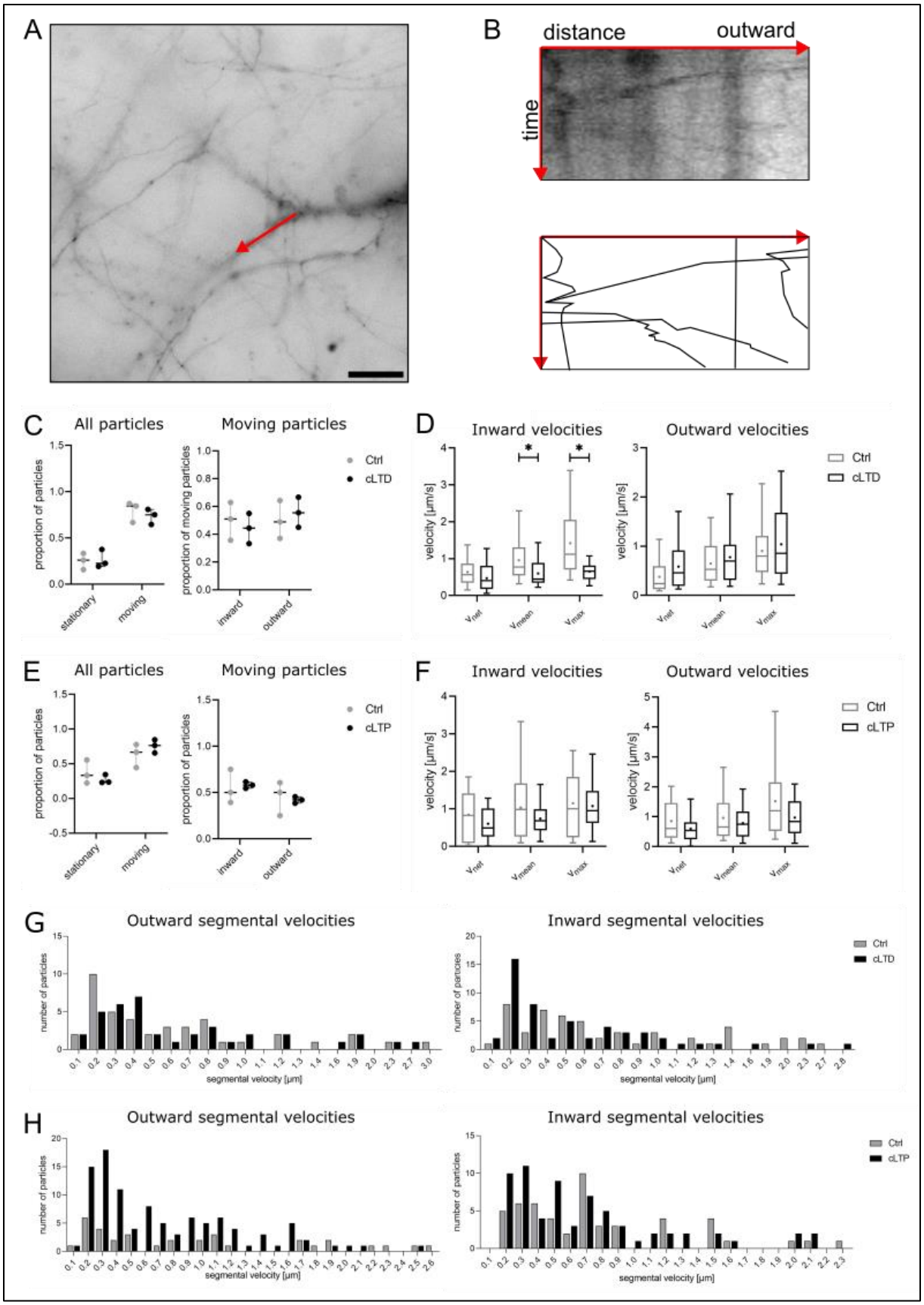

Figure 3.3: YFP-PrP^C transport in synaptic plasticity conditions. (**A**) One frame of a live-cell time-lapse imaging series of DIV14 YFP-PrP^C expressing dissociated hippocampal neurons is shown. The scale bar indicates 20 µm. The red arrow shows the ROI used to generate a kymograph along the dendrite,

shown in (B). (**B**) A kymograph graphically displays the spatial position of YFP-PrP^C particles over time within the dendrite ROI indicated in (A). On the bottom, an illustration to better visualize YFP-PrP^C particle trajectories is shown. Most particles do not move continuously with the same velocity but change velocities or direction. (**C**) Analysis of the proportion of moving or stationary particles in ctrl or cLTD conditions and the direction of the moving particles, moving toward the soma (inward) or away (outward). The dot plots show the median, which is indicated by a line and the error bars show 95% CI. A proportion of 0.240 ± 0.051 of all particles are stationary and 0.760 ± 0.051 are moving in ctrl conditions, while a proportion of 0.262 ± 0.041 are stationary and 0.738 ± 0.041 are moving in cLTD conditions. Of the moving particles a 0.499 ± 0.079 proportion move inward and 0.501 ± 0.079 are moving outward in ctrl conditions, while in cLTD conditions 0.443 ± 0.063 move inward and 0.557 ± 0.063 move outward. Statistical analysis was performed by Mann-Whitney Rank Sum Test (n= 114 particles (ctrl), 80 (cLTD); 3 independent experiments). (**D**) Analysis of segmental velocities of moving particles in ctrl or cLTD conditions. The box-and-whisker plot presents velocities for inward and outward-moving vesicles. For reasons of space, the values of the velocities are shown in the appendix. The results were analyzed by Mann-Whitney Rank Sum Test (*p < 0.05), (n(inward)= 19 particles (ctrl), 16 (cLTD); n(outward)= 13 particles (ctrl), 16 (cLTD); 3 independent experiments). (**E**) Analysis of the proportion of moving or stationary particles in ctrl or cLTP conditions and of the direction of moving particles. The dot plots show the median, which is indicated by a line, while the error bars are representing 95% CI. Of the overall particles 0.370 ± 0.098 are stationary and 0.630 ± 0.098 are moving in ctrl conditions, while 0.265 ± 0.040 are stationary and 0.735 ± 0.040 are moving in cLTP conditions. Of the moving particles 0.547 ± 0.106 move inward and 0.452 ± 0.106 are moving outward ctrl conditions, while in cLTP conditions 0.580 ± 0.020 move inward and 0.420 ± 0.020 move outward. Statistical analysis was performed by Mann-Whitney Rank Sum Test (n= 54 particles (ctrl), 60 (cLTP); 3 independent experiments). (**F**) Analysis of segmental velocities of moving particles in ctrl or cLTP conditions. For reasons of space, the values of the velocities are shown in the appendix. The results were analyzed by Mann-Whitney Rank Sum Test (n(inward)= 18 particles (ctrl), 30 (cLTP); n(outward)= 17 particles (ctrl), 20 (cLTP); 3 independent experiments). (**G**) The numbers of particles moving with a certain segmental velocity (without pauses) were sorted according to their velocity and are shown in a histogram for inward or outward transport in ctrl and cLTD conditions. (n(inward)= 53 (ctrl, cLTD); n(outward)= 43 (ctrl), 38 (cLTD) segments from 3 independent experiments). (**H**) The numbers of particles moving with a certain segmental velocity (without pauses) were sorted by velocity and are shown in a histogram for inward or outward transport in ctrl and cLTP conditions (n(inward)= 34 segments (ctrl), 103 (cLTD); n(outward)= 52 (ctrl), 66 (cLTD); 3 independent experiments).

Because vesicles can change their velocities or directions over time during recording, the particle trajectories were segmented, and individual sections were analyzed for segmental velocities. First, the proportion of moving and stationary particles was explored in dendrites. The population of moving particles was further divided into outward-directed particles, moving away from the soma, and inward-directed particles, moving toward the soma. No differences in the proportion of moving or stationary

particles could be observed between the control and cLTD or cLTP conditions, see figures 3.3C and E. There were also no changes in the proportion of particles moving inward or outward between cLTD or cLTP and control conditions. Overall velocities (v_{net}), segmental velocities without pauses (v_{mean}), and maximum segmental velocities (v_{max}) were determined. For each of the dynamic parameters, the velocities were further differentiated between inward and outward-moving particles, as shown in figures 3.3D and F. YFP-PrP^C velocities v_{mean} and v_{max} for particles moving inward toward the soma were significantly reduced by roughly 40% in cLTD conditions compared to control conditions. No significant changes in velocities could be observed for outward-moving vesicles, or for vesicles in control and cLTP conditions.
The histograms in figures 3.3G and H show the distribution of all segmental velocities for inward and outward movements, divided between control and cLTD conditions or control and cLTP conditions. The segmental velocities show a right-skewed distribution in the histograms, indicating that most vesicles move with a velocity between 0.1 and 0.5 µm/s. For inward-moving particles, a shift in the population of particles toward lower velocities could be observed under cLTD conditions compared to control conditions.

These results show that the active vesicular transport of PrP^C is modulated by the induction of synaptic plasticity. This might lead to a redistribution of PrP^C localization within stimulated neurons.

3.3 Effect of tau overexpression on intracellular transport of PrP^C

Synaptic dysfunction is a common symptom in neurodegenerative diseases like TSE and AD (Budka 2003; Bear et al. 2016). Intracellular neurofibrillary tangles and extracellular amyloid plaques are the molecular characteristics of AD (Grundke-Iqbal et al. 1986). The neurofibrillary tangles are composed of hyperphosphorylated tau. In physiological conditions tau is mainly associated with axonal MTs, regulating its stability and therefore axonal transport. In diseases like AD it is missorted into the somatodendritic compartments (Lee et al. 2001). The hyperphosphorylation of tau leads to the destabilization of MTs and may result in impaired cellular transport causing synaptic dysfunction (Ittner and Ittner 2018).

Since transport is important for synaptic function and synaptic plasticity influenced PrP^C transport velocity, the effect of overexpression of human tau (htau) on vesicular

transport of PrP^C was investigated. Overexpression of htau leads to its hyperphosphorylation and dissociation from MTs in mice (Andorfer et al. 2003). Dissociated hippocampal neurons were co-transfected with plasmids containing either YFP-PrP^C and enhanced cyan fluorescent protein (ECFP)-htau or ECFP at DIV12 and imaged on DIV14 using time-lapse microscopy. A representative frame is shown in figure 3.4A.

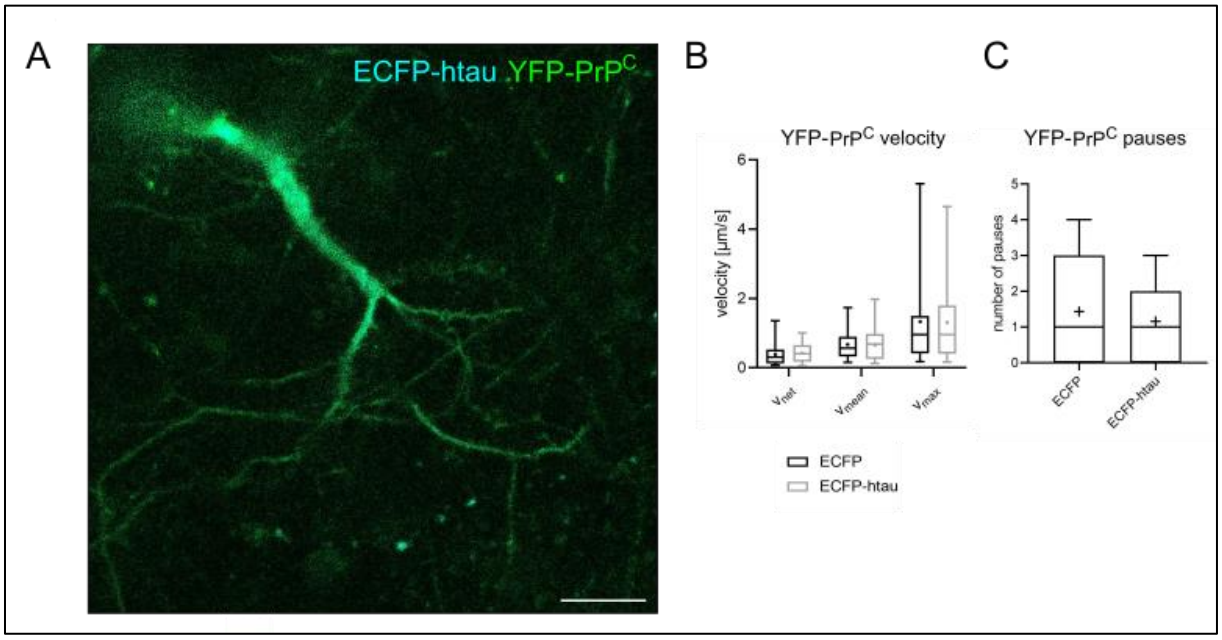

Figure 3.4: PrP^C transport velocity in neurons overexpressing htau. (**A**) One exemplary still image from an imaging series of YFP-PrP^C and ECFP-htau expressing DIV14 dissociated hippocampal neurons is shown. The scale bar represents 20 µm. (**B**) The velocities of inward-moving YFP-PrP^C transport vesicles are plotted in a box-and-whiskers plot, with the median represented by a line, and the mean presented as a cross. YFP-PrP^C vesicles are transported with v_{net} at 0.317 ± 0.145 µm/s, v_{mean} at 0.592 ± 0.143 µm/s, and v_{max} at 0.960 ± 0.238 µm/s for ECFP coexpression. In ECFP-htau coexpressing cells YFP-PrP^C vesicles are transported with v_{net} at 0.408 ± 0.058 µm/s, v_{mean} at 0.714 ± 0.146 µm/s, and v_{max} at 0.959 ± 0.231 µm/s. No significant changes in YFP-PrP^C vesicle transport velocity could be observed between ECFP and ECFP-htau expressing cells. Statistical analysis was performed by Mann-Whitney Rank Sum Test (n(inward)= 30 segments (ECFP), 25 (ECFP-htau); n(outward)= 25 segments (ECFP), 35 (ECFP-htau); 3 independent experiments). (**C**) The pauses of YFP-PrP^C transport vesicles are plotted in a box-and-whiskers plot, with the median represented by a line, and the mean presented as a cross. No significant difference in the median number of pauses of YFP-PrP^C particles is observed between ECFP (1 ± 0.241) and ECFP-htau (1 ± 0.229) overexpressing cells. Statistical analysis was performed by Mann-Whitney Rank Sum Test (n(inward)= 30 segments (ECFP), 25 (ECFP-htau); n(outward)= 25 segments (ECFP), 35 (ECFP-htau); 3 independent experiments).

ECFP-htau is diffusely expressed in the neuron, while YFP-PrP^C is slightly diffuse with a more concentrated fluorescence in moving transport vesicles. The velocities of YFP-

PrP^C segmental transport vesicles were analyzed as described before, but no significant differences in YFP-PrP^C segmental transport velocities or number of pauses of YFP-PrP^C transport vesicles between ECFP and ECFP-htau overexpression could be discerned. Figure 3.4C shows the results of inward-moving YFP-PrP^C. Both, inward and outward-moving YFP-PrP^C vesicles did not change in velocities or number of pauses, the results of outward-moving particles are not shown in this work.

Taken together, the overexpression of htau did not affect dendritic PrP^C transport.

3.4 PrP^C localization to endosomal and lysosomal compartments during neuronal activity processes

Endosomes play an important role in synaptic plasticity. They control the recycling, storing, and degradation of pre- and postsynaptic membrane proteins, which is important for activity-dependent receptor turnover in neurons (Park et al. 2016; Parkinson and Hanley 2018). For sorting endocytic ubiquitinated cargo into ILVs and the formation of MVBs, TSG101 is one important component of the ESCRT complex (Henne et al. 2011). Degradation is an important process for maintaining cellular homeostasis and mainly occurs in lysosomes and proteasomes (Goo et al. 2017). In lysosomes, Lamp1 is a lysosome-associated membrane protein that plays an important role in lysosome biogenesis and autophagy (Eskelinen 2006). In the endolysosome, these two types of organelles are combined in a dynamic system of intracellular membranous organelles, where the endocytic, biosynthetic, and degradative pathways intersect (Maxfield and McGraw 2004). It is the key sorting station to distribute cargo to different membrane domains, to regulate cellular metabolism, degradation, and extracellular release (Klumperman and Raposo 2014; Naslavsky and Caplan 2018).

3.4.1. Changes in PrP^C intensity in endosomal and lysosomal compartments during synaptic plasticity

To this point, it was shown here that PrP^C was affected by the induction of cLTD. PrP^C intensity was reduced at synapses and active transport was slowed after cLTD induction compared to control conditions. After its internalization, PrP^C in principle can be recycled or transported toward the endolysosomal pathway from where it can be stored, degraded, or released on exosomes (Aguzzi et al. 2008). Because endolysosomes are important during synaptic plasticity, PrP^C targeting to

endolysosomal compartments following the induction of synaptic plasticity was investigated.

DIV14 dissociated hippocampal neurons were treated with previously described cLTD and cLTP protocols or untreated as control. After the induction, the cells were fixed and immunofluorescently stained for Lamp1, serving as a lysosomal marker, TSG101, serving as an endosomal marker, and PrP^C. Representative images from the three conditions are shown in figure 3.5A. Lamp1- and TSG101-labeled vesicular structures showed a high amount of colocalization in the soma. The fluorescent intensity of PrP^C was increased around the soma and its distribution there was similar to that of the endosomal and lysosomal markers. The percentage of the area of colocalization between PrP^C and either Lamp1 or TSG101 was measured and amounted to roughly 40% between PrP^C and Lamp1-labeled compartments and around 50% for PrP^C and TSG101-labeled compartments. The results are not shown because the area of colocalization did not change with the induction of synaptic plasticity. When measuring PrP^C intensity in the TSG101-labeled compartments in the soma, however, the intensity of PrP^C was reduced by roughly 25% in TSG101-positive compartments in cLTD treated neurons compared to control conditions, as seen in figure 3.5B. No significant changes could be observed for PrP^C intensity in TSG101-labeled compartments after the induction of cLTP compared to control conditions. In Lamp1-labeled compartments, PrP^C intensity was reduced by about 25% in cLTD treated neurons compared to control conditions. Again, no significant changes could be observed in PrP^C intensity in Lamp1-labeled compartments after the induction of cLTP compared to control conditions. PrP^C intensity and colocalization with TSG101 or Lamp1 labeled compartments were also measured in dendrites, which revealed similar but less pronounced effects compared to those observed in the soma (results not shown).

Taken together, PrP^C targeting to endosomal and lysosomal compartments appears to be moderately affected by the induction of synaptic plasticity. This could hint at a possible function of PrP^C in endolysosomal compartments during synaptic plasticity.

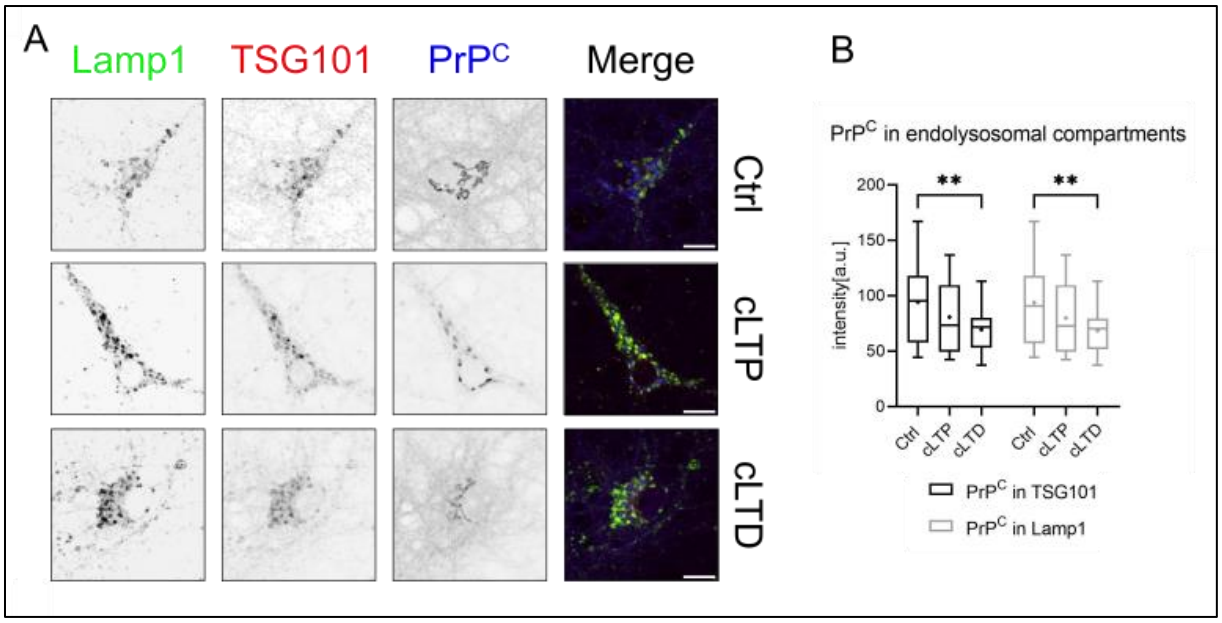

Figure 3.5: Effect of synaptic plasticity on PrP^C targeting to endolysosomal compartments. (**A**) Immunofluorescence staining of DIV14 dissociated hippocampal neurons for PrP^C, TSG101, and Lamp1. Neurons were treated to induce chemical synaptic plasticity (cLTP or cLTD) or left untreated as ctrl. The somata of neurons and proximal dendrites are shown. On the right, the merge of the three channels is shown. Inverted greyscale images of individual channels are shown on the left. There is a high amount of colocalization of PrP^C with TSG101- and Lamp1-labeled compartments. The scale bars represent 10 µm. (**B**) PrP^C intensities in Lamp1- or TSG101-labeled compartments in the soma are quantified by box-and-whiskers plot, with the median represented by a line, and the mean presented as a cross. The median fluorescent intensity of PrP^C in TSG101-labeled compartments is reduced in cLTD (71.547 ± 3.483) compared to ctrl conditions (95.170 ± 5.893), while they remain unchanged after the induction of cLTP (73.171 ± 4.536). The median fluorescent intensity of PrP^C in Lamp1-labeled compartments is decreased after the induction of cLTD (70.802 ± 8.835) compared to ctrl conditions (101 ± 5.732), while it is unchanged in cLTP conditions (80.203 ± 4.339). The results were analyzed by Kruskal-Wallis one way ANOVA on ranks (**$p < 0.01$), (n (TSG101) = 39 cells (Ctrl), 39 (cLTP), 34 (cLTD); n (Lamp1) = 39 cells (Ctrl), 39 (cLTP), 37 (cLTD); 4 independent experiments).

Since the formation of MVBs is a prerequisite for their downstream maturation and fusion with the plasma membrane or lysosomes, a possible effect of inhibiting specific routes of ILV formation on PrP^C localization was investigated. GW4869 is an inhibitor of the nSMase, which has been shown to regulate the formation of ILVs and thus the formation of MVBs in a pathway independent of the ESCRT-mediated ILV formation in which TSG101 plays a role (Colombo et al. 2014; Essandoh et al. 2015; Menck et al. 2017). Dissociated hippocampal neurons at DIV13 were treated for 24 h with 20 µM GW4869 or with DMSO serving as a control. Subsequently, chemical synaptic plasticity was induced in these neurons on DIV14, followed by immunofluorescence

staining for TSG101, Lamp1, and PrP^C. The intensity of PrP^C was measured at TSG101-labeled compartments in the soma, see figure 3.6A.

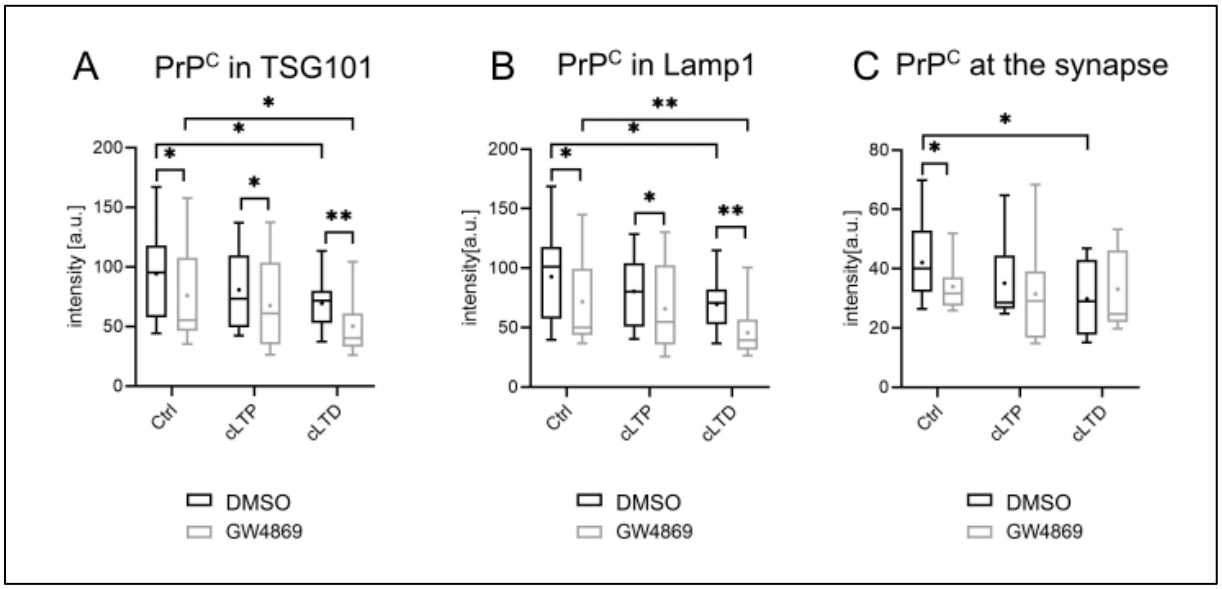

Figure 3.6: *Effect of GW4869 treatment of PrP^C localization*. (**A**) Quantification of PrP^C fluorescence intensities in TSG101-labeled compartments in GW4869- or DMSO-treated DIV14 neurons. PrP^C intensities in TSG101-labeled compartments in cells treated with DMSO are reduced after the induction of cLTD (71.547 ± 3.483) compared to ctrl conditions (95.170 ± 5.893), while no changes could be observed after cLTP induction (73.171 ± 4.536). In GW4869-treated cells PrP^C intensities are reduced in cLTD (40.283 ± 4.124) compared to ctrl conditions (55.337 ± 6.711), while there are no changes after cLTP induction (60.997 ± 5.570). The fluorescent intensities of PrP^C in TSG101-labeled compartments are reduced in GW4869 as compared to DMSO-treated neurons for all, ctrl, cLTP, and cLTD conditions (n (DMSO) = 39 cells (Ctrl), 39 (cLTP), 34 (cLTD); n (GW4869) = 32 cells (Ctrl), 39 (cLTP), 34 (cLTD); 4 independent experiments). (**B**) Quantification of PrP^C fluorescence intensities in Lamp1-labeled compartments in GW4869- or DMSO-treated DIV14 neurons. PrP^C intensities in Lamp1-labeled compartments in cells treated with DMSO are reduced after cLTD induction (70.802 ± 8.835) compared to ctrl conditions (101 ± 5.732), while they remain similar in cLTP conditions (80.203 ± 4.339). In GW4869-treated cells PrP^C intensities are reduced in cLTD (39.315 ± 4.225) compared to ctrl conditions (49.947 ± 6.335), they remain unchanged in cLTP conditions (54.696 ± 5.545) compared to the ctrl. The fluorescent intensities of PrP^C in Lamp1-labeled compartments are reduced in GW4869 as compared to DMSO-treated neurons for all, ctrl, cLTP, and cLTD conditions (ctrl and cLTD) (n (DMSO) = 39 cells (Ctrl), 39 (cLTP), 37 (cLTD); n (GW4869) = 32 cells (Ctrl), 39 (cLTP), 34 (cLTD); 4 independent experiments). (**C**) Quantification of fluorescence intensity of PrP^C at synaptic regions of DIV14 dissociated hippocampal neurons. They were defined as regions where PSD95, synaptophysin, and F-actin signals colocalize. Fluorescent intensities of PrP^C at synaptic regions in DMSO-treated cells are reduced in cLTD (29.015 ± 2.893) compared to ctrl conditions (40.119 ± 2.716), while they are not significantly different in cLTP conditions (28.618 ± 2.633). In cells treated with GW4869 PrP^C fluorescent intensities at synaptic regions are comparable between cLTD (24.798 ± 3.290), cLTP (29.138 ± 4.050) and ctrl conditions (31.624 ± 1.917). GW4869 compared to DMSO treatment in ctrl conditions reduced

PrP^C intensity (n (DMSO) = 19 cells (Ctrl), 19 (cLTP), 16 (cLTD); n (GW4869) = 18 cells (Ctrl), 15 (cLTP), 16 (cLTD); 3 independent experiments). All plots in figure 3.6 represent box-and-whiskers plots, with the line showing the median and the dot the mean. To test for statistical significance between ctrl, cLTP, and cLTD conditions the Kruskal-Wallis one way ANOVA on ranks test was used, while statistical significance between the treatment groups DMSO and GW4869 was assessed by using the Mann-Whitney U test for all data shown in this figure (*$p < 0.05$, **$p < 0.01$).

In both GW4869- and DMSO-treated cells, PrP^C intensity was reduced in cLTD compared to control conditions in TSG101-labeled compartments. In DMSO-treated cells, the fluorescent intensity of PrP^C was reduced by about 25% in cLTD compared to control conditions, while in GW4869-treated neurons it was reduced by over 30% in cLTD compared to control conditions. In contrast, the PrP^C fluorescent intensities in the same compartments did not change with the induction of cLTP compared to control conditions. The fluorescent intensity of PrP^C in TSG101-labeled compartments was reduced in GW4869 treated cells compared to DMSO-treated cells in all conditions. PrP^C intensity in TSG101-positive compartments was reduced by roughly 20% in the control and cLTP conditions, while under cLTD conditions it was decreased by more than 25% in cells treated with GW4869 compared to DMSO-treated neurons. The area of colocalization of PrP^C with TSG101 did not significantly change in synaptic plasticity conditions or in cells treated with GW4869 (results not shown). Figure 3.6B shows the intensity of PrP^C at Lamp1-labeled compartments in the soma. Fluorescent intensity of PrP^C was significantly reduced between control and cLTD conditions in DMSO-treated cells by about 25% and in GW4869-treated neurons by over 30%. GW4869 treatment reduced PrP^C intensity in Lamp1-labeled compartments compared to DMSO control conditions by roughly 20% in cLTP and control conditions and by over 30% in cLTD conditions. However, PrP^C intensity in Lamp1-positive compartments was not altered by the induction of cLTP compared to control conditions in DMSO- or GW4869-treated cells.

To investigate variations of PrP^C intensity at synaptic regions, cells treated with GW4869 or DMSO and chemically induced synaptic plasticity were immunofluorescently stained for F-actin, synaptophysin, PSD95, and PrP^C. The results are shown in figure 3.6C. Under control conditions, PrP^C intensity was reduced by 20% in GW4869 treated cells compared to DMSO treatment but remained unaffected by GW4869 treatment after the induction of cLTP or cLTD. On the other hand, PrP^C intensity at synaptic regions was reduced by 30% in cLTD compared to control conditions in DMSO, but not in GW4869-treated neurons.

GW4869 treatment led to reduced PrP^C intensity in endolysosomal compartments compared to DMSO treatment. The reduction of PrP^C intensity due to GW4869 was less pronounced at the synapses, but it was also detectable under control conditions. These results show that GW4869 has a more significant effect on PrP^C in endolysosomal compartments compared to at the synapse.

3.4.2. Effect of neuronal activity processes on the release of exosomes

Exosomes are small membranous vesicles that are generated by the invagination of endosomal membranes to form ILVs in MVBs and their release into the extracellular space (Colombo et al. 2014). PrP^C is enriched in neuronal exosomes that originate from endosomal compartments (Hartmann et al. 2017). Further, it was shown that general induction of neuronal activity increases the release of exosomes from neurons (Artola and Singer 1993; Cummings et al. 1996; Chivet et al. 2014). Possible alterations of exosome release during plasticity-related processes have scarcely been investigated to date. Since PrP^C intensity was decreased in endolysosomal compartments under cLTD conditions and following GW4869 treatment, the effect of homeostatic plasticity on exosome release and their potential effect on synapse numbers of neurons was investigated. Long-term homeostatic plasticity protocols were chosen since high concentrations of exosomes are needed for these analyses. The blocking of the nSMase by GW4869 also decreases the release of exosomes (Essandoh et al. 2015). This characteristic was used to investigate the effect of blocking exosome release over a long time on synapse numbers or PrP^C localization to synaptic regions in dissociated hippocampal neurons. Additionally, it was explored whether increasing exosome concentration in the ambient media influenced PrP^C synaptic localization or the number of synaptic regions. Furthermore, it was investigated whether the induction of homeostatic plasticity on neurons releasing these exosomes would modulate a potential effect of exosomes on synapses.

DIV12 dissociated hippocampal neurons were incubated with TTX, Bic, or left untreated as control for 48 h at 37 °C. At DIV14 the exosomes were isolated from the medium of the neurons and added to neurons from the same preparation (DIV14) and additionally GW4869 or DMSO for 6 days. On DIV20 the neurons were immunochemically stained for synaptophysin, F-actin, PDS95, and PrP^C. The number of synapses, defined by spots co-labeled for synaptophysin, PSD95, and F-actin, along a dendrite was calculated. The results are shown in figure 3.7A. There were no

significant differences in the number of synapses between DMSO- or GW4869-treated neurons with or without added exosomes. The intensity of PrP^C was also measured in these synaptic regions. The results are shown in figure 3.7B. The intensity of PrP^C at the synapse was reduced in GW4869- compared to DMSO-treated cells that were treated with exosomes isolated from Bic stimulated neurons.

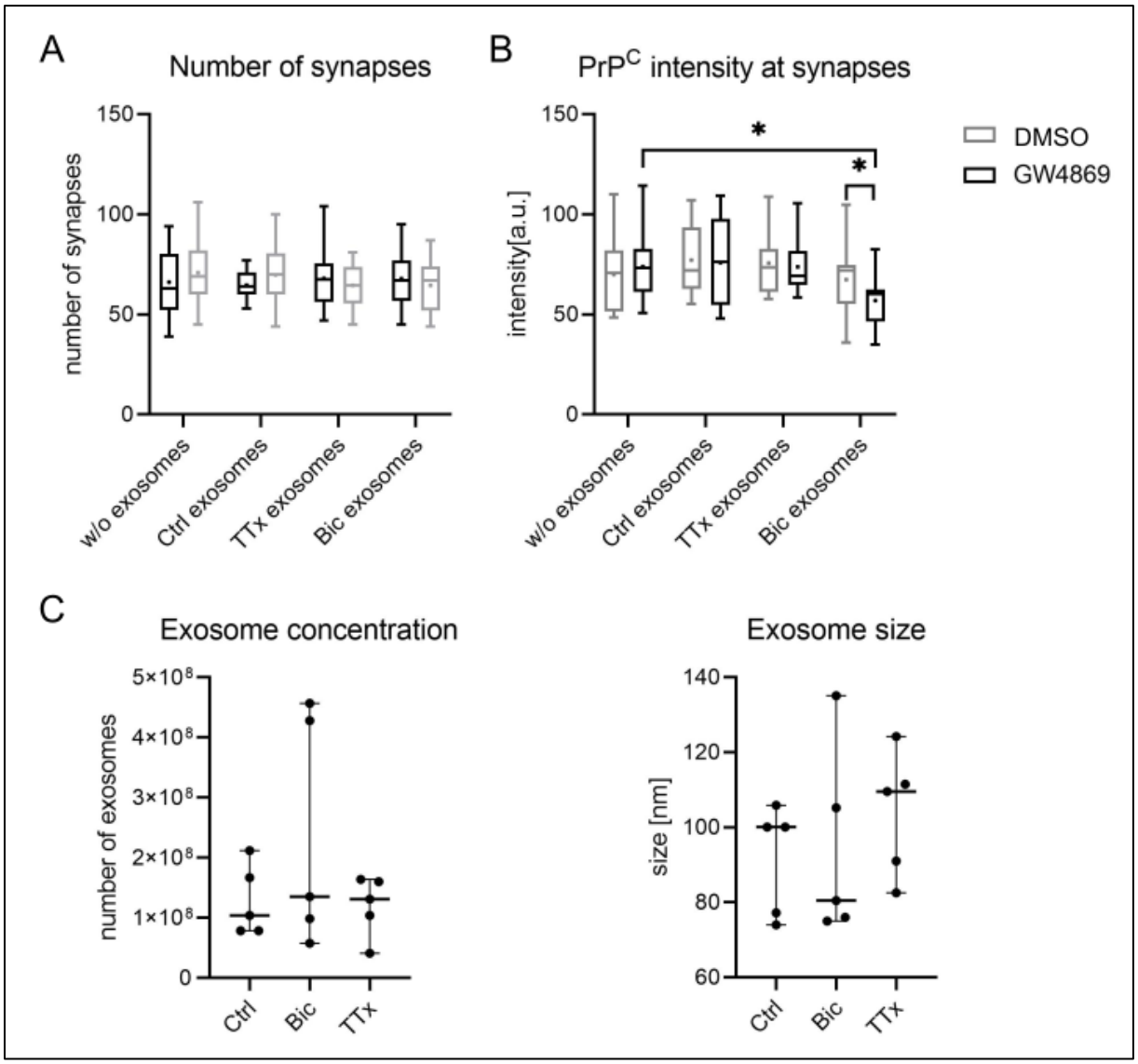

Figure 3.7: *Effect of exosomes released from neurons under homeostatic plasticity conditions*. (**A and B**) Quantification of the number of synapses or PrP^C intensity at synaptic regions in neurons treated with GW4869 or DMSO; and without added exosomes (w/o exosomes), with exosomes from unstimulated neurons (Ctrl exosomes), exosomes from TTX stimulated neurons (TTX exosomes), or exosomes from Bic stimulated neurons (Bic exosomes) added. The results are plotted in a box-and-whiskers plot with the median shown as a line and the mean indicated by a dot. (**A**) The number of synapses along a dendritic section in DMSO-treated neurons is 63.0 ± 3.889 for w/o exosomes, 64.5 ± 2.421 for Ctrl exosomes, 67.5 ± 3.417 for TTX exosomes, and 67.0 ± 3.127 for Bic exosomes. The number of synapses along a dendritic section in GW4869-treated neurons is 69.0 ± 3.679 for w/o exosomes, 70.0

± 3.516 for Ctrl exosomes, 64.5 ± 2.529 for TTX exosomes, and 67.0 ± 2.798 for Bic exosomes. Analysis of synapse numbers reveals similar values between the different conditions. A two-way ANOVA was performed for statistical analysis (n (DMSO) = 18 cells (w/o exosomes), 20 (ctrl exosomes), 18 (TTx exosomes), 18 (Bic exosomes); n (GW4869) = 19 cells (w/o exosomes), 18 (ctrl exosomes), 18 (TTx exosomes), 21 (Bic exosomes); 3 independent experiments). (**B**) PrP^C intensities at synaptic regions in DMSO-treated neurons are 70.756 ± 4.669 for w/o exosomes, 71.895 ± 3.656 for Ctrl exosomes, 73.603 ± 3.726 for TTX exosomes, 71.904 ± 3.712 for Bic exosomes. PrP^C intensities at synaptic regions in GW4869-treated neurons are 73.291 ± 3.553 for w/o exosomes, 76.247 ± 5.077 for Ctrl exosomes, 69.130 ± 3.153 for TTX exosomes, and 60.145 ± 2.475 for Bic exosomes. PrP^C intensity at the synapse is reduced in GW4869- compared to DMSO-treated cells that were treated with exosomes isolated from Bic stimulated cells. The addition of Bic exosomes also reduces PrP^C intensity at the synapse compared to cells without additional exosomes that were treated with GW4869. The Kruskal-Wallis one way ANOVA on ranks was performed for statistical analysis between the different exosome treatment conditions; the Mann-Whitney Rank Sum Test was used to evaluate differences between DMSO and GW4869 conditions (*$p < 0.05$) (n (DMSO) = 18 cells (w/o exosomes), 20 (ctrl exosomes), 18 (TTx exosomes), 18 (Bic exosomes); n (GW4869) = 19 cells (w/o exosomes), 18 (ctrl exosomes), 18 (TTx exosomes), 21 (Bic exosomes); 3 independent experiments). (**C**) Concentration and size of exosomes isolated from DIV14 dissociated hippocampal neurons are presented in a scatter dot plot. The number of exosomes isolated from neurons under control conditions is $1.04 \cdot 10^8$ $\pm 2.7 \cdot 10^7$/µL, for Bic stimulation $1.35 \cdot 10^8 \pm 8.6 \cdot 10^7$/µL, and for TTX stimulation $1.31 \cdot 10^8 \pm 2.3 \cdot 10^7$/µL exosomes were isolated. The mode size of the isolated exosomes is 100.1 ± 6.58 nm from unstimulated neurons, 80.5 ± 11.579 nm from Bic stimulated, and 109.6 ± 7.491 nm from TTX stimulated neurons. The median is shown as a line and the error bars represent 95% CI. The concentration and size of exosomes isolated from stimulated or unstimulated cells show no significant differences (n= 5 independent experiments).

The addition of exosomes for Bic-stimulated cells also reduced PrP^C intensity at the synapse compared to cells without additional exosomes that were treated with GW4869.The exosomes isolated from neuron-conditioned medium were analyzed by nanoparticle tracking analysis, before adding the exosomes to the neurons for 6 days. The results are shown in figure 3.7C. Neither the size nor the concentration of released exosomes changed significantly between exosomes isolated from TTX-, Bic- or untreated neurons.

In general, no significant changes in synapse number were detected by blocking the release of exosomes. The addition of exosomes isolated from stimulated or unstimulated neurons did not have a long-term effect on synapse numbers. PrP^C intensity at the synapse was moderately reduced after 6 days of incubation with GW4869 and additional treatment with exosomes isolated from Bic stimulated neurons compared to DMSO-treated neurons incubated with the same exosomes and

GW4869-treated neurons without the addition of exosomes. Finally, homeostatic plasticity did not affect the size or concentration of released exosomes.

3.5 PrP^C interactions

Synapses are organized by cell adhesion molecules bridging the synaptic cleft. The synaptic cell adhesion molecules are important in synapse assembly and formation as well as synaptic plasticity and memory formation (Missler et al. 2012). PrP^C has been shown to play critical a role in cell adhesion and was shown in this work to be present at inhibitory and excitatory synapses with its localization modulated by synaptic plasticity (Martins et al. 2002; Petit et al. 2013). This work therefore next aimed to identify novel synaptic cell adhesion molecules as PrP^C interaction partners. N-cadherin is a cell adhesion molecule abundant in the brain where it is concentrated at excitatory synapses (Benson and Tanaka 1998). There, N-cadherin mediates homophilic Ca^{2+}-dependent transsynaptic adhesion, regulating synapse formation, spine morphology, and synaptic plasticity (Takeichi and Abe 2005; Brusés 2006; Takeichi 2007; Mysore et al. 2008; Hirano and Takeichi 2012). It has been described to colocalize with PrP^C, however, whether both proteins interact with each other was not known (Bodrikov et al. 2011).

To study a potential interaction of PrP^C with N-cadherin, IP from whole adult mouse brains was performed. The brains were lysed with 1% Triton X-100 and the lysates were incubated with beads coupled with an antibody directed against PrP^C, to precipitate PrP^C together with potential interaction partners. As a control, the lysate was incubated with beads coupled to unspecific rabbit IgG. The IPs were loaded onto a polyacrylamide gel together with the lysate and analyzed by western blotting and immunodetection. The results are shown in figure 3.8A. Precipitation of PrP^C led to the co-precipitation of N-cadherin. To validate this finding, the IP vice versa was conducted with beads coupled to antibodies directed against N-cadherin, as seen in figure 3.8B. Indeed, PrP^C was found to co-precipitate with N-cadherin in these experiments.

PrP^C and N-cadherin are synaptic proteins, so their area of colocalization in DIV19 dissociated hippocampal neurons was investigated at F-actin hotspots and in dendrites. The results are shown in figure 3.8C.

The area of colocalization of immunochemically-labeled PrP^C and N-cadherin did not significantly differ between dendrites and F-actin hotspots, it was about 40% in both.

One representative image of a dendrite immunochemically stained for N-cadherin, PrP^C, and F-actin is shown in figure 3.8D.

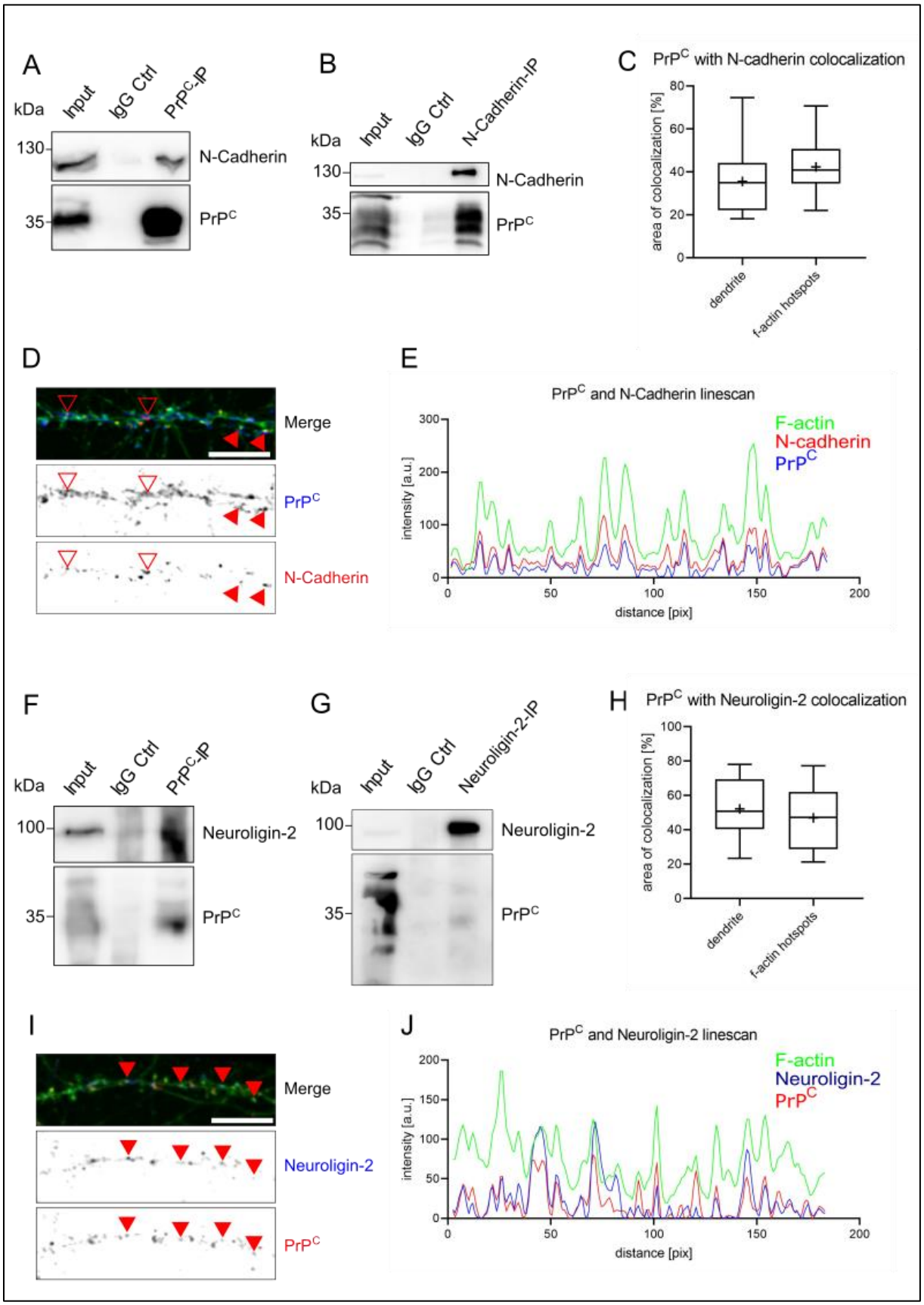

Figure 3.8: PrP^C interaction with cell adhesion proteins. (**A and B**) Western blot analysis of

representative IPs from whole adult mouse brain lysates. Brains from adult mice were lysed (input) and incubated with magnetic beads coupled to unspecific IgG (IgG Ctrl) or antibodies specific for PrP^C (A) or N-cadherin (B). Markers are displayed on the left. **(A)** The input shows bands for PrP^C and N-cadherin at around 35 kDa and 130 kDa, respectively. The lane for the IgG ctrl shows no signal. The PrP^C signal is enhanced in the IP and N-cadherin shows a signal (n=3 independent experiments). (**B**) The input shows three bands for PrP^C at around 35 kDa and one band for N-cadherin at approximately 130 kDa, while the lane for the IgG ctrl hardly shows any signal. The N-cadherin signal is enhanced in the IP and PrP^C shows a clear signal (n=3 independent experiments). (**C**) Quantification of the area of colocalization of immunochemically labeled PrP^C and N-cadherin in DIV19 dissociated hippocampal neurons at F-actin hotspots and in dendrites. The box-and-whisker plot shows the percentage of the area of colocalization, with a line representing the median and a cross at the mean. No significant differences in the area of colocalization of N-cadherin and PrP^C are observed between dendrites (35.042 ± 4.351%) or at F-actin hotspots (40.834 ± 3.848%). Statistical analysis was performed by unpaired, two-tailed t-test. (n= 13 cells, 3 independent experiments). (**D**) A dendrite section of DIV19 dissociated hippocampal neurons immunochemically labeled for PrP^C, N-cadherin, and F-actin. The merge is shown at the top, while the inverted greyscale images of the individual channels for PrP^C and N-cadherin are shown below. Filled red arrows show colocalization of labeled PrP^C and N-cadherin at F-actin hotspots, while red-framed arrows show colocalization in dendrites. The scale bar represents 5 µm. (**E**) A line scan generated from D shows the intensity values for fluorescently-labeled PrP^C, N-cadherin, and F-actin along the dendrite and the correlation with each other. (**F and G**) Western blot analysis of representative IPs from whole adult mouse brain lysates. Brains from adult mice were lysed (input) and incubated with magnetic beads coupled to unspecific IgG (IgG Ctrl) or antibodies specific for PrP^C (F) or neuroligin-2 (G). Markers are displayed on the left. (**F**) The input shows signals for three PrP^C bands at around 35 kDa and one band for neuroligin-2 at 100 kDa. These bands are not present in the IgG ctrl lane, while they are visible in the PrP^C-IP lane (n= 3 independent experiments). (**G**) The input shows signals for three PrP^C bands at around 35 kDa and one band for neuroligin-2 at 100 kDa, as expected. These bands are also visible in the neuroligin-2-IP lane, while the IgG ctrl lane does not show specific signals (n= 3 independent experiments). (**H**) The percentage of the area of colocalization between PrP^C and neuroligin-2 at F-actin hotspots and in dendrites is shown in a box-and-whiskers plot. The median is indicated by a line, while the mean is shown as a cross. No significant differences in the area of colocalization of N-cadherin and PrP^C are observed between dendrites (50.773 ± 4.393%) or at F-actin hotspots (47.301 ± 4.541%). Statistical analysis was performed by unpaired, two-tailed t-test (n= 15 cells, 3 independent experiments). (**I**) DIV19 dissociated hippocampal neurons are immunochemically stained for PrP^C, neuroligin-2, and F-actin. The merge is shown on top, while the inverted grey-scale images of the individual channels for PrP^C and neuroligin-2 are below. Filled arrows show colocalization of PrP^C and neuroligin-2 at F-actin hotspots. The scale bar signifies 5 µm. (**J**) A line scan generated from I shows the intensity values of PrP^C, neuroligin, and F-actin along the dendrite and their correlation with each other.

N-cadherin and PrP^C colocalized in regions with and without F-actin hotspots. To better visualize the fluorescent signals of the labeled proteins, a line scan was generated

from the image in figure 3.8D and presented in figure 3.8E. Here, PrP^C intensity was reduced compared to N-cadherin, especially at F-actin hotspots, but generally, both intensities showed a high degree of correlation. Correspondingly, the calculation of a Pearson correlation coefficient between N-cadherin and PrP^C revealed a value of 0.871.

Since it was shown in this work that PrP^C localizes to inhibitory synapses, its interaction with neuroligin-2, a cell adhesion molecule at inhibitory synapses was investigated (Varoqueaux et al. 2004). First, IP of PrP^C or neuroligin-2 was performed from lysates of whole adult mouse brains, as seen in figures 3.8F and G. Neuroligin-2 co-precipitated with PrP^C and, vice versa, the precipitation of Neuroligin-2 led to weak co-precipitation of PrP^C. Next, the area of colocalization of immunochemically stained PrP^C and neuroligin-2 was measured in dendrites and at F-actin hotspots of DIV19 dissociated hippocampal neurons. The results are shown in figure 3.8H. Amounting to roughly 50%, similar areas of colocalization at F-actin hotspots compared to colocalization in dendrites were observed. A representative image of a dendrite from a DIV19 dissociated hippocampal neuron immunocytochemically stained for neuroligin-2, PrP^C, and F-actin is shown in figure 3.8I. A line scan generated along the dendrite shown in figure 3.8I and depicted in figure 3.8J was used to visualize the intensities of labeled proteins along the dendrite. The intensity values of PrP^C and neuroligin-2 showed a good degree of correlation, which was further corroborated by the calculation of the Pearson correlation coefficient, which revealed a value of 0.759.

3.5.1 PrP^C interactions over development

Cell adhesion molecules are important during development (Thiery 2003; Togashi et al. 2009). PrP^C is already expressed a few days after implantation in murine development, suggesting a possible role during development and it has been shown that PrP^C promotes neurite outgrowth (Manson et al. 1992; Lopes et al. 2005; Santuccione et al. 2005). That PrP^C plays a role in neurodevelopment is underlined by the fact that it interacts with cell adhesion molecules, as shown in other works and above (Schmitt-Ulms et al. 2001). During development, N-cadherin contributes to cell-cell adhesion in neuronal progenitor cells and neurons (Miyamoto et al. 2015). Neuroligin-2 is required for the maturation of inhibitory synapses (Hines et al. 2008; Fu and Vicini 2009; Chubykin et al. 2007). Since PrP^C does interact with cell adhesion molecules, its intensity and colocalization with N-cadherin or neuroligin-2 during development in dissociated hippocampal neurons were investigated.

For this purpose, dissociated hippocampal neurons from different points of development were immunochemically stained for PrP^C and F-actin, as well as synaptophysin, N-cadherin, or neuroligin-2. Functional polarization in dissociated hippocampal neurons begins with synapse formation at DIV7 (Moutin et al. 2020; Kaech and Banker 2006). Between DIV7 and 21, the branching of the dendrites and expression of synaptic markers increase, with dendritic spines occurring around DIV14. Representative images of dendrites from these neurons are shown in figure 3.9A.

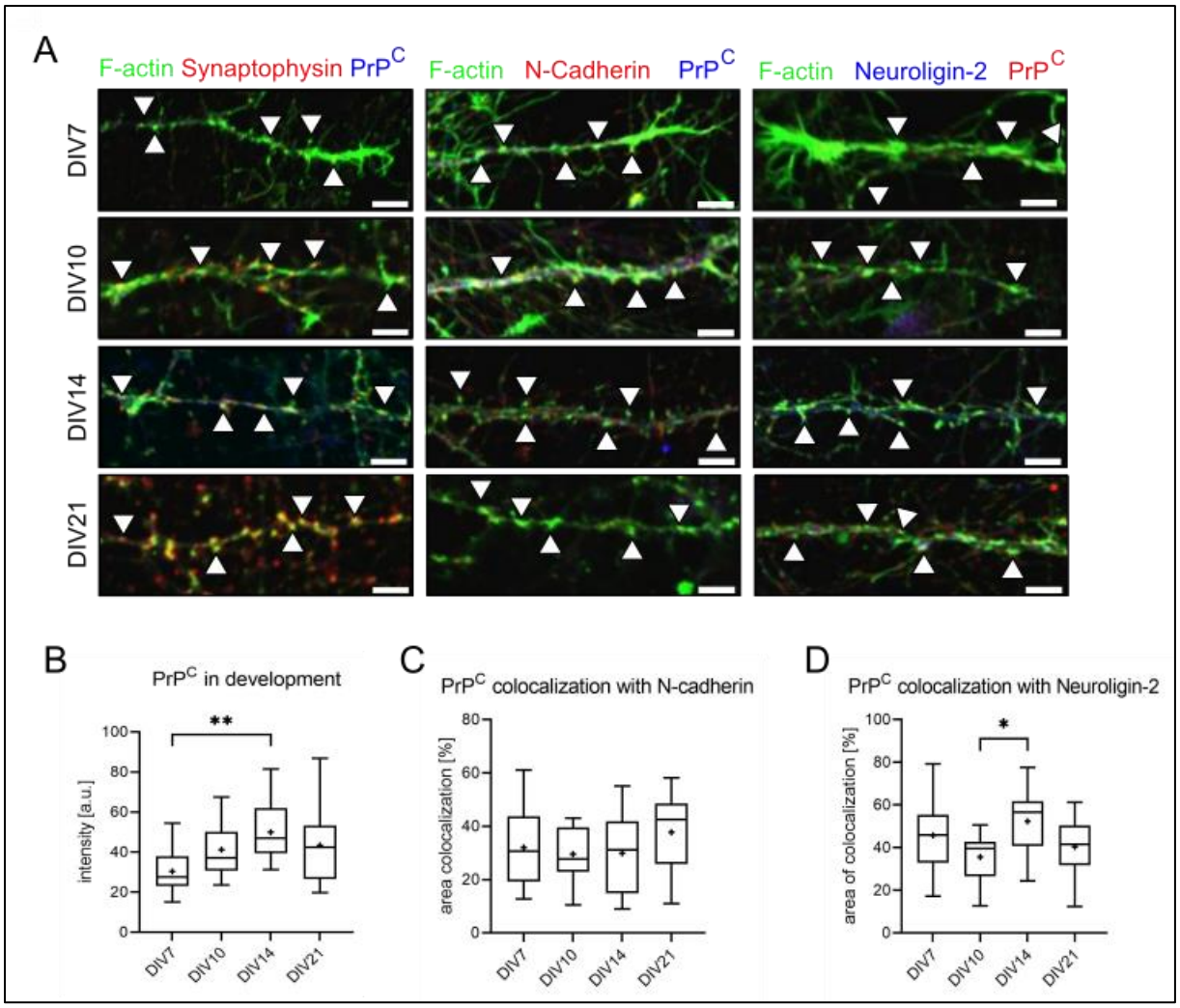

Figure 3.9: PrP^C in development. (**A**) Dissociated hippocampal neurons at different points of development (DIV7, 10, 14, and 21) were immunochemically stained for F-actin and PrP^C, as well as synaptophysin, N-cadherin, or neuroligin-2 (left to right). The scale bar indicates 5 µm. The filled arrows show points of triple colocalization. (**B**) Quantification of the intensity of PrP^C at F-actin hotspots in dissociated hippocampal neurons at DIV7, 10, 14, and 21. PrP^C median intensity at F-actin hotspots increases from 27.514 ± 2.364 at DIV7, over 37.033 ± 3.077 at DIV10, to 46.973 ± 4.473 at DIV14, and 42.354 ± 4.824 at DIV21. PrP^C median intensity at F-actin hotspots increases from DIV7 to DIV14. Statistical analysis was performed by Kruskal-Wallis one way ANOVA on ranks with Dunn's Post Hoc

test (**p < 0.01) (n = 17 cells (DIV7), 16 (DIV10), 11 (DIV14), 16 (DIV21); 3 independent experiments). (**C**) Quantification of the percentage of the area of colocalization between N-cadherin and PrP^C at F-actin hotspots in dissociated hippocampal neurons at DIV7, 10, 14, and 21. The median percentage of the area of colocalization of PrP^C and N-cadherin is 32.228 ± 3.387% at DIV7, 38.666 ± 4.888% at DIV10, 33.105 ±4.188% at DIV14, and 37.806 ± 3.099% at DIV21. The percentage of the area of colocalization of PrP^C and N-cadherin does not change significantly. Statistical analysis was performed by One Way ANOVA (n = 17 cells (DIV7), 15 (DIV10), 14 (DIV14), 17 (DIV21); 3 independent experiments) (**D**) Quantification of the percentage of the area of colocalization between neuroligin-2 and PrP^C at F-actin hotspots in dissociated hippocampal neurons at DIV7, 10, 14, and 21. The median percentage of the area of colocalization of PrP^C and neuroligin-2 is 45.955 ± 5.804% at DIV7, 39.558 ± 3.372 at DIV10, 57.628 ± 4.85 at DIV14, and 41.662 ± 4.256 at DIV21. Between DIV 10 and 14, the percentage of the area of colocalization of PrP^C and neuroligin-2 does increase significantly. Statistical analysis was performed by One Way ANOVA (*p < 0.05) (n = 12 cells (DIV7), 11 (DIV10), 11 (DIV14), 11 (DIV21); 3 independent experiments).
All results in figure 3.9 are plotted in box-and-whiskers plots, with the line showing the median and the cross the mean. (*p < 0.05, **p < 0.01).

Colocalization of PrP^C with neuroligin-2 or N-cadherin at F-actin hotspots could be observed for all time points analyzed. Furthermore, the intensity of PrP^C at F-actin hotspots during the development of disassociated hippocampal neurons was analyzed, the results are shown in figure 3.9B. PrP^C intensity at F-actin hotspots increased from DIV7 to DIV14 by approximately 40%. The percentage of the area of colocalization was measured for PrP^C and N-cadherin or neuroligin-2, see figures 3.9C and D. Between PrP^C and N-cadherin the percentage of the area of colocalization did not change significantly during the development, it was around 30% to 40%. Meanwhile, the percentage of the area of colocalization between PrP^C and neuroligin-2 did increase by around 30% from approximately 40% at DIV10 to over 55% at DIV14.

These results demonstrated that PrP^C colocalizes with N-cadherin and neuroligin-2 at F-actin hotspots over neuronal maturation in DIV7 to DIV21 hippocampal neurons to a similar extent. However, the levels of PrP^C appear to increase in a time window when synaptogenesis occurs and further stay high after synapse maturation at DIV21.

3.5.2 PrP^C co-transport with interaction partners

Since PrP^C and N-cadherin colocalization could be observed in dendrites at non-synaptic sites, this raised the question whether both interaction partners also would undergo vesicular co-transport. To this end, first YFP-PrP^C and monomeric red fluorescent protein (mRFP)-N-cadherin fluorescent fusion proteins were expressed in

N2a cells and imaged 24 h after transfection. Time-lapse videos were acquired in SDC and TIRF mode at a live cell imaging microscope. Indeed, moving particles co-labeled for YFP-PrP^C and mRFP-N-cadherin fluorescence could be observed in TIRF as well as in SDC settings, an example of frames from TIRF imaging is shown in figure 3.10A. It depicts a mobile particle that is positive for both mRFP-N-cadherin and YFP-PrP^C fluorescence.

Several events of this type could be observed in TIRF mode. Since the setting only allowed excitation of molecules within regions less than 100 nm away from the plasma membrane, both mRFP-N-cadherin and YFP-PrP^C are transported within the same vesicles at the cellular cortex. Frequently, events of vesicular co-transport of mRFP-N-cadherin and YFP-PrP^C were also observed at SDC mode at the more equatorial regions of N2a cell bodies (data not shown). Therefore both, mRFP-N-cadherin and YFP-PrP^C, are also co-transported in vesicles within the central cellular cytoplasm. Because co-transport could be observed in N2a cells, dissociated hippocampal neurons were transfected with the same plasmids at DIV12 and imaged on DIV14 by using SDC time-lapse microscopy. The videos frequently showed vesicles co-labeled for YFP-PrP^C and mRFP-N-cadherin. Kymographs were generated from the movies to better illustrate these co-transport events, an example is shown in figure 3.10B. Some particles were co-labeled for mRFP-N-cadherin and YFP-PrP^C, while others were only positive for one of the fluorescently-labeled proteins. It was published that N-cadherin binds GRIP1 (Heisler et al. 2014). GRIP1 is an adaptor protein that binds the motor protein KIF5, regulates the transport of different synaptic proteins, and their turnover during synaptic plasticity (Setou et al. 2002; Geiger et al. 2014). To determine whether PrP^C interacts with GRIP1, IPs from whole mouse brains were performed. The IPs were analyzed by western blot, as shown in figure 3.10C.

Indeed, PrP^C and N-cadherin were co-immunoprecipitated with GRIP1, while the unspecific IgG control did not show bands for either protein. Vice versa, IPs with PrP^C-specific antibodies from the whole mouse brain were performed to validate PrP^C binding to GRIP1. Indeed, GRIP1 co-precipitated with PrP^C as shown in figure 3.10D. These findings indicate that PrP^C and GRIP1 interact within the mouse brain. To further investigate a potential role of GRIP1 in PrP^C vesicle trafficking, neurons expressing YFP-PrP^C and mRFP-GRIP1 were used to investigate potential vesicular co-transport of PrP^C and GRIP1.

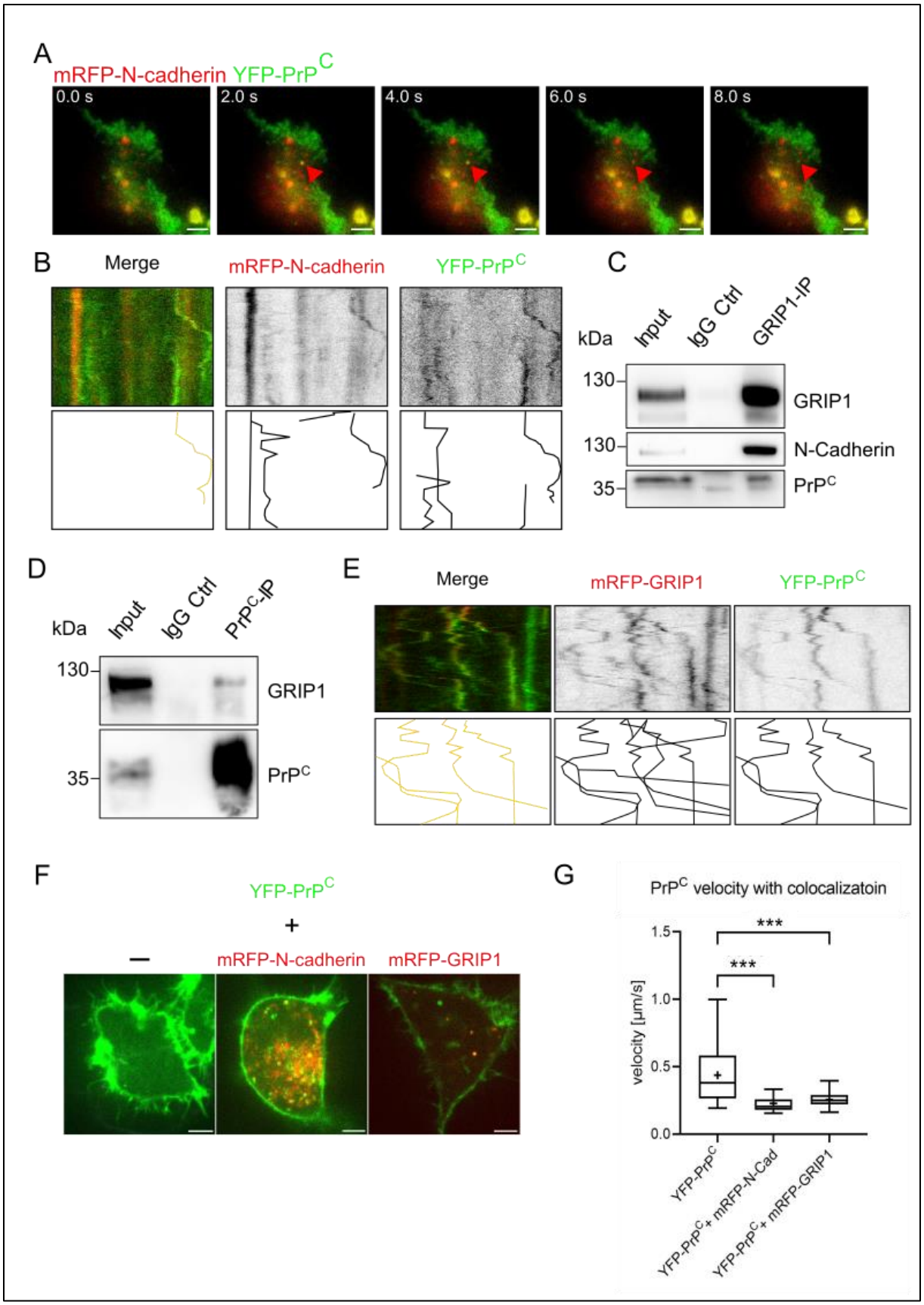

Figure 3.10: PrP^C co-transport with interaction partners. (**A**) Frames from time-lapse TIRF microscopy of N2a cells expressing mRFP-N-cadherin and YFP-PrP^C. Arrows show a double labeled vesicle entering the focal TIRF plane over time. The scale bar represents 5 µm. (**B**) A kymograph generated

from SDC time-lapse microscopy of DIV14 dissociated hippocampal neurons expressing mRFP-N-cadherin and YFP-PrP^C. Kymographs from individual channels are shown in inverted greyscale on the right, while the merge is shown on the right. Below the kymographs, illustrations to better visualize YFP-PrP^C and mRFP-N-cadherin particle trajectories are shown. For the merge, only the colocalized tracks are shown. (**C and D**) Western blot analysis of representative IPs from whole adult mouse brain lysates. Brains from adult mice were lysed (input) and incubated with magnetic beads coupled to unspecific IgG (IgG Ctrl) or antibodies specific for GRIP1 (C) or PrP^C (D). Markers are displayed on the left. (**C**) The input from the whole lysate shows bands for GRIP1 at 130 kDa, N-cadherin at 130 kDa, and PrP^C at roughly 35 kDa. In the IgG ctrl lane, no specific bands are detected. In the GRIP1-IP lane, all three proteins are detected (n=3 independent experiments). (**D**) The input from the whole lysate shows bands for GRIP1 at 130 kDa and PrP^C at roughly 35 kDa. In the lane from the IgG ctrl, no specific bands are visible. In the PrP^C-IP, both proteins are detected (n=3 independent experiments). (**E**) A kymograph generated from SDC time-lapse microscopy of DIV14 dissociated hippocampal neurons co-expressing YFP-PrP^C and mRFP-GRIP1. Inverted kymographs generated from individual channels are shown on the right, the merge is shown on the left. To better visualize mRFP-GRIP1 and YFP-PrP^C particle trajectories, they were traced for the individual channels as shown below the kymographs, in the merge only colocalized tracks are illustrated. (**F**) N2a cells were transfected with YFP-PrP^C alone, or together with mRFP-N-cadherin or mRFP-GRIP1. The scale bar indicates 5 µm. (**G**) The box-and-whisker plot shows the velocities of YFP-PrP^C particles alone or co-labeled with mRFP-N-cadherin (mRFP-N-Cad) or mRFP-GRIP1. The median is represented by a line, while a cross indicates the mean. YFP-PrP^C alone has a velocity of 0.38 ± 0.039 µm/s, compared to 0.205 ± 0.015 µm/s with mRFP-N-cadherin and 0.250 ± 0.011 µm/s for mRFP-GRIP1 co-labeled particles. The velocities of vesicles co-labeled with YFP-PrP^C and mRFP-N-cadherin or mRFP-GRIP1 are reduced compared to vesicles containing only YFP-PrP^C. Kruskal-Wallis one way ANOVA on ranks with Dunn's Post Hoc test was performed as statistical analysis (***$p < 0.001$). (n= 30 particles (YFP-PrP^C), 14 (YFP-PrP^C and mRFP-NCad), 30 (YFP-PrP^C and mRFP-GRIP1); 3 independent experiments).

At DIV14, 48 h after transfection, the cells were imaged using SDC time-lapse microscopy. In the acquired videos, transport vesicles frequently containing YFP-PrP^C and mRFP-GRIP1 were observed. Kymographs were generated from the videos to visualize the co-transport; one example is shown in figure 3.10E. It shows multiple vesicles positive for YFP-PrP^C and mRFP-GRIP1, indicating that these fluorescently labeled proteins are co-transported in neurons.

Finally, N2a cells were transfected with plasmids coding for YFP-PrP^C, either alone, or together with plasmids containing either mRFP-N-cadherin or mRFP-GRIP1. The transfected cells were recorded using SDC time-lapse microscopy, examples of single frames are shown in figure 3.10F. They show that YFP-PrP^C labeled particles could be observed that were co-labeled for mRFP-N-cadherin or -GRIP1. However, particles without co-labeling, only containing YFP-PrP^C or mRFP-tagged proteins were also

detected. The velocities of particles co-labeled for both YFP-PrP^C and mRFP-N-cadherin or -GRIP1 were analyzed. As control, the velocities of only YFP-PrP^C labeled particles were analyzed in N2a cells only expressing YFP-PrP^C. The results were plotted in figure 3.10G. The velocity of YFP-PrP^C and mRFP-GRIP1 co-labeled particles was reduced by approximately 40% compared to YFP-PrP^C particle velocity. The velocity of particles co-labeled with mRFP-N-cadherin and YFP-PrP^C was also significantly reduced by almost 50% compared to the velocity of particles only labeled with YFP-PrP^C.

Together, these experiments show that PrP^C is co-transported with N-cadherin in N2a cells and in neurons. GRIP1, a known regulator of N-cadherin transport, also interacts with PrP^C. PrP^C is co-transported with GRIP1 in transport vesicles in N2a cells and in neurons. The overexpression of fluorescently tagged N-cadherin or GRIP1 reduced the transport velocity of PrP^C vesicles co-labeled for either of the two proteins.

3.5.3 PrP^C overexpression affects N-cadherin targeting to endolysosomal compartments

PrP^C undergoes constant internalization and is trafficked toward endosomes, from where it can be recycled, degraded, stored, or released on exosomes (Aguzzi et al. 2008; Alves et al. 2020). N-Cadherin is also internalized and transported toward endosomes from where it can be stored, recycled, or degraded in lysosomes (Tai et al. 2007). These processes are important for N-Cadherin-mediated plastic changes at synapses. Because N-cadherin and PrP^C are co-transported it was hypothesized that PrP^C might be involved in regulating the endocytic trafficking of N-cadherin. To investigate the potential effects the proteins may have on each other on the targeting to endolysosomal compartments, they were overexpressed in hippocampal neurons and their localizations were investigated by immunocytochemistry.

DIV14 dissociated hippocampal neurons expressing either YFP-PrP^C or YFP as control were stimulated with the protocols to chemically induce synaptic plasticity as described before (Otmakhov et al. 2004; Bhattacharyya et al. 2009). Unstimulated cells were used as control. After stimulation, the cells were fixed and immunocytochemically stained for TSG101, Lamp1, and N-cadherin. Figure 3.10A shows a representative image of an immunocytochemically stained neuron expressing YFP-PrP^C. The intensities of N-cadherin at TSG101 or Lamp1 compartments at the soma were analyzed, the results are shown in figures 3.10B and C.

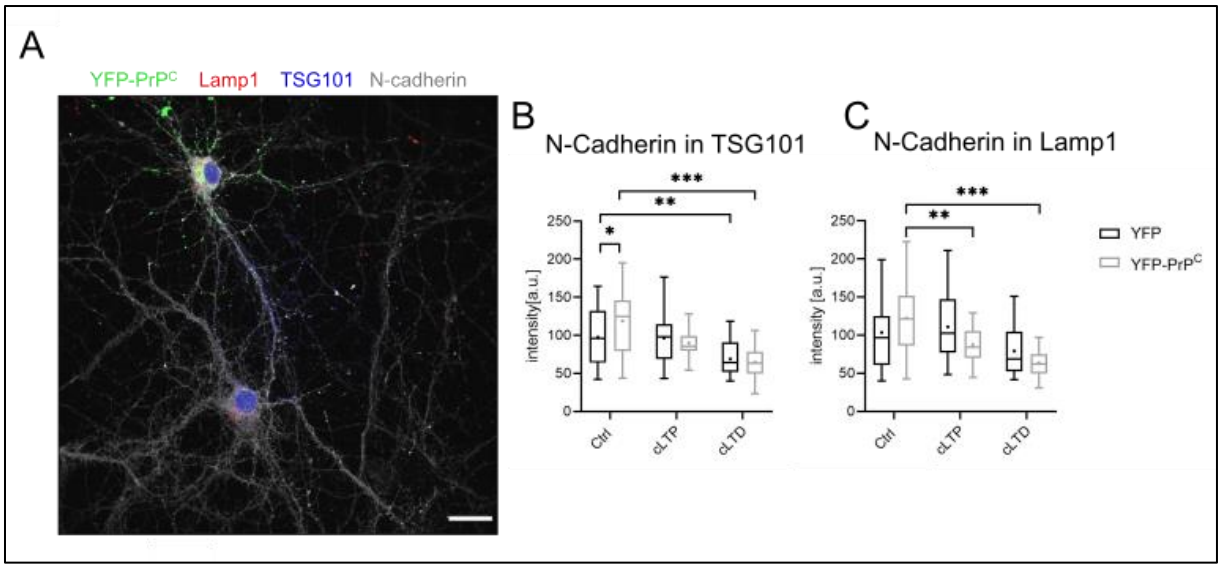

Figure 3.11: N-cadherin localization to endolysosomal compartments following PrP^C overexpression. (**A**) DIV14 dissociated hippocampal neurons immunochemically stained for TSG101, Lamp1, and N-cadherin are shown. YFP-PrP^C is expressed in the upper neuron. The scale bar represents 20 µm. (**B)** Quantification of N-cadherin intensity in TSG101-positive compartments in YFP-PrP^C or YFP overexpressing cells in ctrl, cLTP, or cLTD conditions. N-cadherin median intensity in TSG101-labeled compartments in YFP overexpressing cells is 95.879 ± 7.270 in ctrl conditions, 98.003 ± 6.278 in cLTP, and 63.963 ± 4.478 in cLTD conditions. In cells overexpressing YFP-PrP^C, N-cadherin intensity in TSG101-labeled compartments is 124.963 ± 6.986 in ctrl, 85.72 ± 3.435 in cLTP, and 63.486 ± 3.76 in cLTD conditions. N-Cadherin intensity in TSG101-labeled compartments is significantly increased in ctrl conditions in neurons overexpressing YFP-PrP^C compared to YFP-expressing cells. Meanwhile, N-cadherin intensity in the same compartments is reduced in cLTD conditions compared to ctrl in both YFP and YFP-PrP^C overexpressing cells (n (YFP)= 27 cells (ctrl), 28 (cLTP), 26 (cLTD); n (YFP-PrP^C) = 32 cells (Ctrl), 26 (cLTP), 28 (cLTD); 5 independent experiments). (**C**) Quantification of N-cadherin intensity in Lamp1-positive compartments with YFP-PrP^C or YFP overexpression in ctrl, cLTP, or cLTD conditions. N-cadherin median intensity in Lamp1-labeled compartments in YFP overexpressing cells is 96.488 ± 8.965 in ctrl conditions, 102.419 ± 7.752 in cLTP, and 68.769 ± 5.798 in cLTD conditions. In cells overexpressing YFP-PrP^C, N-cadherin intensity in Lamp1-labeled compartments is 121.218 ± 7.433 in ctrl, 84.144 ± 4.053 in cLTP, and 62.499 ± 3.810 in cLTD conditions. N-Cadherin intensity in Lamp1-positive compartments is significantly reduced after the chemical induction of synaptic plasticity compared to ctrl conditions in YFP-PrP^C overexpressing neurons (n (YFP)= 27 cells (ctrl), 31 (cLTP), 29 (cLTD); n(YFP-PrP^C) = 33 cells (Ctrl), 29 (cLTP), 27 (cLTD); 5 independent experiments). All plots in figure 3.11 represent box-and-whiskers plots, with the line showing the median and the dot the mean. To test for statistical significance between the ctrl, cLTP, and cLTD conditions the Kruskal-Wallis ANOVA on ranks was used, while statistical significance between YFP and YFP-PrP^C overexpressing cells was assessed by using the Mann-Whitney U test for all data shown in this figure (*$p < 0.05$, **$p < 0.01$, ***$p < 0.001$).

In TSG101 compartments, N-cadherin intensity was significantly increased by over 20% when overexpressing PrP^C compared to the YFP control in control conditions. Meanwhile, N-cadherin intensity was reduced in TSG101 compartments in cLTD conditions by approximately 35% in cells overexpressing YFP and by almost 50% in cells overexpressing YFP-PrP^C compared to control conditions. In Lamp1 compartments, however, N-cadherin intensity was decreased by over 45% after cLTD and 30% after cLTP induction compared to untreated control conditions, but only for neurons overexpressing YFP-PrP^C while no changes were observed for YFP overexpressing cells after synaptic plasticity induction. The reverse experiment was performed by overexpressing mRFP-N-cadherin or mRFP as control, these results are not shown. Here, PrP^C intensity did not change significantly between mRFP-N-cadherin and mRFP overexpression following the induction of synaptic plasticity.

These data show that elevated PrP^C levels lead to an increase in the amount of N-cadherin localized to endosomes. However, the effect of increased N-cadherin localization to endosomes in PrP^C overexpressing cells without stimulation was no longer observed after induction of synaptic plasticity. When inducing cLTD, N-cadherin intensity was decreased in TSG101-labeled compartments in both YFP and YFP-PrP^C expressing cells, although the intensity was slightly further decreased in YFP-PrP^C overexpressing cells compared to control conditions. In contrast, N-cadherin lysosomal intensity was reduced in synaptic plasticity conditions only when PrP^C was overexpressed. Together these results indicate that PrP^C influences N-cadherin endosomal and lysosomal targeting.

4. Discussion

PrP^C is a ubiquitously expressed protein with high expression levels in neurons and glial cells of the nervous system (Bendheim et al. 1992). It plays a physiological role in neurite outgrowth, neuroprotection during oxidative stress, apoptosis during ER stress, copper ion binding, synaptic plasticity, peripheral myelination, and regulation of sleep pattern (Kanaani et al. 2005; Linden et al. 2008; Bounhar et al. 2001; Roucou et al. 2005; Vassallo and Herms 2003; Brown et al. 1997; Laurén et al. 2009). PrP^C was also implicated in the regulation of intracellular vesicle formation, thus regulating signaling (Aguzzi et al. 2008). This thesis aimed to elucidate the role of PrP^C at the synapse, during synaptic plasticity processes, and for its transport and sorting into endolysosomal compartments. The following chapter will provide a detailed discussion of the key findings of this thesis.

4.1 The role of PrP^C at the synapse and in synaptic plasticity

The first aim of this thesis was to investigate the role of PrP^C at the synapse. The predominant synaptic localization of PrP^C has been shown previously by electron micrographs, western blots, and confocal microscopy in dendritic postsynaptic regions and brain slices (Salès et al. 1998; Moya et al. 2000; Kretzschmar et al. 2001; Um et al. 2012; Herms et al. 1999). Here, to investigate the role of PrP^C, dissociated hippocampal neurons grown on glass coverslips were used. This allowed studying PrP^C expression on the single cell level, reducing the possibility of overlapping dendrites or axons, which could obscure the results of the confocal microscopy. Although one could argue that these conditions are different from the endogenous *in vivo* environment in the brain, a single layer of neurons makes cellular observations easier by the reduction of the background in the microscopy images. The investigation of the localization of proteins to a specific compartment such as the synapse is more straightforward in neurons grown in a single layer compared to brain slices, where while the neurons did develop in the endogenous environment, but, due to the thickness of the slices, individual dendrites or synapses are very difficult to distinguish. The results of the confocal microscopy show that PrP^C does localize to inhibitory and excitatory synapses in dissociated hippocampal neurons. Mature mouse dissociated hippocampal neurons were immunochemically stained for excitatory and inhibitory synaptic markers and co-labeled for PrP^C. It was shown that PrP^C fluorescence did overlap with synaptic marker proteins, such as F-actin, presynaptic synaptophysin, and

postsynaptic PSD95. These novel results suggest that PrP^C localizes to inhibitory and excitatory synapses in line with the current view that PrP^C is a synaptic protein. However, PrP^C has not been shown to localize to synaptic regions using confocal microscopy in dissociated neuronal cells. The results of the surface staining of PrP^C sustain and further expand these findings, showing that PrP^C is enriched at the synaptic membrane rather than the extrasynaptic membrane. In this work, PrP^C colocalized with synaptophysin and F-actin, defined as synapses here. To investigate synapses using ICC staining, both a pre- and postsynaptic marker should be chosen to certify the localization of PrP^C, and those were used in the following experiments. While the staining of an additional synaptic marker such as PSD95 would have underlined these findings even more, synaptophysin is enriched in the presynaptic region, while F-actin is enriched at both pre- and postsynaptic regions and a colocalization at their hotspots is an indicator for synaptic regions (Matus et al. 1982; Wiedenmann and Franke 1985; Halpain et al. 1998). PrP^C has been described in the formation and extension of filopodia in N2a cells and developing neurons (Schrock et al. 2009; Santos et al. 2013). In this current work, only 20% of protrusions in adult dissociated hippocampal neurons were positive for PrP^C. These results do not contradict each other, since the protrusions (F-actin hotspots without co-labeling of synaptophysin) observed in the dissociated hippocampal neurons were not further characterized. F-actin hotspots at dendrites most likely represent filopodia but, due to limitations in confocal microscopy, F-actin expressed in axons near the observed dendrite or overlapping dendrites could also appear as F-actin hotspots. PrP^C is a known interaction partner of NCAMs and here it was described for the first time that it also interacts with N-cadherin and neuroligin-2. All three molecules are important cell adhesion molecules that play essential roles in neurogenesis and the formation of synapses (Santuccione et al. 2005; Brusés 2006; Chih et al. 2005). So far, PrP^C has not been directly linked to functions at the inhibitory synapses, but prior findings indicated that PrP^C KO in mice leads to weakened $GABA_A$ receptor-mediated fast inhibition (Collinge et al. 1994). In this thesis, it was shown that PrP^C colocalized with gephyrin and VGAT in mature dissociated hippocampal neurons. This now strongly supports the presence of PrP^C at inhibitory synapses and is further supported by immunoprecipitation experiments conducted in this work. The co-precipitation of neuroligin-2 with PrP^C underlines a direct interaction of the two proteins at inhibitory synapses. To further elucidate the role of PrP^C at inhibitory synapses, a surface

staining of PrP^C with inhibitory marker proteins in dissociated neurons could confirm a role of PrP^C at inhibitory synapse membranes. It has been shown that PrP^C interacts with glutamate receptors like AMPA and mGluR5 receptors, (Um et al. 2013; Watt et al. 2012), therefore the interaction of PrP^C with GABA receptors would be interesting to investigate in future research. Several hypotheses have been published to date, including PrP^C involvement in neuronal transmission, cell adhesion, and neuroprotection (Curtis et al. 2003; Criado et al. 2005; Maglio et al. 2006; Caiati et al. 2013; Kishimoto et al. 2020; Matamoros-Angles et al. 2022; White et al. 1999; Carulla et al. 2015; Schrock et al. 2009; Málaga-Trillo et al. 2009; Brown et al. 1999). To discern the specific role PrP^C plays in each of those processes, further investigations are required.

Synaptic plasticity refers to changes in a synapse's efficacy in an activity-dependent manner (Bear et al. 2016). The localization of PrP^C to excitatory synapses is reinforced by the fact that chemically induced synaptic plasticity influences PrP^C localization and transport. Since PrP^C is a synaptic protein and some PrP^C KO mouse models showed impaired synaptic plasticity, it was of interest to see, how PrP^C localization and transport changes with synaptic plasticity induction. Investigating whole and surface PrP^C at synaptic regions with ICC staining after the induction of synaptic plasticity revealed a significant reduction in fluorescence labeled PrP^C intensity after the induction of cLTD compared to control conditions. However, no significant changes were observed in PrP^C intensities in cLTP compared to control conditions. The results were similar in surface and whole PrP^C protein staining, indicating that PrP^C is reduced on the synaptic membrane as well as in post- or presynaptic regions. This is in line with the hypothesis that PrP^C localization is affected by synaptic plasticity. These experiments provide a novel insight into the behavior of PrP^C after the induction of synaptic plasticity. It is worth mentioning that the antibody used for surface staining was recently shown to induce PrP^C clustering at the membrane followed by its internalization. However, these experiments were done in N2a cells over 18 h at 37 °C and cannot be directly translated to dissociated hippocampal neurons treated with the same antibody for 2 h at 4 °C (Linsenmeier et al. 2021). In addition, the internalization inducing effect of this antibody would be expected to cause a decrease in PrP^C for all conditions analyzed, however, the intensity of PrP^C was specifically reduced after cLTD induction compared to control conditions. Furthermore, a similar effect was observed when labeling whole PrP^C, indicating that this reduction was due to the induction of

cLTD. Surprisingly, PrP^C did not change significantly at the synapse after cLTP induction compared to control conditions. However, reproducing synaptic plasticity chemically is difficult. Thus, it is possible that the cells were not sufficiently stimulated to observe any specific effects. Synaptic plasticity is an effect that concentrates on one synapse. With chemical induction, however, the whole neuron is stimulated, therefore possibly reducing the effect at the synapse, because proteins need to be distributed between all synapses simultaneously. PrP^C is cleaved by the a-disintegrin-and-metalloproteinase 10 (ADAM10) (Altmeppen et al. 2011). ADAM10 is a cell surface protease, acting as an α-secretase and is involved in the proteolytic processing of various membrane proteins, including cytokines, growth factors, and adhesion molecules (Seals and Courtneidge 2003; Schlöndorff and Blobel 1999). The activity of ADAM10 is increased with LTD induction while ADAM10 is internalized during LTP (Musardo et al. 2014). PrP^C can undergo multiple forms of proteolytic processing, including α-cleavage and shedding. The α-cleavage takes place between amino acids 109 and 110, resulting in a soluble N1 fragment and a truncated membrane-attached C1 fragment (Altmeppen et al. 2012; McDonald and Millhauser 2014). On the other hand, shedding takes place between amino acids 228 and 229 only three amino acids removed from the GPI anchor, leading to the release of the full length form of PrP^C (Altmeppen et al. 2011; Taylor et al. 2009; Endres et al. 2009). Involvement of ADAM10 has been suggested in both processes in previous publications (Taylor et al. 2009; Endres et al. 2009; Altmeppen et al. 2011; Altmeppen et al. 2012; McDonald and Millhauser 2014; Wik et al. 2012). ADAM10 may very well process PrP^C at the plasma membrane after cLTD induction, while PrP^C would be unchanged after cLTP induction. Since the antibodies used in both experiments to label PrP^C (proteintech, 12555-1-AP; POM2 (Polymenidou et al. 2008)) have binding sites at the N-terminal region, they would not bind to the truncated C1 fragment left over by the α-cleavage, so it cannot be deduced if the PrP^C signal is reduced due to cleavage or shedding (Linsenmeier et al. 2021). PrP^C could either be completely shed from the plasma membrane, or it might be cleaved with the C1-terminal still attached to the membrane. It is also known that PrP^C interacts with AMPA receptors (Watt et al. 2012) and it has been shown in this work that PrP^C also interacts with N-cadherin. The internalization of both of these proteins is crucial during the induction of LTD (Carroll et al. 1999; Heynen et al. 2000; Tai et al. 2007). The full length PrP^C may stabilize synaptic proteins like N-cadherin and AMPA receptors at the synapses. The processing of PrP^C by either cleavage or

shedding may destabilize this interaction complex and lead to an internalization of these proteins. On the other hand, the internalization of its interaction partners could lead to the internalization of PrP^C and thus, PrP^C intensity would be reduced at the synapse under cLTD conditions. Nonetheless the induction of cLTD influences PrP^C localization at the synapse. Further research is required to establish whether the concentration of PrP^C at the synapse is reduced due to cleavage or shedding by for example ADAM10 or by endocytosis together with its cooperation partners. It will be interesting to see how the reduction of either will influence the function of PrP^C.

The active transport of YFP-PrP^C was investigated in dissociated hippocampal neurons since changes in PrP^C concentration at the synapse were not only observed at the synaptic membrane but also for the whole PrP^C at synaptic regions. Synaptic plasticity leads to changes in protein compositions at the synapse by removing or targeting proteins to synaptic sites. It depends on receptor transport in response to changes in synaptic activity (Collingridge et al. 2004; Hirokawa and Takemura 2004; Kennedy and Ehlers 2006; Caviston and Holzbaur 2006; Maas et al. 2009). However, to date, the effect of synaptic plasticity on active vesicular transport of synaptic proteins has not been investigated. PrP^C active transport is especially interesting, as it is known that PrP^C interacts with the GluA1 and GluA2 subunits of AMPA receptors (Watt et al. 2012). In this thesis, active transport of YFP-PrP^C was investigated in dissociated hippocampal neurons. While the number of stationary and moving particles, as well as their directionality, did not change, moderate changes in mean velocities could be observed between cLTD and control conditions. These changes were only observed when discounting pauses, suggesting that the motor proteins were affected in their processivity after the induction of cLTD. This might be due to changes in MAPs binding to MTs or PTMs of the motor proteins or to adaptor proteins that affect motor protein activity (Maas et al. 2009; Aiken and Holzbaur 2021). The motor proteins kinesin and dynein can be posttranslationally modified, which affects their function. The best studied PTM is phosphorylation, which can affect the binding of motor proteins to adaptor proteins (Guillaud et al. 2008). Some MAPs such as MAP9 can enhance motor protein processivity, while others, for example, the tau protein, will slow down kinesin transport (Monroy et al. 2020). Studies have suggested that MAPs expression and phosphorylation are affected by synaptic plasticity (Cuveillier et al. 2021; Takei et al. 2015; Avila et al. 1994). Adaptor proteins such as GRIP1 can also be affected by synaptic plasticity. The phosphorylation of GluA2 enhances GRIP1-AMPA receptor

binding and AMPA receptor insertion into the synaptic membrane (Tan et al. 2020). Together these complex mechanisms can influence the processivity with which transport complexes move along MTs after the induction of synaptic plasticity. In the experiments presented here, PrP^C was overexpressed with a fluorescent protein attached. This could lead to different transport characteristics compared to endogenous PrP^C. However, this method is an established way to investigate protein transport, which needs to be visualized. Measuring the velocity of YFP-PrP^C particles was complicated somewhat by the disappearance of particles from the observed plane, and thus could not be further investigated. On the other hand, particles could also move into the observed plane, thus, more particles could be studied. This phenomenon was observed under control and cLTD conditions and one can reason that it did therefore not affect the outcome significantly. These results reinforce the hypothesis that active transport is affected by synaptic plasticity. The induction of cLTP did not result in any significant changes compared to control conditions. This could be due to a default of the applied protocol in the experiments for this thesis. One could envision testing different cLTP protocols to investigate whether the lack of significant results here was associated with the protocol used, or whether this condition does not influence the localization and active transport PrP^C.

Taken together, this work shows convincingly that PrP^C localizes to excitatory and inhibitory synapses. PrP^C was present at most excitatory synaptic sites and enriched at the synaptic membrane. It was shown for the first time that PrP^C localization to synaptic regions was reduced after the induction of cLTD. Furthermore, this work corroborated that active transport of the synaptic protein PrP^C was altered by the induction of synaptic plasticity.

4.2 The overexpression of htau has no effect PrP^C dendritic transport

Synaptic plasticity is impaired in neurodegenerative diseases such as AD (Cuestas Torres and Cardenas 2020; Skaper et al. 2017; Benarroch 2018; Calabresi et al. 2007). AD is characterized at the molecular level by intracellular neurofibrillary tangles and extracellular amyloid plaques (Grundke-Iqbal et al. 1986). Neurofibrillary tangles are composed of hyperphosphorylated tau, an MT-associated protein that mainly binds to axonal MTs, regulating their stability and therefore axonal transport. The hyperphosphorylation of tau may interfere with cellular transport resulting in synaptic

dysfunction (Ittner and Ittner 2018). Tau is also missorted into the somatodendritic compartments in AD (Lee et al. 2001).

Since transport is important for synaptic function and changes in PrP^C transport were observed after the induction of synaptic plasticity, the effect of htau overexpression on active PrP^C transport was investigated. The overexpression of htau leads to aggregation and hyperphosphorylation of the protein (Andorfer et al. 2003). Dissociated hippocampal neurons were co-transfected with YFP-PrP^C and either ECFP-htau or ECFP as a control. ECFP-htau was diffusely present in axons and dendrites, as well as in the soma, as expected according to the literature (Lee et al. 2001). Since dendritic transport was the focus of this work, PrP^C transport vesicles were investigated in dendrites. Interestingly, no changes in YFP-PrP^C transport could be observed. This was an unexpected finding since htau should destabilize MT, making transport less processive, leading to longer pauses and slower transport (Ittner and Ittner 2018). In this work, the overexpression led to ECFP-htau accumulation in dendrites. However, the destabilization of MTs by htau or hyperphosphorylated tau was primarily described for axons. This might explain why no effect on PrP^C transport after overexpression of htau was observed. However, these results indicate that transport in dendrites is less affected by tau hyperphosphorylation, which might be interesting for future studies. Further studies are needed to investigate how the overexpression of htau affects the axonal transport of PrP^C.

4.3 Synaptic plasticity influences PrP^C targeting to endolysosomal compartments

The effect of PrP^C targeting to endolysosomes was investigated since it was shown in this work that the induction of synaptic plasticity influenced PrP^C localization to the synapse as well as its transport. PrP^C is rapidly internalized from the cell membrane by multiple pathways (Taylor et al. 2005; Taylor and Hooper 2006; Peters et al. 2003; Prado et al. 2004; Vorberg 2019; Aguzzi et al. 2008). After internalization, PrP^C is transported to early endosomes from where it is either recycled back to the plasma membrane or the early endosomes may mature to MVBs. In the MVBs, PrP^C can either be degraded in lysosomes or be released on exosomes (Borchelt et al. 1990; Campana et al. 2005; MacDermott et al. 1986; Mays and Soto 2016). These pathways could be important for PrP^C function. The investigation of whole PrP^C in endosomal and lysosomal compartments with ICC staining after the induction of synaptic plasticity

revealed a reduction in immunofluorescently-labeled PrP^C intensity after the induction of cLTD compared to control conditions in endosomal and lysosomal compartments, while no significant changes could be observed in PrP^C intensities in cLTP compared to control conditions. These findings in endosomal and lysosomal compartments are reminiscent of the findings at the synapse: PrP^C intensity is reduced after the induction of cLTD compared to control conditions. These results indicate a redistribution of PrP^C after the induction of cLTD. The concentration of PrP^C in endolysosomal compartments during synaptic plasticity induction was not investigated previously, but these results are in line with other research that showed that endosomes play an important role during synaptic plasticity (Park et al. 2016; Parkinson and Hanley 2018). While AMPA receptors are reported to be increasingly sorted into endolysosomal compartments during LTD, PrP^C levels appear to be decreased in these compartments. The inward transport for PrP^C containing vesicles is decelerated, thus, this may be an explanation for the lower levels of PrP^C detected in endosomes and lysosomes. Instead, PrP^C might be stored in recycling compartments in dendrites. On the other hand, the internalization of its interaction partners N-cadherin and AMPA receptors in LTD conditions might alleviate the anchoring of PrP^C at the synapse leading to its diffusion along the membrane (Carroll et al. 1999; Heynen et al. 2000; Tai et al. 2007). Another possibility is that PrP^C is released either on exosomes or by ADAM10-dependent shedding PrP^C, as discussed in the previous section, reducing the overall concentration of PrP^C in the neurons (Altmeppen et al. 2011; Taylor et al. 2009; Endres et al. 2009; Hartmann et al. 2017). The release of exosomes is regulated by Ca^{2+}-dependent mechanisms (Savina et al. 2003). Both LTD and LTP require an elevation of intracellular Ca^{2+} (Artola and Singer 1993; Cummings et al. 1996). These circumstances suggest that PrP^C concentration in endosomal and lysosomal compartments might be decreased due to the enhanced release on exosomes after the induction of synaptic plasticity, which leads to an increase in intracellular Ca^{2+}. Even though no significant changes in PrP^C intensity in endosomal and lysosomal compartments were observed after the induction of cLTP, the level of PrP^C intensity was lower than under control conditions by trend. It is possible that the experimental conditions were not stringent enough to induce a significant effect. The decrease after the induction of both cLTD and to a lesser extent in cLTP could be due to the enhanced release of PrP^C carrying exosomes. As described before, using the protocol for cLTP in this work did not yield significant results in any of the experiments described, thus it

may be worthwhile to use different protocols in subsequent studies. Nevertheless, PrP^C concentration in the neurons could also be reduced by shedding or cleavage of PrP^C from the plasma membrane by ADAM10. Synaptic plasticity affects ADAM10 localization and activity. During LTD, ADAM10 is increasingly presented at the cell surface and its activity is stimulated. Conversely, LTP promotes ADAM10 endocytosis (Musardo et al. 2014). PrP^C is usually constantly internalized and transported to endosomes, from where it can be recycled, degraded, or released on exosomes (Borchelt et al. 1990; Campana et al. 2005; Taylor et al. 2005; Aguzzi et al. 2008). Removal from the plasma membrane would result in a decrease of internalization of PrP^C in the endosomal pathway. Therefore, intracellular PrP^C would be reduced. Another possibility is that if PrP^C is cleaved by ADAM10, the antibody used for the staining of PrP^C (proteintech, 12555-1-AP) does not detect the remaining C1 fragment attached to the membrane. The C1 fragment is possibly internalized and moves along the endosomal route, but it would not be detected by the antibody used in this work. Since ADAM10 can either cleave or lead to the shedding of PrP^C, it cannot be determined here, if PrP^C is shed or simply cleaved and the remaining C1 fragment is internalized. The use of antibodies like POM1, specific for the C1 fragment of PrP^C, together with an antibody that only recognizes full length PrP^C might elucidate this circumstance (Polymenidou et al. 2008; Linsenmeier et al. 2021). It would be interesting if ICC experiments with antibodies like POM1 would yield similar results as those of the antibodies directed against full length PrP^C.

However, PrP^C is reduced in endosomal and lysosomal compartments, and this fits well with the reduction of full length PrP^C at the synapse after the induction of cLTD compared to untreated cells. The reduced PrP^C intensity may be due to an increased release of PrP^C either by the endocytic pathway as exosomes or at the plasma membrane by ADAM10 cleavage. Both possibilities could occur at the same time during cLTD, increasing the effect of cLTD on the localization of PrP^C.

GW4869 was used to inhibit the nSMase, which is important for the ceramide pathway and involved in endosome maturation into MVB. In addition, GW4869 was reported to decrease the number of exosomes released from MVBs (Essandoh et al. 2015). In this work, the application of GW4869 caused a significant decrease in PrP^C intensities in TSG101- and Lamp1-positive compartments compared to DMSO control conditions (figure 3.6). The decrease in PrP^C intensity in endosomal and lysosomal compartments

persisted in GW4869-treated neurons with cLTD induction compared to control conditions. Gou et al. (2015) showed that packaging of PrP^C into exosomes depends partly on nSMase and is reduced with GW4869 treatment compared to controls (Guo et al. 2015). This indicates that PrP^C intensity is not reduced due to an increased release of exosomes positive for PrP^C. This might occur when the typical route for sorting PrP^C into ILVs is increased to compensate for the inhibition of the ceramide pathway by GW4869. PrP^C intensity at the synapse was also investigated in neurons treated with GW4869 or DMSO as control. Here, PrP^C intensity was only markedly reduced in control conditions with GW4869 compared to DMSO only treated neurons. The reduction of PrP^C intensity after the induction of cLTD was lost in cells treated with GW4869. The overall reduction of PrP^C intensity may indicate a reduction of PrP^C concentration throughout the cell. GW4869 blocks the ceramide pathway involved in the maturation of endosomes into MVBs, the reduction of PrP^C intensity in endosomal compartments of neurons treated with GW4869 indicates that PrP^C sorting into ILVs is partly dependent on this pathway and that this sorting process may regulate the distribution, and thus the function of PrP^C (Trajkovic et al. 2008). The nSMase that is inhibited by GW4869 catalyzes the hydrolytic cleavage of sphingomyelin to ceramide and phosphocholine (Chatterjee 1993; Spence 1993; Liu et al. 1997). Sphingomyelin and ceramide are essential components of lipid rafts, where the GPI anchor of PrP^C is preferentially located (Tabatadze et al. 2010). GW4869 treatment would disrupt the lipid metabolism and could change lipid raft composition. This may influence PrP^C presentation at the synapse, which could explain why the reduction of PrP^C under cLTD was lost. GW4869 treatment could lead to lower concentrations of PrP^C at the synapses of neurons and therefore would be less affected by changes in synaptic plasticity. The effect might still be detectable when using a higher number of cells. PrP^C intensity is still slightly reduced in cells treated with GW4869 after the induction of cLTD compared to control conditions, but under these conditions, the effect is no longer significant. To investigate if PrP^C expression is overall reduced after 24 h of GW4869 treatment compared to DMSO alone, cells could be lysed, and protein levels analyzed by western blot. The mRNA levels of PrP^C in neurons with GW4869 or DMSO treatment could also be compared.

MVB can fuse with lysosomes to degrade their contents or fuse with the plasma membrane to release the ILVs as exosomes. PrP^C is enriched on neuronal exosomes (Hartmann et al. 2017). Levels of exosomes generated by hippocampal neurons during

a time interval matching synaptic plasticity induction and maintenance were too low to be analyzed by western blot or mass spectrometry. However, possible effects of exosomes on synapses and the induction of long-term homeostatic plasticity affecting exosome release were investigated. It is known that the release of exosomes increases with elevated Ca^{2+} levels, which are observed during synaptic plasticity (Artola and Singer 1993; Cummings et al. 1996; Chivet et al. 2014). Due to the difficulty of isolating enough exosomes to analyze, long-term stimulation protocols were used to induce homeostatic plasticity for 48 h. The cells were chronically stimulated with the $GABA_A$ receptor antagonist Bic or activity was completely blocked by sodium channel blocker TTX for 48 h (Narahashi et al. 1967; Curtis et al. 1970). This long-term blocking or overstimulation of neurons leads to a feedback mechanism to adjust synaptic strength (Pozo and Goda 2010). The exosomes were isolated from these stimulated neurons after 48 h, analyzed, and added for 6 days to neurons from the same preparation. Additionally, the neurons were treated with GW4869, to suppress the release of exosomes, or DMSO as control. After 6 days the cells were fixed and immunochemically stained for synaptic proteins and PrP^C. The synapses were counted for each condition, but no differences in the number of synapses under the different conditions could be observed. These results contradict those of Sharma et al. (2019), who found that treatment of human induced pluripotent stem cell (hiPSC)-derived neurospheres with exosomes increased the number of synapses. However, these hiPSCs exhibited a decreased number of synapses compared to control WT neurons due to methyl CpG binding protein (MECP2) loss of function (Sharma et al. 2019). Thus, this observation may be limited to neurons with fewer synapses present initially compared to control neurons. Unfortunately, the group did not use WT control iPSC neurons as a control, which would make their study and this study more comparable. Tabatadze et al. treated neurons with GW4869 and showed an altered synaptic structure with increased PSD95 and AMPA receptor concentrations at the synapse, but no changes in synapse number (Tabatadze et al. 2010). This is similar to the results of this thesis showing that GW4869 treatment of primary adult dissociated hippocampal neurons does not affect the number of synapses.

Changes were observed when measuring PrP^C concentration at the synapse after stimulation with exosomes and GW4869 treatment. The intensity of PrP^C at synaptic regions in cells treated with GW4869 and stimulated with exosomes isolated from neurons treated with Bic was significantly reduced compared DMSO treated neurons

stimulated with the same exosomes as control or to GW4869 treated cells without additional exosomes. Previously, the treatment of dissociated hippocampal neurons for 24 h with GW4869 significantly decreased PrP^C intensity at synaptic regions under control conditions compared to DMSO treatment. After the treatment of dissociated hippocampal neurons with GW4869 for 6 days, PrP^C intensities did not change significantly with the treatment of GW4869 alone. This might be due to the long exposure of the neurons to GW4869, resulting in a restored balance of PrP^C endocytic turnover. The intensity of PrP^C is only significantly reduced at synaptic regions in GW4869 treated neurons additionally treated with exosomes from Bic stimulated neurons, compared to neurons treated with GW4869 without additional exosomes or compared to PrP^C in DMSO treated neurons with added exosomes from Bic stimulated neurons. This decrease of PrP^C intensity at synaptic regions in neurons treated with GW4869 and exosomes from Bic stimulated cells might be due to a shrinkage of the synapses due to the exosomes added and exacerbated by the addition of GW4869. Also, the neurons used in these experiments were cultured longer (more than a week) than the neurons studied in the previous experiments. The longer time in culture could influence the PrP^C turnover at the synapse. It would be interesting to investigate this combined effect on AMPA and NMDA receptors at the synapse since it is known that GW4869 affects both (Tabatadze et al. 2010). In general, GW4869 impacts lipid metabolism significantly, thus rendering the interpretation of the results difficult. GW4869 has been described to inhibit the release of exosomes, however, this inhibition appears to be incomplete (Essandoh et al. 2015). Future studies could investigate other pathways of exosome release together with PrP^C localization.

Finally, exosomes released from neurons treated with Bic, TTX, or water as control did not show any significant differences in number or size, although there was a big variance in the size and concentration of exosomes from neurons treated with Bic. It was shown by Lachenal et al. (2011) that enhanced glutamatergic activity increased the release of exosomes after 10 min of treatment. However, these findings could not be reproduced or elaborated upon because the number of exosomes was too low to analyze the content of the different exosomes. This was probably due to the different number of neurons used to produce exosomes in Lachenal et al. compared to this work. The generalization of these results is limited by the variance in the results of size and concentration of the exosomes. Further experiments should investigate the possible differences of exosomes isolated from Bic stimulated neurons. Also, more

dissociated hippocampal neurons could be used or even better cortical neurons as they yield higher cell numbers.

This work showed that GW4869 treatment generally reduces the concentration of PrP^C in neurons compared to DMSO treatment alone, especially in endosomal and lysosomal compartments, which was not investigated before. After 6 days of GW4869 treatment, this effect was decreased at least at synapses. The treatment of neurons with exosomes isolated from stimulated neurons showed no effect on synapse number, while it moderately reduced PrP^C intensity at synaptic regions when combined with GW4869 treatment. Further research with higher neuron numbers is needed to investigate the effect of different stimulation on exosome composition and their effect on PrP^C at the synapse and in endolysosomal compartments.

4.4 PrP^C interacts with cell adhesion molecules

The results obtained in this work show that PrP^C localizes to inhibitory as well as to excitatory synapses in dissociated hippocampal neurons and that its localization and active transport change with the induction of cLTD. The molecular function of a protein is best investigated together with its interaction partners.

PrP^C does not have an intracellular domain, which would be needed for direct interactions with intracellular molecules. The seemingly contracting functions reported for PrP^C may be explained by PrP^C interacting with different binding partners leading to different downstream pathways. Therefore, identifying and rigorously testing new interaction partners and their downstream effect is essential. These interactions are cell type- and context-dependent. One of the functions attributed to PrP^C is cell adhesion (Mangé et al. 2002; Martins et al. 2002; Málaga-Trillo et al. 2009; Kaiser et al. 2012; Petit et al. 2013). Due to the interconnected nature of the nervous system, cell adhesion is very important in the development of the brain and the maintenance of connectivity, also during synaptic plasticity changes (Togashi et al. 2009). N-cadherin is a transmembrane protein expressed in multiple tissues where it mediates cell-to-cell adhesion through homophilic interactions. It belongs to the Ca^{2+}-dependent cell adhesion molecule family of cadherins (Brusés 2006). N-cadherin is important for synaptic development. It contributes to cell-cell adhesion in neuronal progenitor cells and neurons (Miyamoto et al. 2015). Through its binding partners α- and ß-catenins, N-cadherin interacts with F-actin filaments which enables N-cadherin to regulate the synaptic structure (Kosik et al. 2005). In cultured hippocampal neurons, N-cadherin is

lost at inhibitory synapses during development and preferentially localizes to excitatory synapses (Benson and Tanaka 1998). Studies have shown that hippocampal CA1 synapses lacking N-cadherin show impairment in LTP persistence and do not show the usual spine enlargement typical in LTP (Bozdagi et al. 2010). Meanwhile, the internalization of N-cadherin is important for LTD (Tai et al. 2007). It was shown that PrP^C promotes growth cone development by affecting N-cadherin distribution and colocalization of PrP^C with N-cadherin was reported (Bodrikov et al. 2011). This raised the question of whether PrP^C may interact with N-cadherin. Indeed, PrP^C co-immunoprecipitated together with N-cadherin from whole adult mouse brain lysates and vice versa. In dissociated hippocampal neurons PrP^C and N-cadherin showed around 40% colocalization, independent of F-actin hotspots. These results indicate that PrP^C and N-cadherin might interact physically, either direct or indirect, in the brain and possibly in neurons.

PrP^C interactions with cell adhesion proteins mainly found at inhibitory synapses such as neuroligin-2 were of interest (Varoqueaux et al. 2004) since PrP^C was found to localize to inhibitory synapses as discussed in chapter 4.1. Neuroligins are postsynaptic adhesion proteins that bind to presynaptic neurexins to regulate synapse formation and function (Krueger et al. 2012). Neuroligin-2 recruits gephyrin and $GABA_A$ receptors to inhibitory synaptic clusters (Poulopoulos et al. 2009). Neuroligin-2 co-immunoprecipitated together with PrP^C from whole adult mouse brain lysates and vice versa, indicating an interaction between the two proteins. Neuroligin-2 and PrP^C frequently colocalized in developed dissociated hippocampal neurons at around 50% in dendrites and at F-actin hotspots, as shown in figure 3.8. This interaction of PrP^C with neuroligin-2 further supports the hypothesis that PrP^C plays a role at inhibitory synapses. While the area of colocalization between PrP^C and neuroligin-2 was larger than between PrP^C and N-cadherin, the Pearson's coefficient was higher for PrP^C and N-cadherin colocalization than for neuroligin-2 and PrP^C. Also, the signal intensity of PrP^C in the N-cadherin-IP was higher than in the neuroligin-2-IP. These results hint at a stronger interaction between PrP^C and N-cadherin. From these experiments, it is not clear whether PrP^C and N-cadherin or neuroligin-2 are covalently bound in the brain or in dissociated hippocampal neurons. However, these experiments do suggest that PrP^C and N-cadherin or neuroligin-2 interact in the brain and dissociated hippocampal neurons. The experiments contribute to a clearer understanding of the connection between N-cadherin and PrP^C which was first shown by Bodrikov et al. in 2011. The

results expand on the existing evidence that PrP^C does play a role in cell adhesion as reviewed by Petit et al. in 2013.

In murine development, PrP^C is already expressed a few days after implantation, suggesting a possible role in the development of the brain (Manson et al. 1992). PrP^C has been shown to promote neurite outgrowth (Chen et al. 2003; Lopes et al. 2005; Santuccione et al. 2005). The interaction of PrP^C with different cell adhesion molecules underlines its importance in neurodevelopment. In this work, it was discovered that PrP^C interacts with N-cadherin and neuroligin-2. This led to the investigation of PrP^C colocalization with these interaction partners in developing dissociated hippocampal neurons. Dissociated hippocampal neurons were immunochemically stained for PrP^C and F-actin, as well as for N-cadherin, synaptophysin, or neuroligin-2 at DIV7, 10, 14, and 21. PrP^C intensity at F-actin hotspots increased from DIV7 to DIV14. This is probably because F-actin hotspots in DIV7 and 10 are larger and not as punctate as they are in developed neurons. This might reduce the average intensity of PrP^C at F-actin hotspots, because PrP^C intensity could be higher at certain points in the F-actin hotspots but probably not as widespread as the hotspots themselves, leading to a reduced average intensity per area. On the other hand, PrP^C intensity may be reduced because expression levels are lower than in adult hippocampal neurons. However, PrP^C RNA levels were described not to change significantly during development in hamsters (McKinley et al. 1987). This should be further investigated by for example western blot analysis of PrP^C expression levels in dissociated hippocampal neurons. Looking at the colocalization of PrP^C with N-cadherin, there are no significant changes in the area of colocalization over time. This would be expected since PrP^C does regulate N-cadherin transport in development, so their interaction might play a role already early in development (Bodrikov et al. 2011). PrP^C colocalization with neuroligin-2 did vary during development. The difference was significant between DIV10 and 14 (figure 3.9). This coincides with the time when N-cadherin is no longer associated with inhibitory neurons in dissociated hippocampal neurons (Benson and Tanaka 1998). It is therefore possible that PrP^C is more involved in regulating the formation of excitatory synapses together with N-cadherin. When the synapses are completely developed, PrP^C is expressed higher on inhibitory synapses. The interactions between PrP^C and cell adhesion molecules during development are worthwhile to initiate further investigations, based on the data provided by this thesis. For example, fetal mouse brains or dissociated hippocampal neurons at early DIVs could be used to

immunoprecipitate PrP^C and its interaction partners during development. These results build on research that attributes a role in development to PrP^C and suggests that PrP^C interactions with neuroligin-2 and N-cadherin discovered in this work play a crucial role during developmental processes.

PrP^C has been described to regulate N-cadherin trafficking and N-cadherin and PrP^C colocalization was observed in dendrites without F-actin hotspots. This led to the hypothesis that PrP^C and N-cadherin might be co-transported in dissociated hippocampal neurons. In time-lapse videos of YFP-PrP^C and mRFP-N-cadherin expressing N2a cells, mobile transport vesicles positive for both fluorescently labeled proteins could be observed close to the plasma membrane in TIRF and SDC settings. Co-transport could be observed in YFP-PrP^C and mRFP-N-cadherin expressing DIV14 dissociated hippocampal neurons. The reliability of these experiments is impacted by the fact that both proteins are overexpressed, which increases the chance of them being in the same transport vesicle. Also, N-cadherin and PrP^C are fluorescently tagged, which could alter their binding affinity. However, this is an established experiment to investigate co-transport and binding and colocalization of N-cadherin and PrP^C has been shown by other experiments as well. Therefore, it was further examined if PrP^C would interact with GRIP1, a known regulator of N-cadherin transport and localization. GRIP1 binds N-cadherin and AMPA receptors and regulates their transport (Heisler et al. 2014; Setou et al. 2002). As previously reported, PrP^C binds AMPA receptor subunits (Watt et al. 2012), so the possible interaction with GRIP1 is worthwhile to investigate. Indeed, PrP^C and N-cadherin could be co-immunoprecipitated with GRIP1 from whole adult mouse brains. GRIP1 is also co-immunoprecipitated together with PrP^C from adult mouse brains. Importantly, PrP^C cannot directly bind an adaptor protein because it lacks a transmembrane and cytosolic domain. This indicates that PrP^C is transported in a complex together with proteins that have a transmembrane and cytosolic domain to interact with GRIP1. Other proteins could be investigated as a linker between GRIP1 and PrP^C such as N-cadherin or AMPA receptors. This also raises the question of whether PrP^C directly interacts with N-cadherin and neuroligin-2. However, these proteins do interact with each other in a complex and this interaction could be a crucial part of the molecular function of PrP^C. Co-transport could be observed in dissociated hippocampal neurons expressing mRFP-GRIP1 and YFP-PrP^C. To investigate whether the co-transport with its interaction partners influenced YFP-PrP^C transport vesicle velocity, N2a cells were

transfected to express either YFP-PrP^C alone or together with mRFP-N-cadherin or mRFP-GRIP1. Interestingly, a significant reduction in YFP-PrP^C transport velocity was detected for particles co-labeled for either mRFP-N-cadherin or mRFP-GRIP1 (figure 3.10). Particles co-labeled with YFP and mRFP were usually brighter and slower moving. This may be attributed to the presence of two fluorescently labeled proteins in one vesicle. It could also be that the higher concentration of GRIP1 or N-cadherin leads to the reduction in velocities because these proteins could bind more motor or adaptor proteins, which might lead to a tug-of-war and less processive transport. Further experiments would be needed to investigate mRFP-GRIP1 and -N-cadherin processivity, by overexpressing one of the proteins in N2a cells and analyzing their velocities. The experiments reported here show that the overexpression of fluorescently labeled proteins could impact the dynamics of these proteins. The particles observed were usually quite bright suggesting that multiple fluorescently labeled proteins were transported in the same vesicle, influencing the binding to motor proteins or adaptor proteins and therefore also their transportation. These experiments elaborate further on the interaction of PrP^C and AMPA receptors. In this work, it was shown that PrP^C interacts with N-cadherin and GRIP1, both of which have been suggested to regulate AMPA receptor trafficking and localization (Setou et al. 2002; Nuriya and Huganir 2006; Heisler et al. 2014). PrP^C may stabilize the interaction between N-cadherin and AMPA receptors. The regulation of the complex needs further investigation.

It was proposed, that PrP^C may contribute to endocytic and exocytic protein trafficking (Alves et al. 2020). In N2a cells expressing a truncated version of PrP^C, lacking the octarepeat region, internalization of glypican-1 was reduced, suggesting a possible role for PrP^C in co-internalizing other proteins (Cheng et al. 2006). To investigate the function of the PrP^C-N-cadherin interaction, YFP-PrP^C or mRFP-N-cadherin were overexpressed in dissociated hippocampal neurons. The endosomal and lysosomal compartments of the neurons were labeled using ICC. After overexpression of YFP-PrP^C, a significant increase in N-cadherin intensity in endosomal compartments labeled with TSG101 was observed under control conditions compared to neurons expressing YFP. This could be due to increased internalization of N-cadherin together with the overexpressed PrP^C. After induction of cLTD a reduction of N-cadherin intensity was observed for both, YFP-PrP^C and YFP overexpressing cells compared to unstimulated conditions. This showed that YFP-PrP^C overexpression does not have a

direct effect on N-cadherin targeting to endosomal compartments with cLTD induction. However, N-cadherin intensity in endosomal and lysosomal compartments was further reduced in YFP-PrP^C expressing than in YFP expressing neurons after induction of cLTD compared to control conditions. This may indicate that transport is slowed to redistribute proteins along the neurites, as shown in this work, or the proteins could be released in exosomes which are released in greater quantities with Ca^{2+} signaling (Savina et al. 2003). Interestingly, N-cadherin is also cleaved by ADAM10 (Reiss et al. 2005). Many interaction partners of PrP^C are bound and processed by ADAM10, including PrP^C itself. (Hinkle et al. 2006; Parkyn et al. 2008; Liu et al. 2009; Altmeppen et al. 2011). One possible function of PrP^C could be to act as a hub to organize proteins for cleavage or other ways of removal from the plasma membrane. Surface levels and activity of ADAM10 are increased after induction of LTD (Musardo et al. 2014). This might lead to increased shedding of both, PrP^C and N-cadherin, under cLTD conditions compared to control conditions. The shedding may be increased by PrP^C overexpression. PrP^C might be indirectly involved in the removal or cleavage of proteins not needed in LTP induction, explaining the fact that PrP^C intensity and transport were less affected by cLTP induction. The N-cadherin intensity in Lamp1 labeled lysosomes was significantly decreased in cLTP and cLTD conditions after YFP-PrP^C overexpression, while there were no changes in N-cadherin intensity in cLTP or cLTD compared to control conditions in YFP overexpressing neurons. In chapter 3.4.1 it was shown that endogenous PrP^C intensity in lysosomes was only reduced in cLTD compared to control conditions, but the decrease in PrP^C intensity observed after cLTP induction was only by trend compared to control conditions. This effect might be enhanced in cells overexpressing PrP^C and the increased concentration of PrP^C might increase proteolytic cleavage of N-cadherin by ADAM10 or increase the release of N-cadherin containing exosomes, leading to lower levels of N-cadherin targeted for degradation. In cLTP conditions, ADAM10 activity is decreased and cannot be the reason for a decrease in N-cadherin intensity after the induction of cLTP. It is possible that PrP^C is internalized at lower levels during cLTP conditions compared to control, which may then stabilize N-cadherin at the synapse, leading to a lower amount of N-cadherin for degradation. This hypothesis needs further study though, to investigate N-cadherin expression levels at the synapse in the setting of PrP^C overexpression. PrP^C does also interact with GRIP1 and therefore it may play a role in the endocytosis of N-cadherin and AMPA receptors. This complex needs to be further

investigated, especially during synaptic plasticity. No significant changes were observed for PrP^C intensity in endosomal and lysosomal compartments when overexpressing mRFP-N-cadherin or mRFP as control, so the results were not shown. This supports the theory that the increased intensity of N-cadherin in endosomal compartments is due to the overexpression of PrP^C specifically and not a general effect of overexpressing synaptic proteins with a fluorescent tag.

4.5 Conclusions

In this thesis, the cellular function of PrP^C in hippocampal neurons was investigated with focus on a possible involvement of PrP^C in synaptic plasticity related processes. To this end, a search for novel PrP^C interaction partners was conducted and PrP^C subcellular localization and vesicle trafficking during synaptic plasticity changes were analyzed.

This thesis demonstrates that PrP^C localizes to both, excitatory and inhibitory synapses in dissociated hippocampal neurons. PrP^C was identified to interact with the synaptic cell adhesion molecules N-cadherin and neuroligin-2. A third novel interaction partner identified is GRIP1, a direct binding partner of N-cadherin and AMPA receptors and a regulator of synaptic protein turnover during plasticity changes. Frequent colocalization of PrP^C with N-cadherin or with neuroligin-2 was observed at synaptic and non-synaptic compartments. Neuronal live imaging revealed that PrP^C together with N-Cadherin or GRIP1 is co-transported within the same vesicles close beneath the plasma membrane and along the dendrites of hippocampal neurons. Further, it was shown that synaptic plasticity induces the subcellular redistribution of PrP^C. PrP^C levels at the synapse and in endolysosomal compartments were decreased after the induction of cLTD but not cLTP. Notably, the induction of cLTD also had a significant impact on the transport parameters of PrP^C containing vesicles. PrPC trafficking towards the soma was considerably slower. The decrease in synaptic PrP^C levels following cLTD induction might be due to increased ADAM10 activity, leading to increased endocytosis or shedding of PrP^C and its interaction partners, such as N-cadherin and AMPA receptors. The reduction of PrP^C in endolysosomal compartments after cLTD induction could be explained by the observed deceleration in PrP^C soma-directed vesicle trafficking. However, this would suggest that the excess of internalized PrP^C is either stored in recycling compartments, recycled back to the plasma membrane, or released into the extracellular environment via exosomes. With respect to N-cadherin turnover, the

overexpression of PrP^C functionally facilitated N-cadherin targeting to endosomes under basal conditions and led to a decrease in its synaptic plasticity-dependent lysosomal targeting.

Together this work elucidated the cellular function of PrP^C in neurons and for the first time describes the involvement of PrP^C in synaptic plasticity related processes. Future experiments based on this work may investigate the molecular mechanisms and the functional impact of altered PrP^C turnover during cLTD on synapse function.

References

Publication bibliography

Aguzzi, A.; Polymenidou, M. (2004): Mammalian prion biology: one century of evolving concepts. In *Cell* 116 (2), pp. 313–327.

Aguzzi, Adriano; Baumann, Frank; Bremer, Juliane (2008): The prion's elusive reason for being. In *Annual review of neuroscience* 31, pp. 439–477. DOI: 10.1146/annurev.neuro.31.060407.125620.

Aguzzi, Adriano; Lakkaraju, Asvin K. K. (2016): Cell Biology of Prions and Prionoids: A Status Report. In *Trends in cell biology* 26 (1), pp. 40–51. DOI: 10.1016/j.tcb.2015.08.007.

Aiken, Jayne; Holzbaur, Erika L. F. (2021): Cytoskeletal regulation guides neuronal trafficking to effectively supply the synapse. In *Current biology : CB* 31 (10), R633-R650. DOI: 10.1016/j.cub.2021.02.024.

Alberts, Bruce (2015): Molecular biology of the cell. Sixth edition. New York NY: Garland Science Taylor and Francis Group.

Alenquer, Marta; Amorim, Maria João (2015): Exosome Biogenesis, Regulation, and Function in Viral Infection. In *Viruses* 7 (9), pp. 5066–5083. DOI: 10.3390/v7092862.

Allison, Daniel W.; Gelfand, Vladimir I.; Spector, Ilan; Craig, Ann Marie (1998): Role of Actin in Anchoring Postsynaptic Receptors in Cultured Hippocampal Neurons: Differential Attachment of NMDA versus AMPA Receptors. In *J. Neurosci.* 18 (7), pp. 2423–2436. DOI: 10.1523/JNEUROSCI.18-07-02423.1998.

Altman, David; Sweeney, H.Lee; Spudich, James A. (2004): The Mechanism of Myosin VI Translocation and Its Load-Induced Anchoring. In *Cell* 116 (5), pp. 737–749. DOI: 10.1016/S0092-8674(04)00211-9.

Altmeppen, Hermann C.; Prox, Johannes; Puig, Berta; Kluth, Mark A.; Bernreuther, Christian; Thurm, Dana et al. (2011): Lack of a-disintegrin-and-metalloproteinase ADAM10 leads to intracellular accumulation and loss of shedding of the cellular prion protein in vivo. In *Molecular neurodegeneration* 6 (1), p. 36. DOI: 10.1186/1750-1326-6-36.

Altmeppen, Hermann C.; Puig, Berta; Dohler, Frank; Thurm, Dana K.; Falker, Clemens; Krasemann, Susanne; Glatzel, Markus (2012): Proteolytic processing of the prion protein in health and disease. In *American Journal of Neurodegenerative Diseases* 1 (1), pp. 15–31. Available online at https://www.researchgate.net/publication/235403306_Proteolytic_processing_of_the_prion_in_health_and_disease.

Alvarez-Erviti, Lydia; Seow, Yiqi; Yin, HaiFang; Betts, Corinne; Lakhal, Samira; Wood, Matthew J. A. (2011): Delivery of siRNA to the mouse brain by systemic injection of targeted exosomes. In *Nat Biotechnol* 29 (4), pp. 341–345. DOI: 10.1038/nbt.1807.

Alves, Rodrigo Nunes; Iglesia, Rebeca Piatniczka; Prado, Mariana Brandão; Melo Escobar, Maria Isabel; Boccacino, Jacqueline Marcia; Fernandes, Camila Felix de Lima et al. (2020): A New Take on Prion Protein Dynamics in Cellular Trafficking. In *International journal of molecular sciences* 21 (20). DOI: 10.3390/ijms21207763.

An, Kyongman; Klyubin, Igor; Kim, Youngkyu; Jung, Jung Hoon; Mably, Alexandra J.; O'Dowd, Sean T. et al. (2013): Exosomes neutralize synaptic-plasticity-disrupting activity of Aβ assemblies in vivo. In *Molecular brain* 6, p. 47. DOI: 10.1186/1756-6606-6-47.

Andorfer, Cathy; Kress, Yvonne; Espinoza, Marisol; Silva, Rohan de; Tucker, Kerry L.; Barde, Yves-Alain et al. (2003): Hyperphosphorylation and aggregation of tau in mice expressing

normal human tau isoforms. In *Journal of neurochemistry* 86 (3), pp. 582–590. DOI: 10.1046/j.1471-4159.2003.01879.x.

Artola, Alain; Singer, Wolf (1993): Long-term depression of excitatory synaptic transmission and its relationship to long-term potentiation. In *Trends in Neurosciences* 16 (11), pp. 480–487. DOI: 10.1016/0166-2236(93)90081-V.

Avila, J.; Domínguez, J.; Díaz-Nido, J. (1994): Regulation of microtubule dynamics by microtubule-associated protein expression and phosphorylation during neuronal development. In *The International journal of developmental biology* 38 (1), pp. 13–25.

Bacci, Alberto; Coco, Silvia; Pravettoni, Elena; Schenk, Ursula; Armano, Simona; Frassoni, Carolina et al. (2001): Chronic Blockade of Glutamate Receptors Enhances Presynaptic Release and Downregulates the Interaction between Synaptophysin-Synaptobrevin–Vesicle-Associated Membrane Protein 2. In *J. Neurosci.* 21 (17), pp. 6588–6596. DOI: 10.1523/JNEUROSCI.21-17-06588.2001.

Bahloul, Amel; Chevreux, Guillaume; Wells, Amber L.; Martin, Davy; Nolt, Jocelyn; Yang, Zhaohui et al. (2004): The unique insert in myosin VI is a structural calcium-calmodulin binding site. In *Proc Natl Acad Sci USA* 101 (14), pp. 4787–4792. DOI: 10.1073/pnas.0306892101.

Bahrini, Insaf; Song, Ji-hoon; Diez, Diego; Hanayama, Rikinari (2015): Neuronal exosomes facilitate synaptic pruning by up-regulating complement factors in microglia. In *Sci Rep* 5, p. 7989. DOI: 10.1038/srep07989.

Bakhti, Mostafa; Winter, Christine; Simons, Mikael (2011): Inhibition of myelin membrane sheath formation by oligodendrocyte-derived exosome-like vesicles. In *The Journal of biological chemistry* 286 (1), pp. 787–796. DOI: 10.1074/jbc.M110.190009.

Bear, Mark F.; Connors, Barry W.; Paradiso, Michael A. (2016): Neuroscience. Exploring the brain. 4th edition, international edition. Philadelphia, Baltimore, New York, London: Wolters Kluwer.

Benarroch, Eduardo E. (2018): Glutamatergic synaptic plasticity and dysfunction in Alzheimer disease: Emerging mechanisms. In *Neurology* 91 (3), pp. 125–132. DOI: 10.1212/WNL.0000000000005807.

Bendheim, P. E.; Brown, H. R.; Rudelli, R. D.; Scala, L. J.; Goller, N. L.; Wen, G. Y. et al. (1992): Nearly ubiquitous tissue distribution of the scrapie agent precursor protein. In *Neurology* 42 (1), pp. 149–156. DOI: 10.1212/wnl.42.1.149.

Benson, Deanna L.; Tanaka, Hidekazu (1998): N-Cadherin Redistribution during Synaptogenesis in Hippocampal Neurons. In *J. Neurosci.* 18 (17), pp. 6892–6904. DOI: 10.1523/JNEUROSCI.18-17-06892.1998.

Bhattacharyya, Samarjit; Biou, Virginie; Xu, Weifeng; Schlüter, Oliver; Malenka, Robert C. (2009): A critical role for PSD-95/AKAP interactions in endocytosis of synaptic AMPA receptors. In *Nature neuroscience* 12 (2), pp. 172–181. DOI: 10.1038/nn.2249.

Biasini, Emiliano; Turnbaugh, Jessie A.; Massignan, Tania; Veglianese, Pietro; Forloni, Gianluigi; Bonetto, Valentina et al. (2012): The toxicity of a mutant prion protein is cell-autonomous, and can be suppressed by wild-type prion protein on adjacent cells. In *PloS one* 7 (3), e33472. DOI: 10.1371/journal.pone.0033472.

Bodrikov, V.; Solis, G. P.; Stuermer, C. A. (2011): Prion protein promotes growth cone development through reggie/flotillin-dependent N-cadherin trafficking. In *J Neurosci* 31 (49), pp. 18013–18025. DOI: 10.1523/JNEUROSCI.4729-11.2011.

Borchelt, D. R.; Scott, M.; Taraboulos, A.; Stahl, N.; Prusiner, S. B. (1990): Scrapie and cellular prion proteins differ in their kinetics of synthesis and topology in cultured cells. In *The Journal of cell biology* 110 (3), pp. 743–752. DOI: 10.1083/jcb.110.3.743.

Bounhar, Y.; Zhang, Y.; Goodyer, C. G.; LeBlanc, A. (2001): Prion protein protects human neurons against Bax-mediated apoptosis. In *Journal of Biological Chemistry* 276 (42), pp. 39145–39149. DOI: 10.1074/jbc.C100443200.

Bozdagi, Ozlem; Wang, Xiao-bin; Nikitczuk, Jessica S.; Anderson, Tonya R.; Bloss, Erik B.; Radice, Glenn L. et al. (2010): Persistence of coordinated long-term potentiation and dendritic spine enlargement at mature hippocampal CA1 synapses requires N-cadherin. In *J. Neurosci.* 30 (30), pp. 9984–9989. DOI: 10.1523/JNEUROSCI.1223-10.2010.

Braithwaite, Steven P.; Xia, Houhui; Malenka, Robert C. (2002): Differential roles for NSF and GRIP/ABP in AMPA receptor cycling. In *Proc Natl Acad Sci USA* 99 (10), pp. 7096–7101. DOI: 10.1073/pnas.102156099.

Branco, Tiago; Staras, Kevin; Darcy, Kevin J.; Goda, Yukiko (2008): Local dendritic activity sets release probability at hippocampal synapses. In *Neuron* 59 (3), pp. 475–485. DOI: 10.1016/j.neuron.2008.07.006.

Bredesen, Dale E.; Rao, Rammohan V.; Mehlen, Patrick (2006): Cell death in the nervous system. In *Nature* 443 (7113), pp. 796–802. DOI: 10.1038/nature05293.

Bridgman, Paul C. (2004): Myosin-dependent transport in neurons. In *Journal of neurobiology* 58 (2), pp. 164–174. DOI: 10.1002/neu.10320.

Brody, A. Harrison; Strittmatter, Stephen M. (2018): Synaptotoxic Signaling by Amyloid Beta Oligomers in Alzheimer's Disease Through Prion Protein and mGluR5. In *Advances in pharmacology (San Diego, Calif.)* 82, pp. 293–323. DOI: 10.1016/bs.apha.2017.09.007.

Brown, D. R.; Qin, K.; Herms, J. W.; Madlung, A.; Manson, J.; Strome, R. et al. (1997): The cellular prion protein binds copper in vivo. In *Nature* 390 (6661), pp. 684–687. DOI: 10.1038/37783.

Brown, D. R.; Wong, B. S.; Hafiz, F.; Clive, C.; Haswell, S. J.; Jones, I. M. (1999): Normal prion protein has an activity like that of superoxide dismutase. In *Biochemical Journal* 344 Pt 1 (Pt 1), pp. 1–5. DOI: Study.

Brown, Deborah A.; Rose, John K. (1992): Sorting of GPI-anchored proteins to glycolipid-enriched membrane subdomains during transport to the apical cell surface. In *Cell* 68 (3), pp. 533–544. DOI: 10.1016/0092-8674(92)90189-J.

Brown, Tyler C.; Correia, Susana S.; Petrok, Cortney N.; Esteban, José A. (2007): Functional compartmentalization of endosomal trafficking for the synaptic delivery of AMPA receptors during long-term potentiation. In *J. Neurosci.* 27 (48), pp. 13311–13315. DOI: 10.1523/JNEUROSCI.4258-07.2007.

Brusés, Juan L. (2006): N-Cadherin Signaling in Synapse Formation and Neuronal Physiology. In *MN* 33 (3), pp. 237–252. DOI: 10.1385/MN:33:3:237.

Budka, Herbert (2003): Neuropathology of prion diseases. In *British medical bulletin* 66, pp. 121–130. DOI: 10.1093/bmb/66.1.121.

Büeler, H.; Aguzzi, A.; Sailer, A.; Greiner, R.-A.; Autenried, P.; Aguet, M.; Weissmann, C. (1993): Mice devoid of PrP are resistant to scrapie. In *Cell* 73 (7), pp. 1339–1347. DOI: 10.1016/0092-8674(93)90360-3.

Buss, F.; Arden, S. D.; Lindsay, M.; Luzio, J. P.; Kendrick-Jones, J. (2001): Myosin VI isoform localized to clathrin-coated vesicles with a role in clathrin-mediated endocytosis. In *The EMBO journal* 20 (14), pp. 3676–3684. DOI: 10.1093/emboj/20.14.3676.

Caiati, Maddalena D.; Safiulina, Victoria F.; Fattorini, Giorgia; Sivakumaran, Sudhir; Legname, Giuseppe; Cherubini, Enrico (2013): PrPC controls via protein kinase A the direction of synaptic plasticity in the immature hippocampus. In *The Journal of neuroscience : the official journal of the Society for Neuroscience* 33 (7), pp. 2973–2983. DOI: 10.1523/JNEUROSCI.4149-12.2013.

Calabresi, Paolo; Galletti, Francesca; Saggese, Emanuele; Ghiglieri, Veronica; Picconi, Barbara (2007): Neuronal networks and synaptic plasticity in Parkinson's disease: beyond motor deficits. In *Parkinsonism & Related Disorders* 13, S259-S262. DOI: 10.1016/S1353-8020(08)70013-0.

Cammalleri, Maurizio; Bagnoli, Paola; Bigiani, Albertino (2019): Molecular and Cellular Mechanisms Underlying Somatostatin-Based Signaling in Two Model Neural Networks, the Retina and the Hippocampus. In *International journal of molecular sciences* 20 (10), p. 2506. DOI: 10.3390/ijms20102506.

Campana, Vincenza; Sarnataro, Daniela; Zurzolo, Chiara (2005): The highways and byways of prion protein trafficking. In *Trends in cell biology* 15 (2), pp. 102–111. DOI: 10.1016/j.tcb.2004.12.002.

Carleton, A.; Tremblay, P.; Vincent, J. D.; Lledo, P. M. (2001): Dose-dependent, prion protein (PrP)-mediated facilitation of excitatory synaptic transmission in the mouse hippocampus. In *Pflugers Archiv : European journal of physiology* 442 (2), pp. 223–229. DOI: 10.1007/s004240100523.

Carroll, R. C.; Lissin, D. V.; Zastrow, M. von; Nicoll, R. A.; Malenka, R. C. (1999): Rapid redistribution of glutamate receptors contributes to long-term depression in hippocampal cultures. In *Nat Neurosci* 2 (5), pp. 454–460. DOI: 10.1038/8123.

Carulla, Patricia; Llorens, Franc; Matamoros-Angles, Andreu; Aguilar-Calvo, Patricia; Espinosa, Juan Carlos; Gavín, Rosalina et al. (2015): Involvement of PrP(C) in kainate-induced excitotoxicity in several mouse strains. In *Sci Rep* 5, p. 11971. DOI: 10.1038/srep11971.

Castle, Andrew R.; Gill, Andrew C. (2017): Physiological Functions of the Cellular Prion Protein. In *Frontiers in molecular biosciences* 4, p. 19. DOI: 10.3389/fmolb.2017.00019.

Caviston, Juliane P.; Holzbaur, Erika L. F. (2006): Microtubule motors at the intersection of trafficking and transport. In *Trends in cell biology* 16 (10), pp. 530–537. DOI: 10.1016/j.tcb.2006.08.002.

Chanaday, Natali L.; Cousin, Michael A.; Milosevic, Ira; Watanabe, Shigeki; Morgan, Jennifer R. (2019): The Synaptic Vesicle Cycle Revisited: New Insights into the Modes and Mechanisms. In *J. Neurosci.* 39 (42), pp. 8209–8216. DOI: 10.1523/JNEUROSCI.1158-19.2019.

Chang, Diane T. W.; Honick, Anthony S.; Reynolds, Ian J. (2006): Mitochondrial trafficking to synapses in cultured primary cortical neurons. In *J. Neurosci.* 26 (26), pp. 7035–7045. DOI: 10.1523/JNEUROSCI.1012-06.2006.

Chatterjee, S. (1993): Neutral sphingomyelinase. In *Advances in lipid research* 26, pp. 25–48.

Chen, Jieli; Chopp, Michael (2018): Exosome Therapy for Stroke. In *Stroke* 49 (5), pp. 1083–1090. DOI: 10.1161/STROKEAHA.117.018292.

Chen, L.; Chetkovich, D. M.; Petralia, R. S.; Sweeney, N. T.; Kawasaki, Y.; Wenthold, R. J. et al. (2000): Stargazin regulates synaptic targeting of AMPA receptors by two distinct mechanisms. In *Nature* 408 (6815), pp. 936–943. DOI: 10.1038/35050030.

Chen, Suzhen; Mangé, Alain; Dong, Ling; Lehmann, Sylvain; Schachner, Melitta (2003): Prion protein as trans-interacting partner for neurons is involved in neurite outgrowth and neuronal survival. In *Molecular and Cellular Neuroscience* 22 (2), pp. 227–233. DOI: 10.1016/S1044-7431(02)00014-3.

Cheng, Fang; Lindqvist, Josefin; Haigh, Cathryn L.; Brown, David R.; Mani, Katrin (2006): Copper-dependent co-internalization of the prion protein and glypican-1. In *Journal of neurochemistry* 98 (5), pp. 1445–1457. DOI: 10.1111/j.1471-4159.2006.03981.x.

Chevalier-Larsen, Erica; Holzbaur, Erika L. F. (2006): Axonal transport and neurodegenerative disease. In *Biochimica et biophysica acta* 1762 (11-12), pp. 1094–1108. DOI: 10.1016/j.bbadis.2006.04.002.

Chih, Ben; Engelman, Holly; Scheiffele, Peter (2005): Control of excitatory and inhibitory synapse formation by neuroligins. In *Science (New York, N.Y.)* 307 (5713), pp. 1324–1328. DOI: 10.1126/science.1107470.

Chivet, Mathilde; Javalet, Charlotte; Laulagnier, Karine; Blot, Béatrice; Hemming, Fiona J.; Sadoul, Rémy (2014): Exosomes secreted by cortical neurons upon glutamatergic synapse activation specifically interact with neurons. In *Journal of extracellular vesicles* 3, p. 24722. DOI: 10.3402/jev.v3.24722.

Chubykin, Alexander A.; Atasoy, Deniz; Etherton, Mark R.; Brose, Nils; Kavalali, Ege T.; Gibson, Jay R.; Südhof, Thomas C. (2007): Activity-dependent validation of excitatory versus inhibitory synapses by neuroligin-1 versus neuroligin-2. In *Neuron* 54 (6), pp. 919–931. DOI: 10.1016/j.neuron.2007.05.029.

Cingolani, Lorenzo A.; Goda, Yukiko (2008): Actin in action: the interplay between the actin cytoskeleton and synaptic efficacy. In *Nat Rev Neurosci* 9 (5), pp. 344–356. DOI: 10.1038/nrn2373.

Clayton, Aled; Turkes, Atilla; Dewitt, Sharon; Steadman, Robert; Mason, Malcolm D.; Hallett, Maurice B. (2004): Adhesion and signaling by B cell-derived exosomes: the role of integrins. In *FASEB journal : official publication of the Federation of American Societies for Experimental Biology* 18 (9), pp. 977–979. DOI: 10.1096/fj.03-1094fje.

Colling, Simon B.; Collinge, John; Jefferys, John G.R. (1996): Hippocampal slices from prion protein null mice: disrupted Ca2+-activated K+ currents. In *Neuroscience Letters* 209 (1), pp. 49–52. DOI: 10.1016/0304-3940(96)12596-9.

Collinge, J.; Whittington, M. A.; Sidle, K. C.; Smith, C. J.; Palmer, M. S.; Clarke, A. R.; Jefferys, J. G. (1994): Prion protein is necessary for normal synaptic function. In *Nature* 370 (6487), pp. 295–297. DOI: 10.1038/370295a0.

Collingridge, Graham L.; Isaac, John T. R.; Wang, Yu Tian (2004): Receptor trafficking and synaptic plasticity. In *Nature reviews. Neuroscience* 5 (12), pp. 952–962. DOI: 10.1038/nrn1556.

Colombo, Marina; Moita, Catarina; van Niel, Guillaume; Kowal, Joanna; Vigneron, James; Benaroch, Philippe et al. (2013): Analysis of ESCRT functions in exosome biogenesis, composition and secretion highlights the heterogeneity of extracellular vesicles. In *J Cell Sci* 126 (Pt 24), pp. 5553–5565. DOI: 10.1242/jcs.128868.

Colombo, Marina; Raposo, Graça; Théry, Clotilde (2014): Biogenesis, secretion, and intercellular interactions of exosomes and other extracellular vesicles. In *Annual review of cell and developmental biology* 30, pp. 255–289. DOI: 10.1146/annurev-cellbio-101512-122326.

Cooney, James R.; Hurlburt, Jamie L.; Selig, David K.; Harris, Kristen M.; Fiala, John C. (2002): Endosomal Compartments Serve Multiple Hippocampal Dendritic Spines from a Widespread Rather Than a Local Store of Recycling Membrane. In *J. Neurosci.* 22 (6), pp. 2215–2224. DOI: 10.1523/JNEUROSCI.22-06-02215.2002.

Correia, Susana S.; Bassani, Silvia; Brown, Tyler C.; Lisé, Marie-France; Backos, Donald S.; El-Husseini, Alaa et al. (2008): Motor protein-dependent transport of AMPA receptors into spines during long-term potentiation. In *Nat Neurosci* 11 (4), pp. 457–466. DOI: 10.1038/nn2063.

Criado, José R.; Sánchez-Alavez, Manuel; Conti, Bruno; Giacchino, Jeannie L.; Wills, Derek N.; Henriksen, Steven J. et al. (2005): Mice devoid of prion protein have cognitive deficits that are rescued by reconstitution of PrP in neurons. In *Neurobiology of disease* 19 (1-2), pp. 255–265. DOI: 10.1016/j.nbd.2005.01.001.

Cuestas Torres, Diana Marcela; Cardenas, Fernando P. (2020): Synaptic plasticity in Alzheimer's disease and healthy aging. In *Reviews in the neurosciences* 31 (3), pp. 245–268. DOI: 10.1515/revneuro-2019-0058.

Cullen, Peter J.; Steinberg, Florian (2018): To degrade or not to degrade: mechanisms and significance of endocytic recycling. In *Nat Rev Mol Cell Biol* 19 (11), pp. 679–696. DOI: 10.1038/s41580-018-0053-7.

Cummings, Jennifer A.; Mulkey, Rosel M.; Nicoll, Roger A.; Malenka, Robert C. (1996): Ca2+ Signaling Requirements for Long-Term Depression in the Hippocampus. In *Neuron* 16 (4), pp. 825–833. DOI: 10.1016/S0896-6273(00)80102-6.

Curtis, D. R.; Duggan, A. W.; Felix, D.; Johnston, G. A. (1970): GABA, bicuculline and central inhibition. In *Nature* 226 (5252), pp. 1222–1224. DOI: 10.1038/2261222a0.

Curtis, John; Errington, Mick; Bliss, Tim; Voss, Karen; MacLeod, Nikki (2003): Age-dependent loss of PTP and LTP in the hippocampus of PrP-null mice. In *Neurobiology of disease* 13 (1), pp. 55–62. DOI: 10.1016/S0969-9961(03)00017-2.

Cuveillier, Camille; Boulan, Benoit; Ravanello, Charlotte; Denarier, Eric; Deloulme, Jean-Christophe; Gory-Fauré, Sylvie et al. (2021): Beyond Neuronal Microtubule Stabilization: MAP6 and CRMPS, Two Converging Stories. In *Front. Mol. Neurosci.* 14, p. 665693. DOI: 10.3389/fnmol.2021.665693.

Daw, Michael I.; Chittajallu, Ramesh; Bortolotto, Zuner A.; Dev, Kumlesh K.; Duprat, Fabrice; Henley, Jeremy M. et al. (2000): PDZ Proteins Interacting with C-Terminal GluR2/3 Are Involved in a PKC-Dependent Regulation of AMPA Receptors at Hippocampal Synapses. In *Neuron* 28 (3), pp. 873–886. DOI: 10.1016/S0896-6273(00)00160-4.

Defelipe, Javier (2011): The evolution of the brain, the human nature of cortical circuits, and intellectual creativity. In *Frontiers in neuroanatomy* 5, p. 29. DOI: 10.3389/fnana.2011.00029.

Dekker-Ohno, Kyoko; Hayasaka, Shizu; Takagishi, Yoshiko; Oda, Sen-ichi; Wakasugi, Noboru; Mikoshiba, Katsuhiko et al. (1996): Endoplasmic reticulum is missing in dendritic spines of Purkinje cells of the ataxic mutant rat. In *Brain research* 714 (1-2), pp. 226–230. DOI: 10.1016/0006-8993(95)01560-4.

Desai, A.; Mitchison, T. J. (1997): Microtubule polymerization dynamics. In *Annual review of cell and developmental biology* 13, pp. 83–117. DOI: 10.1146/annurev.cellbio.13.1.83.

Desai, Niraj S. (2003): Homeostatic plasticity in the CNS: synaptic and intrinsic forms. In *Journal of physiology, Paris* 97 (4-6), pp. 391–402. DOI: 10.1016/j.jphysparis.2004.01.005.

Edgar, James R. (2016): Q&A: What are exosomes, exactly? In *BMC biology* 14, p. 46. DOI: 10.1186/s12915-016-0268-z.

Encalada, Sandra E.; Szpankowski, Lukasz; Xia, Chun-hong; Goldstein, Lawrence S. B. (2011): Stable kinesin and dynein assemblies drive the axonal transport of mammalian prion protein vesicles. In *Cell* 144 (4), pp. 551–565. DOI: 10.1016/j.cell.2011.01.021.

Endres, Kristina; Mitteregger, Gerda; Kojro, Elzbieta; Kretzschmar, Hans; Fahrenholz, Falk (2009): Influence of ADAM10 on prion protein processing and scrapie infectiosity in vivo. In *Neurobiology of disease* 36 (2), pp. 233–241. DOI: 10.1016/j.nbd.2009.07.015.

Eskelinen, Eeva-Liisa (2006): Roles of LAMP-1 and LAMP-2 in lysosome biogenesis and autophagy. In *Molecular aspects of medicine* 27 (5-6), pp. 495–502. DOI: 10.1016/j.mam.2006.08.005.

Essandoh, Kobina; Yang, Liwang; Wang, Xiaohong; Huang, Wei; Qin, Dongze; Hao, Jiukuan et al. (2015): Blockade of exosome generation with GW4869 dampens the sepsis-induced inflammation and cardiac dysfunction. In *Biochimica et biophysica acta* 1852 (11), pp. 2362–2371. DOI: 10.1016/j.bbadis.2015.08.010.

Fang, Cheng; Wu, Bei; Le, Nhat T. T.; Imberdis, Thibaut; Mercer, Robert C. C.; Harris, David A. (2018): Prions activate a p38 MAPK synaptotoxic signaling pathway. In *PLoS pathogens* 14 (9), e1007283. DOI: 10.1371/journal.ppat.1007283.

Fauré, J.; Lachenal, G.; Court, M.; Hirrlinger, J.; Chatellard-Causse, C.; Blot, B. et al. (2006): Exosomes are released by cultured cortical neurones. In *Molecular and cellular neurosciences* 31 (4), pp. 642–648. DOI: 10.1016/j.mcn.2005.12.003.

Ferreira, Diana G.; Temido-Ferreira, Mariana; Vicente Miranda, Hugo; Batalha, Vânia L.; Coelho, Joana E.; Szegö, Éva M. et al. (2017): α-synuclein interacts with PrPC to induce cognitive impairment through mGluR5 and NMDAR2B. In *Nature neuroscience* 20 (11), pp. 1569–1579. DOI: 10.1038/nn.4648.

Fioravante, Diasynou; Regehr, Wade G. (2011): Short-term forms of presynaptic plasticity. In *Current opinion in neurobiology* 21 (2), pp. 269–274. DOI: 10.1016/j.conb.2011.02.003.

Fischer, M.; Kaech, S.; Wagner, U.; Brinkhaus, H.; Matus, A. (2000): Glutamate receptors regulate actin-based plasticity in dendritic spines. In *Nat Neurosci* 3 (9), pp. 887–894. DOI: 10.1038/78791.

Fish, Kenneth N. (2009): Total internal reflection fluorescence (TIRF) microscopy. In *Current protocols in cytometry / editorial board, J. Paul Robinson, managing editor … [et al.]* Chapter 12, Unit12.18. DOI: 10.1002/0471142956.cy1218s50.

Fröhlich, Dominik; Kuo, Wen Ping; Frühbeis, Carsten; Sun, Jyh-Jang; Zehendner, Christoph M.; Luhmann, Heiko J. et al. (2014): Multifaceted effects of oligodendroglial exosomes on neurons: impact on neuronal firing rate, signal transduction and gene regulation. In *Philosophical Transactions of the Royal Society B: Biological Sciences* 369 (1652). DOI: 10.1098/rstb.2013.0510.

Fu, Meng-meng; Holzbaur, Erika L. F. (2014): Integrated regulation of motor-driven organelle transport by scaffolding proteins. In *Trends in cell biology* 24 (10), pp. 564–574. DOI: 10.1016/j.tcb.2014.05.002.

Fu, Zhanyan; Vicini, Stefano (2009): Neuroligin-2 accelerates GABAergic synapse maturation in cerebellar granule cells. In *Molecular and cellular neurosciences* 42 (1), pp. 45–55. DOI: 10.1016/j.mcn.2009.05.004.

Gassart, Aude de; Geminard, Charles; Fevrier, Benoit; Raposo, Graca; Vidal, Michel (2003): Lipid raft-associated protein sorting in exosomes. In *Blood* 102 (13), pp. 4336–4344. DOI: 10.1182/blood-2003-03-0871.

Geiger, Julia C.; Lipka, Joanna; Segura, Inmaculada; Hoyer, Susanne; Schlager, Max A.; Wulf, Phebe S. et al. (2014): The GRIP1/14-3-3 pathway coordinates cargo trafficking and dendrite development. In *Developmental cell* 28 (4), pp. 381–393. DOI: 10.1016/j.devcel.2014.01.018.

Gerges, Nashaat Z.; Backos, Donald S.; Esteban, José A. (2004): Local control of AMPA receptor trafficking at the postsynaptic terminal by a small GTPase of the Rab family. In *The Journal of biological chemistry* 279 (42), pp. 43870–43878. DOI: 10.1074/jbc.M404982200.

Ghossoub, Rania; Lembo, Frédérique; Rubio, Aude; Gaillard, Carole Baron; Bouchet, Jérôme; Vitale, Nicolas et al. (2014): Syntenin-ALIX exosome biogenesis and budding into multivesicular bodies are controlled by ARF6 and PLD2. In *Nat Commun* 5 (1), p. 3477. DOI: 10.1038/ncomms4477.

Gill, S. R.; Schroer, T. A.; Szilak, I.; Steuer, E. R.; Sheetz, M. P.; Cleveland, D. W. (1991): Dynactin, a conserved, ubiquitously expressed component of an activator of vesicle motility mediated by cytoplasmic dynein. In *The Journal of cell biology* 115 (6), pp. 1639–1650. DOI: 10.1083/jcb.115.6.1639.

Gois, Stéphanie de; Schäfer, Martin K-H; Defamie, Norah; Chen, Chu; Ricci, Anthony; Weihe, Eberhard et al. (2005): Homeostatic scaling of vesicular glutamate and GABA transporter

expression in rat neocortical circuits. In *J. Neurosci.* 25 (31), pp. 7121–7133. DOI: 10.1523/JNEUROSCI.5221-04.2005.

Goldie, Belinda J.; Dun, Matthew D.; Lin, Minjie; Smith, Nathan D.; Verrills, Nicole M.; Dayas, Christopher V.; Cairns, Murray J. (2014): Activity-associated miRNA are packaged in Map1b-enriched exosomes released from depolarized neurons. In *Nucleic acids research* 42 (14), pp. 9195–9208. DOI: 10.1093/nar/gku594.

Goldsbury, Claire; Mocanu, Maria-Magdalena; Thies, Edda; Kaether, Christoph; Haass, Christian; Keller, Patrick et al. (2006): Inhibition of APP trafficking by tau protein does not increase the generation of amyloid-beta peptides. In *Traffic (Copenhagen, Denmark)* 7 (7), pp. 873–888. DOI: 10.1111/j.1600-0854.2006.00434.x.

Goo, Marisa S.; Sancho, Laura; Slepak, Natalia; Boassa, Daniela; Deerinck, Thomas J.; Ellisman, Mark H. et al. (2017): Activity-dependent trafficking of lysosomes in dendrites and dendritic spines. In *The Journal of cell biology* 216 (8), pp. 2499–2513. DOI: 10.1083/jcb.201704068.

Grundke-Iqbal, I.; Iqbal, K.; Tung, Y. C.; Quinlan, M.; Wisniewski, H. M.; Binder, L. I. (1986): Abnormal phosphorylation of the microtubule-associated protein tau (tau) in Alzheimer cytoskeletal pathology. In *Proc Natl Acad Sci U S A* 83 (13), pp. 4913–4917. DOI: 10.1073/pnas.83.13.4913.

Gu, Yi; Chiu, Shu-Ling; Liu, Bian; Wu, Pei-Hsun; Delannoy, Michael; Lin, Da-Ting et al. (2016): Differential vesicular sorting of AMPA and GABAA receptors. In *Proc Natl Acad Sci USA* 113 (7), E922-31. DOI: 10.1073/pnas.1525726113.

Guescini, Michele; Genedani, Susanna; Stocchi, Vilberto; Agnati, Luigi Francesco (2010): Astrocytes and Glioblastoma cells release exosomes carrying mtDNA. In *Journal of neural transmission (Vienna, Austria : 1996)* 117 (1), pp. 1–4. DOI: 10.1007/s00702-009-0288-8.

Guillaud, Laurent; Wong, Richard; Hirokawa, Nobutaka (2008): Disruption of KIF17-Mint1 interaction by CaMKII-dependent phosphorylation: a molecular model of kinesin-cargo release. In *Nat Cell Biol* 10 (1), pp. 19–29. DOI: 10.1038/ncb1665.

Guo, Belinda B.; Bellingham, Shayne A.; Hill, Andrew F. (2015): The neutral sphingomyelinase pathway regulates packaging of the prion protein into exosomes. In *Journal of Biological Chemistry* 290 (6), pp. 3455–3467. DOI: 10.1074/jbc.M114.605253.

Guo, Xiaoli; Farías, Ginny G.; Mattera, Rafael; Bonifacino, Juan S. (2016): Rab5 and its effector FHF contribute to neuronal polarity through dynein-dependent retrieval of somatodendritic proteins from the axon. In *Proc Natl Acad Sci USA* 113 (36), E5318-27. DOI: 10.1073/pnas.1601844113.

Halpain, Shelley; Hipolito, Arlene; Saffer, Linda (1998): Regulation of F-Actin Stability in Dendritic Spines by Glutamate Receptors and Calcineurin. In *J. Neurosci.* 18 (23), pp. 9835–9844. DOI: 10.1523/JNEUROSCI.18-23-09835.1998.

Hammond, Jennetta W.; Huang, Chun-Fang; Kaech, Stefanie; Jacobson, Catherine; Banker, Gary; Verhey, Kristen J. (2010): Posttranslational modifications of tubulin and the polarized transport of kinesin-1 in neurons. In *Molecular biology of the cell* 21 (4), pp. 572–583. DOI: 10.1091/mbc.e09-01-0044.

Harrington, W. F.; Rodgers, M. E. (1984): Myosin. In *Annual review of biochemistry* 53, pp. 35–73. DOI: 10.1146/annurev.bi.53.070184.000343.

Hartmann, Alexander; Muth, Christiane; Dabrowski, Oliver; Krasemann, Susanne; Glatzel, Markus (2017): Exosomes and the Prion Protein: More than One Truth. In *Frontiers in neuroscience* 11, p. 194. DOI: 10.3389/fnins.2017.00194.

Heisler, F. F.; Loebrich, S.; Pechmann, Y.; Maier, N.; Zivkovic, A. R.; Tokito, M. et al. (2011): Muskelin regulates actin filament- and microtubule-based GABA(A) receptor transport in neurons. In *Neuron* 70 (1), pp. 66–81. DOI: 10.1016/j.neuron.2011.03.008.

Heisler, F. F.; Pechmann, Y.; Wieser, I.; Altmeppen, H. C.; Veenendaal, L.; Muhia, M. et al. (2018): Muskelin Coordinates PrP(C) Lysosome versus Exosome Targeting and Impacts Prion Disease Progression. In *Neuron* 99 (6), 1155-1169 e9. DOI: 10.1016/j.neuron.2018.08.010.

Heisler, Frank F.; Lee, Han Kyu; Gromova, Kira V.; Pechmann, Yvonne; Schurek, Beate; Ruschkies, Laura et al. (2014): GRIP1 interlinks N-cadherin and AMPA receptors at vesicles to promote combined cargo transport into dendrites. In *Proc Natl Acad Sci USA* 111 (13), pp. 5030–5035. DOI: 10.1073/pnas.1304301111.

Hendershott, Melissa C.; Vale, Ronald D. (2014): Regulation of microtubule minus-end dynamics by CAMSAPs and Patronin. In *Proc Natl Acad Sci USA* 111 (16), pp. 5860–5865. DOI: 10.1073/pnas.1404133111.

Hendricks, Adam G.; Perlson, Eran; Ross, Jennifer L.; Schroeder, Harry W.; Tokito, Mariko; Holzbaur, Erika L. F. (2010): Motor coordination via a tug-of-war mechanism drives bidirectional vesicle transport. In *Current biology : CB* 20 (8), pp. 697–702. DOI: 10.1016/j.cub.2010.02.058.

Henne, William M.; Buchkovich, Nicholas J.; Emr, Scott D. (2011): The ESCRT pathway. In *Developmental cell* 21 (1), pp. 77–91. DOI: 10.1016/j.devcel.2011.05.015.

Herms, J.; Tings, T.; Gall, S.; Madlung, A.; Giese, A.; Siebert, H. et al. (1999): Evidence of presynaptic location and function of the prion protein. In *J Neurosci* 19 (20), pp. 8866–8875.

Heynen, Arnold J.; Quinlan, Elizabeth M.; Bae, David C.; Bear, Mark F. (2000): Bidirectional, Activity-Dependent Regulation of Glutamate Receptors in the Adult Hippocampus In Vivo. In *Neuron* 28 (2), pp. 527–536. DOI: 10.1016/S0896-6273(00)00130-6.

Hill, Andrew F. (2019): Extracellular Vesicles and Neurodegenerative Diseases. In *The Journal of neuroscience : the official journal of the Society for Neuroscience* 39 (47), pp. 9269–9273. DOI: 10.1523/JNEUROSCI.0147-18.2019.

Hines, Rochelle M.; Wu, Longjun; Hines, Dustin J.; Steenland, Hendrik; Mansour, Souraya; Dahlhaus, Regina et al. (2008): Synaptic imbalance, stereotypies, and impaired social interactions in mice with altered neuroligin 2 expression. In *J. Neurosci.* 28 (24), pp. 6055–6067. DOI: 10.1523/JNEUROSCI.0032-08.2008.

Hinkle, C. Leann; Diestel, Simone; Lieberman, Jeffrey; Maness, Patricia F. (2006): Metalloprotease-induced ectodomain shedding of neural cell adhesion molecule (NCAM). In *Journal of neurobiology* 66 (12), pp. 1378–1395. DOI: 10.1002/neu.20257.

Hirano, Shinji; Takeichi, Masatoshi (2012): Cadherins in brain morphogenesis and wiring. In *Physiological reviews* 92 (2), pp. 597–634. DOI: 10.1152/physrev.00014.2011.

Hirokawa, Nobutaka; Niwa, Shinsuke; Tanaka, Yosuke (2010): Molecular motors in neurons: transport mechanisms and roles in brain function, development, and disease. In *Neuron* 68 (4), pp. 610–638. DOI: 10.1016/j.neuron.2010.09.039.

Hirokawa, Nobutaka; Takemura, Reiko (2004): Molecular motors in neuronal development, intracellular transport and diseases. In *Current opinion in neurobiology* 14 (5), pp. 564–573. DOI: 10.1016/j.conb.2004.08.011.

Hollmann, M.; Hartley, M.; Heinemann, S. (1991): Ca2+ permeability of KA-AMPA--gated glutamate receptor channels depends on subunit composition. In *Science (New York, N.Y.)* 252 (5007), pp. 851–853. DOI: 10.1126/science.1709304.

Honkura, Naoki; Matsuzaki, Masanori; Noguchi, Jun; Ellis-Davies, Graham C. R.; Kasai, Haruo (2008): The subspine organization of actin fibers regulates the structure and plasticity of dendritic spines. In *Neuron* 57 (5), pp. 719–729. DOI: 10.1016/j.neuron.2008.01.013.

Hotulainen, Pirta; Hoogenraad, Casper C. (2010): Actin in dendritic spines: connecting dynamics to function. In *The Journal of cell biology* 189 (4), pp. 619–629. DOI: 10.1083/jcb.201003008.

Hou, Wenya; Izadi, Maryam; Nemitz, Sabine; Haag, Natja; Kessels, Michael M.; Qualmann, Britta (2015): The Actin Nucleator Cobl Is Controlled by Calcium and Calmodulin. In *PLOS Biology* 13 (9), e1002233. DOI: 10.1371/journal.pbio.1002233.

Hsiao, K. K.; Cass, C.; Schellenberg, G. D.; Bird, T.; Devine-Gage, E.; Wisniewski, H.; Prusiner, S. B. (1991): A prion protein variant in a family with the telencephalic form of Gerstmann-Sträussler-Scheinker syndrome. In *Neurology* 41 (5), pp. 681–684. DOI: 10.1212/wnl.41.5.681.

Hsu, Chieh; Morohashi, Yuichi; Yoshimura, Shin-Ichiro; Manrique-Hoyos, Natalia; Jung, Sangyong; Lauterbach, Marcel A. et al. (2010): Regulation of exosome secretion by Rab35 and its GTPase-activating proteins TBC1D10A-C. In *The Journal of cell biology* 189 (2), pp. 223–232. DOI: 10.1083/jcb.200911018.

Huang, Yu-Mei; Rasband, Matthew N. (2016): Organization of the axon initial segment: Actin like a fence. In *The Journal of cell biology* 215 (1), pp. 9–11. DOI: 10.1083/jcb.201609084.

Huganir, Richard L.; Nicoll, Roger A. (2013): AMPARs and synaptic plasticity: the last 25 years. In *Neuron* 80 (3), pp. 704–717. DOI: 10.1016/j.neuron.2013.10.025.

Hunt, C. A.; Schenker, L. J.; Kennedy, M. B. (1996): PSD-95 is associated with the postsynaptic density and not with the presynaptic membrane at forebrain synapses. In *J. Neurosci.* 16 (4), pp. 1380–1388. DOI: 10.1523/JNEUROSCI.16-04-01380.1996.

Ikonen, Elina (2001): Roles of lipid rafts in membrane transport. In *Current opinion in cell biology* 13 (4), pp. 470–477. DOI: 10.1016/S0955-0674(00)00238-6.

Inoue, Hiroaki; Nojima, Hiroshi; Okayama, Hiroto (1990): High efficiency transformation of Escherichia coli with plasmids. In *Gene* 96 (1), pp. 23–28. DOI: 10.1016/0378-1119(90)90336-P.

Ittner, Arne; Ittner, Lars M. (2018): Dendritic Tau in Alzheimer's Disease. In *Neuron* 99 (1), pp. 13–27. DOI: 10.1016/j.neuron.2018.06.003.

Kaech, Stefanie; Banker, Gary (2006): Culturing hippocampal neurons. In *Nat Protoc* 1 (5), pp. 2406–2415. DOI: 10.1038/nprot.2006.356.

Kaiser, Darcy M.; Acharya, Moulinath; Leighton, Patricia L. A.; Wang, Hao; Daude, Nathalie; Wohlgemuth, Serene et al. (2012): Amyloid beta precursor protein and prion protein have a conserved interaction affecting cell adhesion and CNS development. In *PloS one* 7 (12), e51305. DOI: 10.1371/journal.pone.0051305.

Kanaani, Jamil; Prusiner, Stanley B.; Diacovo, Julia; Baekkeskov, Steinunn; Legname, Giuseppe (2005): Recombinant prion protein induces rapid polarization and development of synapses in embryonic rat hippocampal neurons in vitro. In *Journal of neurochemistry* 95 (5), pp. 1373–1386. DOI: 10.1111/j.1471-4159.2005.03469.x.

Kang, Dukjin; Oh, Sunok; Ahn, Sung-Min; Lee, Bong-Hee; Moon, Myeong Hee (2008): Proteomic analysis of exosomes from human neural stem cells by flow field-flow fractionation and nanoflow liquid chromatography-tandem mass spectrometry. In *Journal of proteome research* 7 (8), pp. 3475–3480. DOI: 10.1021/pr800225z.

Katzmann, David J.; Babst, Markus; Emr, Scott D. (2001): Ubiquitin-Dependent Sorting into the Multivesicular Body Pathway Requires the Function of a Conserved Endosomal Protein Sorting Complex, ESCRT-I. In *Cell* 106 (2), pp. 145–155. DOI: 10.1016/S0092-8674(01)00434-2.

Kennedy, Matthew J.; Ehlers, Michael D. (2006): Organelles and trafficking machinery for postsynaptic plasticity. In *Annual review of neuroscience* 29, pp. 325–362. DOI: 10.1146/annurev.neuro.29.051605.112808.

Kishimoto, Yasushi; Hirono, Moritoshi; Atarashi, Ryuichiro; Sakaguchi, Suehiro; Yoshioka, Tohru; Katamine, Shigeru; Kirino, Yutaka (2020): Impairment of cerebellar long-term

depression and GABAergic transmission in prion protein deficient mice ectopically expressing PrPLP/Dpl. In *Scientific reports* 10 (1), p. 15900. DOI: 10.1038/s41598-020-72753-6.

Klumperman, Judith; Raposo, Graça (2014): The complex ultrastructure of the endolysosomal system. In *Cold Spring Harb Perspect Biol* 6 (10), a016857. DOI: 10.1101/cshperspect.a016857.

Kneussel, Matthias; Brandstätter, Johann Helmut; Laube, Bodo; Stahl, Sabine; Müller, Ulrike; Betz, Heinrich (1999): Loss of Postsynaptic GABA A Receptor Clustering in Gephyrin-Deficient Mice. In *J. Neurosci.* 19 (21), pp. 9289–9297. DOI: 10.1523/JNEUROSCI.19-21-09289.1999.

Kneussel, Matthias; Loebrich, Sven (2007): Trafficking and synaptic anchoring of ionotropic inhibitory neurotransmitter receptors. In *Biology of the cell* 99 (6), pp. 297–309. DOI: 10.1042/BC20060120.

Kneussel, Matthias; Wagner, Wolfgang (2013): Myosin motors at neuronal synapses: drivers of membrane transport and actin dynamics. In *Nat Rev Neurosci* 14 (4), pp. 233–247. DOI: 10.1038/nrn3445.

Köhrmann, M.; Haubensak, W.; Hemraj, I.; Kaether, C.; Lessmann, V. J.; Kiebler, M. A. (1999): Fast, convenient, and effective method to transiently transfect primary hippocampal neurons. In *Journal of neuroscience research* 58 (6), pp. 831–835.

Kornau, H. C.; Schenker, L. T.; Kennedy, M. B.; Seeburg, P. H. (1995): Domain interaction between NMDA receptor subunits and the postsynaptic density protein PSD-95. In *Science (New York, N.Y.)* 269 (5231), pp. 1737–1740. DOI: 10.1126/science.7569905.

Kosaka, Nobuyoshi; Iguchi, Haruhisa; Yoshioka, Yusuke; Takeshita, Fumitaka; Matsuki, Yasushi; Ochiya, Takahiro (2010): Secretory mechanisms and intercellular transfer of microRNAs in living cells. In *The Journal of biological chemistry* 285 (23), pp. 17442–17452. DOI: 10.1074/jbc.M110.107821.

Kosik, Kenneth S.; Donahue, Christine P.; Israely, Inbal; Liu, Xin; Ochiishi, Tomoyo (2005): Delta-catenin at the synaptic-adherens junction. In *Trends in cell biology* 15 (3), pp. 172–178. DOI: 10.1016/j.tcb.2005.01.004.

Kraus, Allison; Groveman, Bradley R.; Caughey, Byron (2013): Prions and the potential transmissibility of protein misfolding diseases. In *Annual review of microbiology* 67, pp. 543–564. DOI: 10.1146/annurev-micro-092412-155735.

Krementsov, Dimitry N.; Krementsova, Elena B.; Trybus, Kathleen M. (2004): Myosin V: regulation by calcium, calmodulin, and the tail domain. In *J Cell Biol* 164 (6), pp. 877–886. DOI: 10.1083/jcb.200310065.

Kretzschmar, H. A.; Tings, T.; Madlung, A.; Giese, A.; Herms, J. (2001): Prion protein as copper-binding protein at the synapse. In *Methods in molecular medicine* 59, pp. 17–30. DOI: 10.1385/1-59259-134-5:17.

Krueger, Dilja D.; Tuffy, Liam P.; Papadopoulos, Theofilos; Brose, Nils (2012): The role of neurexins and neuroligins in the formation, maturation, and function of vertebrate synapses. In *Current opinion in neurobiology* 22 (3), pp. 412–422. DOI: 10.1016/j.conb.2012.02.012.

Kuffer, A.; Lakkaraju, A. K.; Mogha, A.; Petersen, S. C.; Airich, K.; Doucerain, C. et al. (2016): The prion protein is an agonistic ligand of the G protein-coupled receptor Adgrg6. In *Nature* 536 (7617), pp. 464–468. DOI: 10.1038/nature19312.

Kuta, Anna; Deng, Wenhan; Morsi El-Kadi, Ali; Banks, Gareth T.; Hafezparast, Majid; Pfister, K. Kevin; Fisher, Elizabeth M. C. (2010): Mouse cytoplasmic dynein intermediate chains: identification of new isoforms, alternative splicing and tissue distribution of transcripts. In *PloS one* 5 (7), e11682. DOI: 10.1371/journal.pone.0011682.

La Vitola, Pietro; Beeg, Marten; Balducci, Claudia; Santamaria, Giulia; Restelli, Elena; Colombo, Laura et al. (2019): Cellular prion protein neither binds to alpha-synuclein oligomers

nor mediates their detrimental effects. In *Brain : a journal of neurology* 142 (2), pp. 249–254. DOI: 10.1093/brain/awy318.

Lachenal, Gaelle; Pernet-Gallay, Karin; Chivet, Mathilde; Hemming, Fiona J.; Belly, Agnès; Bodon, Gilles et al. (2011): Release of exosomes from differentiated neurons and its regulation by synaptic glutamatergic activity. In *Molecular and cellular neurosciences* 46 (2), pp. 409–418. DOI: 10.1016/j.mcn.2010.11.004.

Lambert, M. P.; Barlow, A. K.; Chromy, B. A.; Edwards, C.; Freed, R.; Liosatos, M. et al. (1998): Diffusible, nonfibrillar ligands derived from Abeta1-42 are potent central nervous system neurotoxins. In *Proc Natl Acad Sci USA* 95 (11), pp. 6448–6453. DOI: 10.1073/pnas.95.11.6448.

Lauren, J.; Gimbel, D. A.; Nygaard, H. B.; Gilbert, J. W.; Strittmatter, S. M. (2009): Cellular prion protein mediates impairment of synaptic plasticity by amyloid-beta oligomers. In *Nature* 457 (7233), pp. 1128–1132. DOI: 10.1038/nature07761.

Laurén, Juha; Gimbel, David A.; Nygaard, Haakon B.; Gilbert, John W.; Strittmatter, Stephen M. (2009): Cellular prion protein mediates impairment of synaptic plasticity by amyloid-beta oligomers. In *Nature* 457 (7233), pp. 1128–1132. DOI: 10.1038/nature07761.

Lee, Gloria; Thangavel, Ramasamy; Sharma, Vandana M.; Litersky, Joel M.; Bhaskar, Kiran; Fang, Sandy M. et al. (2004): Phosphorylation of tau by fyn: implications for Alzheimer's disease. In *J. Neurosci.* 24 (9), pp. 2304–2312. DOI: 10.1523/JNEUROSCI.4162-03.2004.

Lee, Hey-Kyoung; Kirkwood, Alfredo (2019): Mechanisms of Homeostatic Synaptic Plasticity in vivo. In *Frontiers in cellular neuroscience* 13, p. 520. DOI: 10.3389/fncel.2019.00520.

Lee, V. M.; Goedert, M.; Trojanowski, J. Q. (2001): Neurodegenerative tauopathies. In *Annual review of neuroscience* 24, pp. 1121–1159. DOI: 10.1146/annurev.neuro.24.1.1121.

Lee, Yi; El Andaloussi, Samir; Wood, Matthew J. A. (2012): Exosomes and microvesicles: extracellular vesicles for genetic information transfer and gene therapy. In *Human molecular genetics* 21 (R1), R125-34. DOI: 10.1093/hmg/dds317.

Li, Guangwen; Ma, Qingfeng; Wang, Rongliang; Fan, Zhibin; Tao, Zhen; Liu, Ping et al. (2018): Diagnostic and Immunosuppressive Potential of Elevated Mir-424 Levels in Circulating Immune Cells of Ischemic Stroke Patients. In *Aging and disease* 9 (2), pp. 172–181. DOI: 10.14336/AD.2017.0602.

Ligon, Lee A.; Steward, Oswald (2000): Role of microtubules and actin filaments in the movement of mitochondria in the axons and dendrites of cultured hippocampal neurons. In *J. Comp. Neurol.* 427 (3), pp. 351–361. DOI: 10.1002/1096-9861(20001120)427:3<351::aid-cne3>3.0.co;2-r.

Linden, Rafael; Martins, Vilma R.; Prado, Marco A. M.; Cammarota, Martín; Izquierdo, Iván; Brentani, Ricardo R. (2008): Physiology of the prion protein. In *Physiological reviews* 88 (2), pp. 673–728. DOI: 10.1152/physrev.00007.2007.

Linsenmeier, Luise; Mohammadi, Behnam; Shafiq, Mohsin; Frontzek, Karl; Bär, Julia; Shrivastava, Amulya N. et al. (2021): Ligands binding to the prion protein induce its proteolytic release with therapeutic potential in neurodegenerative proteinopathies. In *Science Advances* 7 (48), eabj1826. DOI: 10.1126/sciadv.abj1826.

Lissin, D. V.; Gomperts, S. N.; Carroll, R. C.; Christine, C. W.; Kalman, D.; Kitamura, M. et al. (1998): Activity differentially regulates the surface expression of synaptic AMPA and NMDA glutamate receptors. In *Proc Natl Acad Sci USA* 95 (12), pp. 7097–7102. DOI: 10.1073/pnas.95.12.7097.

Liu; Obeid; Hannun (1997): Sphingomyelinases in cell regulation. In *Seminars in cell & developmental biology* 8 (3), pp. 311–322. DOI: 10.1006/scdb.1997.0153.

Liu, Qiang; Zhang, Juan; Tran, Hien; Verbeek, Marcel M.; Reiss, Karina; Estus, Steven; Bu, Guojun (2009): LRP1 shedding in human brain: roles of ADAM10 and ADAM17. In *Mol Neurodegeneration* 4 (1), p. 17. DOI: 10.1186/1750-1326-4-17.

Lledo, P. M.; Tremblay, P.; DeArmond, S. J.; Prusiner, S. B.; Nicoll, R. A. (1996): Mice deficient for prion protein exhibit normal neuronal excitability and synaptic transmission in the hippocampus. In *Proc Natl Acad Sci USA* 93 (6), pp. 2403–2407. DOI: 10.1073/pnas.93.6.2403.

Lopes, M. H.; Hajj, G. N.; Muras, A. G.; Mancini, G. L.; Castro, R. M.; Ribeiro, K. C. et al. (2005): Interaction of cellular prion and stress-inducible protein 1 promotes neuritogenesis and neuroprotection by distinct signaling pathways. In *J Neurosci* 25 (49), pp. 11330–11339. DOI: 10.1523/JNEUROSCI.2313-05.2005.

Lu, Wen-Jing; Zeng, Li-Li; Wang, Yang; Zhang, Yu; Liang, Huai-Bin; Tu, Xuan-Qiang et al. (2018): Blood microRNA-15a Correlates with IL-6, IGF-1 and Acute Cerebral Ischemia. In *Current neurovascular research* 15 (1), pp. 63–71. DOI: 10.2174/1567202615666180319143509.

Lv, Kaosheng; Chen, Liang; Li, Yuanjun; Li, Zenglong; Zheng, Pengli; Liu, Yingying et al. (2015): Trip6 promotes dendritic morphogenesis through dephosphorylated GRIP1-dependent myosin VI and F-actin organization. In *J. Neurosci.* 35 (6), pp. 2559–2571. DOI: 10.1523/JNEUROSCI.2125-14.2015.

Maas, Christoph; Belgardt, Dorthe; Lee, Han Kyu; Heisler, Frank F.; Lappe-Siefke, Corinna; Magiera, Maria M. et al. (2009): Synaptic activation modifies microtubules underlying transport of postsynaptic cargo. In *Proc Natl Acad Sci USA* 106 (21), pp. 8731–8736. DOI: 10.1073/pnas.0812391106.

MacDermott, A. B.; Mayer, M. L.; Westbrook, G. L.; Smith, S. J.; Barker, J. L. (1986): NMDA-receptor activation increases cytoplasmic calcium concentration in cultured spinal cord neurones. In *Nature* 321 (6069), pp. 519–522. DOI: 10.1038/321519a0.

Maglio, Laura E.; Martins, Vilma R.; Izquierdo, Iván; Ramirez, Oscar A. (2006): Role of cellular prion protein on LTP expression in aged mice. In *Brain research* 1097 (1), pp. 11–18. DOI: 10.1016/j.brainres.2006.04.056.

Maglio, Laura E.; Perez, Mariela F.; Martins, Vilma R.; Brentani, Ricardo R.; Ramirez, Oscar A. (2004): Hippocampal synaptic plasticity in mice devoid of cellular prion protein. In *Brain research. Molecular brain research* 131 (1-2), pp. 58–64. DOI: 10.1016/j.molbrainres.2004.08.004.

Málaga-Trillo, Edward; Solis, Gonzalo P.; Schrock, Yvonne; Geiss, Corinna; Luncz, Lydia; Thomanetz, Venus; Stuermer, Claudia A. O. (2009): Regulation of embryonic cell adhesion by the prion protein. In *PLoS biology* 7 (3), e55. DOI: 10.1371/journal.pbio.1000055.

Mallucci, G. R.; Ratté, S.; Asante, E. A.; Linehan, J.; Gowland, I.; Jefferys, J. G. R.; Collinge, J. (2002): Post-natal knockout of prion protein alters hippocampal CA1 properties, but does not result in neurodegeneration. In *The EMBO journal* 21 (3), pp. 202–210. DOI: 10.1093/emboj/21.3.202.

Mangé, Alain; Milhavet, Ollivier; Umlauf, David; Harris, David; Lehmann, Sylvain (2002): PrP-dependent cell adhesion in N2a neuroblastoma cells. In *FEBS letters* 514 (2-3), pp. 159–162. DOI: 10.1016/S0014-5793(02)02338-4.

Manson, J.; West, J. D.; Thomson, V.; McBride, P.; Kaufman, M. H.; Hope, J. (1992): The prion protein gene: a role in mouse embryogenesis? In *Development (Cambridge, England)* 115 (1), pp. 117–122. DOI: 10.1242/dev.115.1.117.

Martinez-Arroyo, Olga; Selma-Soriano, Estela; Ortega, Ana; Cortes, Raquel; Redon, Josep (2021): Small Rab GTPases in Intracellular Vesicle Trafficking: The Case of Rab3A/Raphillin-

3A Complex in the Kidney. In *International journal of molecular sciences* 22 (14), p. 7679. DOI: 10.3390/ijms22147679.

Martins, Vilma R.; Linden, Rafael; Prado, Marco A.M; Walz, Roger; Sakamoto, Américo C.; Izquierdo, Ivan; Brentani, Ricardo R. (2002): Cellular prion protein: on the road for functions. In *FEBS letters* 512 (1-3), pp. 25–28. DOI: 10.1016/S0014-5793(02)02291-3.

Masters, C. L.; Kakulas, B. A.; Alpers, M. P.; Gajdusek, D. C.; Gibbs, C. J. (1976): Preclinical lesions and their progression in the experimental spongiform encephalopathies (kuru and Creutzfeldt-Jakob disease) in primates. In *Journal of neuropathology and experimental neurology* 35 (6), pp. 593–605. DOI: 10.1097/00005072-197611000-00001.

Matamoros-Angles, A.; Hervera, A.; Soriano, J.; Martí, E.; Carulla, P.; Llorens, F. et al. (2022): Analysis of co-isogenic prion protein deficient mice reveals behavioral deficits, learning impairment, and enhanced hippocampal excitability. In *BMC biology* 20 (1), p. 17. DOI: 10.1186/s12915-021-01203-0.

Matsuzaki, Masanori; Honkura, Naoki; Ellis-Davies, Graham C. R.; Kasai, Haruo (2004): Structural basis of long-term potentiation in single dendritic spines. In *Nature* 429 (6993), pp. 761–766. DOI: 10.1038/nature02617.

Matus, A. (2000): Actin-based plasticity in dendritic spines. In *Science (New York, N.Y.)* 290 (5492), pp. 754–758. DOI: 10.1126/science.290.5492.754.

Matus, A.; Ackermann, M.; Pehling, G.; Byers, H. R.; Fujiwara, K. (1982): High actin concentrations in brain dendritic spines and postsynaptic densities. In *Proc Natl Acad Sci USA* 79 (23), pp. 7590–7594. DOI: 10.1073/pnas.79.23.7590.

Maxfield, Frederick R.; McGraw, Timothy E. (2004): Endocytic recycling. In *Nature reviews. Molecular cell biology* 5 (2), pp. 121–132. DOI: 10.1038/nrm1315.

Mayer, M. L.; Westbrook, G. L.; Guthrie, P. B. (1984): Voltage-dependent block by Mg2+ of NMDA responses in spinal cord neurones. In *Nature* 309 (5965), pp. 261–263. DOI: 10.1038/309261a0.

Mays, Charles E.; Soto, Claudio (2016): The stress of prion disease. In *Brain research* 1648 (Pt B), pp. 553–560. DOI: 10.1016/j.brainres.2016.04.009.

McConville, M. J.; Ferguson, M. A. (1993): The structure, biosynthesis and function of glycosylated phosphatidylinositols in the parasitic protozoa and higher eukaryotes. In *Biochemical Journal* 294 (Pt 2) (Pt 2), pp. 305–324. DOI: 10.1042/bj2940305.

McDonald, Alex J.; Millhauser, Glenn L. (2014): PrP overdrive: does inhibition of α-cleavage contribute to PrP(C) toxicity and prion disease? In *Prion* 8 (2), pp. 183–191. DOI: 10.4161/pri.28796.

McKinley, Michael P.; Hay, Bruce; Lingappa, Vishwanath R.; Lieberburg, Ivan; Prusiner, Stanley B. (1987): Developmental expression of prion protein gene in brain. In *Developmental Biology* 121 (1), pp. 105–110. DOI: 10.1016/0012-1606(87)90143-6.

Menck, Kerstin; Bleckmann, Annalen; Schulz, Matthias; Ries, Lena; Binder, Claudia (2017): Isolation and Characterization of Microvesicles from Peripheral Blood. In *JoVE* (119). DOI: 10.3791/55057.

Meyer, R. K.; McKinley, M. P.; Bowman, K. A.; Braunfeld, M. B.; Barry, R. A.; Prusiner, S. B. (1986): Separation and properties of cellular and scrapie prion proteins. In *Proc Natl Acad Sci USA* 83 (8), pp. 2310–2314. DOI: 10.1073/pnas.83.8.2310.

Micci, Maria-Adelaide; Krishnan, Balaji; Bishop, Elizabeth; Zhang, Wen-Ru; Guptarak, Jutatip; Grant, Auston et al. (2019): Hippocampal stem cells promotes synaptic resistance to the dysfunctional impact of amyloid beta oligomers via secreted exosomes. In *Mol Neurodegeneration* 14 (1), p. 25. DOI: 10.1186/s13024-019-0322-8.

Mikhaylova, Marina; Bär, Julia; van Bommel, Bas; Schätzle, Philipp; YuanXiang, PingAn; Raman, Rajeev et al. (2018): Caldendrin Directly Couples Postsynaptic Calcium Signals to Actin Remodeling in Dendritic Spines. In *Neuron* 97 (5), 1110-1125.e14. DOI: 10.1016/j.neuron.2018.01.046.

Missler, Markus; Südhof, Thomas C.; Biederer, Thomas (2012): Synaptic cell adhesion. In *Cold Spring Harb Perspect Biol* 4 (4), a005694. DOI: 10.1101/cshperspect.a005694.

Mitchison, T.; Kirschner, M. (1984): Dynamic instability of microtubule growth. In *Nature* 312 (5991), pp. 237–242. DOI: 10.1038/312237a0.

Miterko, Lauren N.; Lackey, Elizabeth P.; Heck, Detlef H.; Sillitoe, Roy V. (2018): Shaping Diversity Into the Brain's Form and Function. In *Frontiers in neural circuits* 12, p. 83. DOI: 10.3389/fncir.2018.00083.

Miyamoto, Yasunori; Sakane, Fumi; Hashimoto, Kei (2015): N-cadherin-based adherens junction regulates the maintenance, proliferation, and differentiation of neural progenitor cells during development. In *Cell Adhesion & Migration* 9 (3), pp. 183–192. DOI: 10.1080/19336918.2015.1005466.

Miyata, Mariko; Finch, Elizabeth A.; Khiroug, Leonard; Hashimoto, Kouichi; Hayasaka, Shizu; Oda, Sen-ichi et al. (2000): Local Calcium Release in Dendritic Spines Required for Long-Term Synaptic Depression. In *Neuron* 28 (1), pp. 233–244. DOI: 10.1016/S0896-6273(00)00099-4.

Monroy, Brigette Y.; Tan, Tracy C.; Oclaman, Janah May; Han, Jisoo S.; Simó, Sergi; Niwa, Shinsuke et al. (2020): A Combinatorial MAP Code Dictates Polarized Microtubule Transport. In *Developmental cell* 53 (1), 60-72.e4. DOI: 10.1016/j.devcel.2020.01.029.

Montecalvo, Angela; Larregina, Adriana T.; Shufesky, William J.; Stolz, Donna Beer; Sullivan, Mara L. G.; Karlsson, Jenny M. et al. (2012): Mechanism of transfer of functional microRNAs between mouse dendritic cells via exosomes. In *Blood* 119 (3), pp. 756–766. DOI: 10.1182/blood-2011-02-338004.

Morris, Shelli M.; Arden, Susan D.; Roberts, Rhys C.; Kendrick-Jones, John; Cooper, Jonathan A.; Luzio, J. Paul; Buss, Folma (2002): Myosin VI binds to and localises with Dab2, potentially linking receptor-mediated endocytosis and the actin cytoskeleton. In *Traffic (Copenhagen, Denmark)* 3 (5), pp. 331–341. DOI: 10.1034/j.1600-0854.2002.30503.x.

Moulder, Krista L.; Jiang, Xiaoping; Taylor, Amanda A.; Olney, John W.; Mennerick, Steven (2006): Physiological activity depresses synaptic function through an effect on vesicle priming. In *J. Neurosci.* 26 (24), pp. 6618–6626. DOI: 10.1523/JNEUROSCI.5498-05.2006.

Moulder, Krista L.; Meeks, Julian P.; Shute, Amanda A.; Hamilton, Clair K.; Erausquin, Gabriel de; Mennerick, Steven (2004): Plastic Elimination of Functional Glutamate Release Sites by Depolarization. In *Neuron* 42 (3), pp. 423–435. DOI: 10.1016/S0896-6273(04)00184-9.

Moutin, Enora; Hemonnot, Anne-Laure; Seube, Vincent; Linck, Nathalie; Rassendren, François; Perroy, Julie; Compan, Vincent (2020): Procedures for Culturing and Genetically Manipulating Murine Hippocampal Postnatal Neurons. In *Front. Synaptic Neurosci.* 12, p. 19. DOI: 10.3389/fnsyn.2020.00019.

Moya, Kenneth L.; Sals, Nicole; Hssig, Raymonde; Crminon, Christophe; Grassi, Jacques; Di Giamberardino, Luigi (2000): Immunolocalization of the cellular prion protein in normal brain. In *Microsc. Res. Tech.* 50 (1), pp. 58–65. DOI: 10.1002/1097-0029(20000701)50:1<58::AID-JEMT9>3.0.CO;2-5.

Murthy, Venkatesh N.; Schikorski, Thomas; Stevens, Charles F.; Zhu, Yongling (2001): Inactivity Produces Increases in Neurotransmitter Release and Synapse Size. In *Neuron* 32 (4), pp. 673–682. DOI: 10.1016/S0896-6273(01)00500-1.

Musardo, Stefano; Marcello, Elena; Gardoni, Fabrizio; Di Luca, Monica (2014): ADAM10 in synaptic physiology and pathology. In *Neuro-degenerative diseases* 13 (2-3), pp. 72–74. DOI: 10.1159/000354233.

Mysore, Shreesh P.; Tai, Chin-Yin; Schuman, Erin M. (2008): N-cadherin, spine dynamics, and synaptic function. In *Frontiers in neuroscience* 2 (2), pp. 168–175. DOI: 10.3389/neuro.01.035.2008.

Nakata, Takao; Hirokawa, Nobutaka (2003): Microtubules provide directional cues for polarized axonal transport through interaction with kinesin motor head. In *J Cell Biol* 162 (6), pp. 1045–1055. DOI: 10.1083/jcb.200302175.

Narahashi, T.; Moore, J. W.; Poston, R. N. (1967): Tetrodotoxin derivatives: chemical structure and blockage of nerve membrane conductance. In *Science (New York, N.Y.)* 156 (3777), pp. 976–979. DOI: 10.1126/science.156.3777.976.

Naslavsky, Naava; Caplan, Steve (2018): The enigmatic endosome - sorting the ins and outs of endocytic trafficking. In *J Cell Sci* 131 (13). DOI: 10.1242/jcs.216499.

Nirschl, Jeffrey J.; Ghiretti, Amy E.; Holzbaur, Erika L. F. (2017): The impact of cytoskeletal organization on the local regulation of neuronal transport. In *Nat Rev Neurosci* 18 (10), pp. 585–597. DOI: 10.1038/nrn.2017.100.

Nozohouri, Saeideh; Vaidya, Bhuvaneshwar; Abbruscato, Thomas J. (2020): Exosomes in Ischemic Stroke. In *Current pharmaceutical design* 26 (42), pp. 5533–5545. DOI: 10.2174/1381612826666200614180253.

Nuriya, Mutsuo; Huganir, Richard L. (2006): Regulation of AMPA receptor trafficking by N-cadherin. In *Journal of neurochemistry* 97 (3), pp. 652–661. DOI: 10.1111/j.1471-4159.2006.03740.x.

O'Brien, Richard J.; Kamboj, Sunjeev; Ehlers, Michael D.; Rosen, Kenneth R.; Fischbach, Gerald D.; Huganir, Richard L. (1998): Activity-Dependent Modulation of Synaptic AMPA Receptor Accumulation. In *Neuron* 21 (5), pp. 1067–1078. DOI: 10.1016/S0896-6273(00)80624-8.

Oertner, Thomas G.; Matus, Andrew (2005): Calcium regulation of actin dynamics in dendritic spines. In *Cell calcium* 37 (5), pp. 477–482. DOI: 10.1016/j.ceca.2005.01.016.

Ondrejcak, Tomas; Hu, Neng-Wei; Qi, Yingjie; Klyubin, Igor; Corbett, Grant T.; Fraser, Graham et al. (2019): Soluble tau aggregates inhibit synaptic long-term depression and amyloid β-facilitated LTD in vivo. In *Neurobiology of disease* 127, pp. 582–590. DOI: 10.1016/j.nbd.2019.03.022.

Ondrejcak, Tomas; Klyubin, Igor; Corbett, Grant T.; Fraser, Graham; Hong, Wei; Mably, Alexandra J. et al. (2018): Cellular Prion Protein Mediates the Disruption of Hippocampal Synaptic Plasticity by Soluble Tau In Vivo. In *The Journal of neuroscience : the official journal of the Society for Neuroscience* 38 (50), pp. 10595–10606. DOI: 10.1523/JNEUROSCI.1700-18.2018.

Osterweil, Emily; Wells, David G.; Mooseker, Mark S. (2005): A role for myosin VI in postsynaptic structure and glutamate receptor endocytosis. In *J Cell Biol* 168 (2), pp. 329–338. DOI: 10.1083/jcb.200410091.

Ostrowski, Matias; Carmo, Nuno B.; Krumeich, Sophie; Fanget, Isabelle; Raposo, Graça; Savina, Ariel et al. (2010): Rab27a and Rab27b control different steps of the exosome secretion pathway. In *Nat Cell Biol* 12 (1), 19-30; sup pp 1-13. DOI: 10.1038/ncb2000.

Otmakhov, Nikolai; Khibnik, Lena; Otmakhova, Nonna; Carpenter, Stephen; Riahi, Shervin; Asrican, Brent; Lisman, John (2004): Forskolin-induced LTP in the CA1 hippocampal region is NMDA receptor dependent. In *Journal of neurophysiology* 91 (5), pp. 1955–1962. DOI: 10.1152/jn.00941.2003.

Pak, Chi W.; Flynn, Kevin C.; Bamburg, James R. (2008): Actin-binding proteins take the reins in growth cones. In *Nat Rev Neurosci* 9 (2), pp. 136–147. DOI: 10.1038/nrn2236.

Pan, K. M.; Baldwin, M.; Nguyen, J.; Gasset, M.; Serban, A.; Groth, D. et al. (1993): Conversion of alpha-helices into beta-sheets features in the formation of the scrapie prion proteins. In *Proc Natl Acad Sci USA* 90 (23), pp. 10962–10966. DOI: 10.1073/pnas.90.23.10962.

Park, Joohyun; Cho, Oh Yeon; Kim, Jung Ah; Chang, Sunghoe (2016): Endosome-mediated endocytic mechanism replenishes the majority of synaptic vesicles at mature CNS synapses in an activity-dependent manner. In *Sci Rep* 6 (1), p. 31807. DOI: 10.1038/srep31807.

Park, Sang Jun; Seog, Joung-Su; Moon, Il Soo; Seog, Dae-Hyun (2017): The Regulation Mechanisms of Kinesin Motor Proteins. In *Journal of Life Science* 27 (7), pp. 840–848. DOI: 10.5352/JLS.2017.27.7.840.

Parkinson, Gabrielle T.; Hanley, Jonathan G. (2018): Mechanisms of AMPA Receptor Endosomal Sorting. In *Frontiers in molecular neuroscience* 11, p. 440. DOI: 10.3389/fnmol.2018.00440.

Parkyn, C. J.; Vermeulen, E. G.; Mootoosamy, R. C.; Sunyach, C.; Jacobsen, C.; Oxvig, C. et al. (2008): LRP1 controls biosynthetic and endocytic trafficking of neuronal prion protein. In *J Cell Sci* 121 (Pt 6), pp. 773–783. DOI: 10.1242/jcs.021816.

Pegtel, D. Michiel; Gould, Stephen J. (2019): Exosomes. In *Annual review of biochemistry* 88, pp. 487–514. DOI: 10.1146/annurev-biochem-013118-111902.

Peters, Peter J.; Mironov, Alexander; Peretz, David; van Donselaar, Elly; Leclerc, Estelle; Erpel, Susanne et al. (2003): Trafficking of prion proteins through a caveolae-mediated endosomal pathway. In *J Cell Biol* 162 (4), pp. 703–717. DOI: 10.1083/jcb.200304140.

Petit, Constance S. V.; Besnier, Laura; Morel, Etienne; Rousset, Monique; Thenet, Sophie (2013): Roles of the cellular prion protein in the regulation of cell-cell junctions and barrier function. In *Tissue barriers* 1 (2), e24377. DOI: 10.4161/tisb.24377.

Polanco, Juan Carlos; Li, Chuanzhou; Durisic, Nela; Sullivan, Robert; Götz, Jürgen (2018): Exosomes taken up by neurons hijack the endosomal pathway to spread to interconnected neurons. In *Acta neuropathologica communications* 6 (1), p. 10. DOI: 10.1186/s40478-018-0514-4.

Pollard, Thomas D.; Cooper, John A. (2009): Actin, a central player in cell shape and movement. In *Science (New York, N.Y.)* 326 (5957), pp. 1208–1212. DOI: 10.1126/science.1175862.

Polymenidou, Magdalini; Moos, Rita; Scott, Mike; Sigurdson, Christina; Shi, Yong-Zhong; Yajima, Bill et al. (2008): The POM monoclonals: a comprehensive set of antibodies to non-overlapping prion protein epitopes. In *PloS one* 3 (12), e3872. DOI: 10.1371/journal.pone.0003872.

Poulopoulos, Alexandros; Aramuni, Gayane; Meyer, Guido; Soykan, Tolga; Hoon, Mrinalini; Papadopoulos, Theofilos et al. (2009): Neuroligin 2 drives postsynaptic assembly at perisomatic inhibitory synapses through gephyrin and collybistin. In *Neuron* 63 (5), pp. 628–642. DOI: 10.1016/j.neuron.2009.08.023.

Pozo, Karine; Goda, Yukiko (2010): Unraveling mechanisms of homeostatic synaptic plasticity. In *Neuron* 66 (3), pp. 337–351. DOI: 10.1016/j.neuron.2010.04.028.

Prado, Marco A. M.; Alves-Silva, Juliana; Magalhães, Ana C.; Prado, Vania F.; Linden, Rafael; Martins, Vilma Regina; Brentani, Ricardo Renzo (2004): PrPc on the road: trafficking of the cellular prion protein. In *Journal of neurochemistry* 88 (4), pp. 769–781. DOI: 10.1046/j.1471-4159.2003.02199.x.

Prusiner, S. B. (1982): Novel proteinaceous infectious particles cause scrapie. In *Science (New York, N.Y.)* 216 (4542), pp. 136–144. DOI: 10.1126/science.6801762.

Quevedo, María Florencia; Bustos, Matías Alberto; Masone, Diego; Roggero, Carlos Marcelo; Bustos, Diego Martín; Tomes, Claudia Nora (2019): Grab recruitment by Rab27A-Rabphilin3a triggers Rab3A activation in human sperm exocytosis. In *Biochimica et biophysica acta. Molecular cell research* 1866 (4), pp. 612–622. DOI: 10.1016/j.bbamcr.2018.12.005.

Rana, Sanyukta; Yue, Shijing; Stadel, Daniela; Zöller, Margot (2012): Toward tailored exosomes: the exosomal tetraspanin web contributes to target cell selection. In *The international journal of biochemistry & cell biology* 44 (9), pp. 1574–1584. DOI: 10.1016/j.biocel.2012.06.018.

Rangel, Alejandra; Madroñal, Noelia; Gruart, Agnès; Gruart i Massó, Agnès; Gavín, Rosalina; Llorens, Franc et al. (2009): Regulation of GABA(A) and glutamate receptor expression, synaptic facilitation and long-term potentiation in the hippocampus of prion mutant mice. In *PloS one* 4 (10), e7592. DOI: 10.1371/journal.pone.0007592.

Raposo, Graça; Stoorvogel, Willem (2013): Extracellular vesicles: exosomes, microvesicles, and friends. In *The Journal of cell biology* 200 (4), pp. 373–383. DOI: 10.1083/jcb.201211138.

Redondo, Roger L.; Morris, Richard G. M. (2011): Making memories last: the synaptic tagging and capture hypothesis. In *Nat Rev Neurosci* 12 (1), pp. 17–30. DOI: 10.1038/nrn2963.

Reiss, Karina; Maretzky, Thorsten; Ludwig, Andreas; Tousseyn, Thomas; Strooper, Bart de; Hartmann, Dieter; Saftig, Paul (2005): ADAM10 cleavage of N-cadherin and regulation of cell-cell adhesion and beta-catenin nuclear signalling. In *The EMBO journal* 24 (4), pp. 742–752. DOI: 10.1038/sj.emboj.7600548.

Roberts, Anthony J.; Kon, Takahide; Knight, Peter J.; Sutoh, Kazuo; Burgess, Stan A. (2013): Functions and mechanics of dynein motor proteins. In *Nat Rev Mol Cell Biol* 14 (11), pp. 713–726. DOI: 10.1038/nrm3667.

Roucou, X.; Giannopoulos, P. N.; Zhang, Y.; Jodoin, J.; Goodyer, C. G.; LeBlanc, A. (2005): Cellular prion protein inhibits proapoptotic Bax conformational change in human neurons and in breast carcinoma MCF-7 cells. In *Cell death and differentiation* 12 (7), pp. 783–795. DOI: 10.1038/sj.cdd.4401629.

Rubinsztein, David C. (2006): The roles of intracellular protein-degradation pathways in neurodegeneration. In *Nature* 443 (7113), pp. 780–786. DOI: 10.1038/nature05291.

Sailer, A. (1994): No propagation of prions in mice devoid of PrP. In *Cell* 77 (7), pp. 967–968. DOI: 10.1016/0092-8674(94)90436-7.

Salès, N.; Rodolfo, K.; Hässig, R.; Faucheux, B.; Di Giamberardino, L.; Moya, K. L. (1998): Cellular prion protein localization in rodent and primate brain. In *The European journal of neuroscience* 10 (7), pp. 2464–2471. DOI: 10.1046/j.1460-9568.1998.00258.x.

Samanta, Saheli; Rajasingh, Sheeja; Drosos, Nicholas; Zhou, Zhigang; Dawn, Buddhadeb; Rajasingh, Johnson (2018): Exosomes: new molecular targets of diseases. In *Acta pharmacologica Sinica* 39 (4), pp. 501–513. DOI: 10.1038/aps.2017.162.

Sankaranarayanan, Sethuraman; Atluri, Pradeep P.; Ryan, Timothy A. (2003): Actin has a molecular scaffolding, not propulsive, role in presynaptic function. In *Nat Neurosci* 6 (2), pp. 127–135. DOI: 10.1038/nn1002.

Santos, Tiago G.; Beraldo, Flavio H.; Hajj, Glaucia N. M.; Lopes, Marilene H.; Roffe, Martin; Lupinacci, Fernanda C. S. et al. (2013): Laminin-γ1 chain and stress inducible protein 1 synergistically mediate PrPC-dependent axonal growth via Ca2+ mobilization in dorsal root ganglia neurons. In *Journal of neurochemistry* 124 (2), pp. 210–223. DOI: 10.1111/jnc.12091.

Santuccione, Antonella; Sytnyk, Vladimir; Leshchyns'ka, Iryna; Schachner, Melitta (2005): Prion protein recruits its neuronal receptor NCAM to lipid rafts to activate p59fyn and to enhance neurite outgrowth. In *The Journal of cell biology* 169 (2), pp. 341–354. DOI: 10.1083/jcb.200409127.

Sarnataro, Daniela; Pepe, Anna; Zurzolo, Chiara (2017): Cell Biology of Prion Protein. In *Progress in molecular biology and translational science* 150, pp. 57–82. DOI: 10.1016/bs.pmbts.2017.06.018.

Savina, Ariel; Fader, Claudio M.; Damiani, María T.; Colombo, María Isabel (2005): Rab11 promotes docking and fusion of multivesicular bodies in a calcium-dependent manner. In *Traffic (Copenhagen, Denmark)* 6 (2), pp. 131–143. DOI: 10.1111/j.1600-0854.2004.00257.x.

Savina, Ariel; Furlán, Marcelo; Vidal, Michel; Colombo, Maria I. (2003): Exosome release is regulated by a calcium-dependent mechanism in K562 cells. In *Journal of Biological Chemistry* 278 (22), pp. 20083–20090. DOI: 10.1074/jbc.M301642200.

Schlöndorff, J.; Blobel, C. P. (1999): Metalloprotease-disintegrins: modular proteins capable of promoting cell-cell interactions and triggering signals by protein-ectodomain shedding. In *J Cell Sci* 112 (Pt 21), pp. 3603–3617. DOI: 10.1242/jcs.112.21.3603.

Schmitt-Ulms, G.; Legname, G.; Baldwin, M. A.; Ball, H. L.; Bradon, N.; Bosque, P. J. et al. (2001): Binding of neural cell adhesion molecules (N-CAMs) to the cellular prion protein. In *J Mol Biol* 314 (5), pp. 1209–1225. DOI: 10.1006/jmbi.2000.5183.

Schrock, Yvonne; Solis, Gonzalo P.; Stuermer, Claudia A. O. (2009): Regulation of focal adhesion formation and filopodia extension by the cellular prion protein (PrPC). In *FEBS letters* 583 (2), pp. 389–393. DOI: 10.1016/j.febslet.2008.12.038.

SCOVILLE, W. B.; MILNER, B. (1957): Loss of recent memory after bilateral hippocampal lesions. In *Journal of neurology, neurosurgery, and psychiatry* 20 (1), pp. 11–21. DOI: 10.1136/jnnp.20.1.11.

Seals, Darren F.; Courtneidge, Sara A. (2003): The ADAMs family of metalloproteases: multidomain proteins with multiple functions. In *Genes & development* 17 (1), pp. 7–30. DOI: 10.1101/gad.1039703.

Setou, Mitsutoshi; Seog, Dae-Hyung; Tanaka, Yosuke; Kanai, Yoshimitsu; Takei, Yosuke; Kawagishi, Masahiko; Hirokawa, Nobutaka (2002): Glutamate-receptor-interacting protein GRIP1 directly steers kinesin to dendrites. In *Nature* 417 (6884), pp. 83–87. DOI: 10.1038/nature743.

Shankar, Ganesh M.; Bloodgood, Brenda L.; Townsend, Matthew; Walsh, Dominic M.; Selkoe, Dennis J.; Sabatini, Bernardo L. (2007): Natural oligomers of the Alzheimer amyloid-beta protein induce reversible synapse loss by modulating an NMDA-type glutamate receptor-dependent signaling pathway. In *J. Neurosci.* 27 (11), pp. 2866–2875. DOI: 10.1523/JNEUROSCI.4970-06.2007.

Sharma, Pranav; Mesci, Pinar; Carromeu, Cassiano; McClatchy, Daniel R.; Schiapparelli, Lucio; Yates, John R. et al. (2019): Exosomes regulate neurogenesis and circuit assembly. In *Proc Natl Acad Sci USA* 116 (32), pp. 16086–16094. DOI: 10.1073/pnas.1902513116.

Shrager, Yael; Bayley, Peter J.; Bontempi, Bruno; Hopkins, Ramona O.; Squire, Larry R. (2007): Spatial memory and the human hippocampus. In *Proc Natl Acad Sci USA* 104 (8), pp. 2961–2966. DOI: 10.1073/pnas.0611233104.

Shrestha, Brikha R.; Vitolo, Ottavio V.; Joshi, Powrnima; Lordkipanidze, Tamar; Shelanski, Michael; Dunaevsky, Anna (2006): Amyloid beta peptide adversely affects spine number and motility in hippocampal neurons. In *Molecular and cellular neurosciences* 33 (3), pp. 274–282. DOI: 10.1016/j.mcn.2006.07.011.

Silverman, M. A.; Kaech, S.; Ramser, E. M.; Lu, X.; Lasarev, M. R.; Nagalla, S.; Banker, G. (2010): Expression of kinesin superfamily genes in cultured hippocampal neurons. In *Cytoskeleton (Hoboken, N.J.)* 67 (12), pp. 784–795. DOI: 10.1002/cm.20487.

Simpson, Richard J.; Jensen, Søren S.; Lim, Justin W. E. (2008): Proteomic profiling of exosomes: current perspectives. In *Proteomics* 8 (19), pp. 4083–4099. DOI: 10.1002/pmic.200800109.

Sirajuddin, Minhajuddin; Rice, Luke M.; Vale, Ronald D. (2014): Regulation of microtubule motors by tubulin isotypes and post-translational modifications. In *Nature cell biology* 16 (4), pp. 335–344. DOI: 10.1038/ncb2920.

Šišková, Zuzana; Reynolds, Richard A.; O'Connor, Vincent; Perry, V. Hugh (2013): Brain region specific pre-synaptic and post-synaptic degeneration are early components of neuropathology in prion disease. In *PloS one* 8 (1), e55004. DOI: 10.1371/journal.pone.0055004.

Skaper, Stephen D.; Facci, Laura; Zusso, Morena; Giusti, Pietro (2017): Synaptic Plasticity, Dementia and Alzheimer Disease. In *CNS & neurological disorders drug targets* 16 (3), pp. 220–233. DOI: 10.2174/1871527316666170113120853.

Smalheiser, Neil R. (2007): Exosomal transfer of proteins and RNAs at synapses in the nervous system. In *Biology direct* 2, p. 35. DOI: 10.1186/1745-6150-2-35.

Snyder, Eric M.; Nong, Yi; Almeida, Claudia G.; Paul, Surojit; Moran, Timothy; Choi, Eun Young et al. (2005): Regulation of NMDA receptor trafficking by amyloid-beta. In *Nat Neurosci* 8 (8), pp. 1051–1058. DOI: 10.1038/nn1503.

Soto, Claudio; Estrada, Lisbell; Castilla, Joaquín (2006): Amyloids, prions and the inherent infectious nature of misfolded protein aggregates. In *Trends in biochemical sciences* 31 (3), pp. 150–155. DOI: 10.1016/j.tibs.2006.01.002.

Spence, M. W. (1993): Sphingomyelinases. In *Advances in lipid research* 26, pp. 3–23.

Sung, Jee Young; Engmann, Olivia; Teylan, Merilee A.; Nairn, Angus C.; Greengard, Paul; Kim, Yong (2008): WAVE1 controls neuronal activity-induced mitochondrial distribution in dendritic spines. In *Proc Natl Acad Sci USA* 105 (8), pp. 3112–3116. DOI: 10.1073/pnas.0712180105.

Sweeney, H. Lee; Houdusse, Anne (2010): Myosin VI rewrites the rules for myosin motors. In *Cell* 141 (4), pp. 573–582. DOI: 10.1016/j.cell.2010.04.028.

Tabatadze, Nino; Savonenko, Alena; Song, Hongjun; Bandaru, Veera Venkata Ratnam; Chu, Michael; Haughey, Norman J. (2010): Inhibition of neutral sphingomyelinase-2 perturbs brain sphingolipid balance and spatial memory in mice. In *Journal of neuroscience research* 88 (13), pp. 2940–2951. DOI: 10.1002/jnr.22438.

Tai, Chin-Yin; Mysore, Shreesh P.; Chiu, Cindy; Schuman, Erin M. (2007): Activity-regulated N-cadherin endocytosis. In *Neuron* 54 (5), pp. 771–785. DOI: 10.1016/j.neuron.2007.05.013.

Takei, Yosuke; Kikkawa, Yayoi S.; Atapour, Nafiseh; Hensch, Takao K.; Hirokawa, Nobutaka (2015): Defects in Synaptic Plasticity, Reduced NMDA-Receptor Transport, and Instability of Postsynaptic Density Proteins in Mice Lacking Microtubule-Associated Protein 1A. In *J. Neurosci.* 35 (47), pp. 15539–15554. DOI: 10.1523/JNEUROSCI.2671-15.2015.

Takeichi, Masatoshi (2007): The cadherin superfamily in neuronal connections and interactions. In *Nature reviews. Neuroscience* 8 (1), pp. 11–20. DOI: 10.1038/nrn2043.

Takeichi, Masatoshi; Abe, Kentaro (2005): Synaptic contact dynamics controlled by cadherin and catenins. In *Trends in cell biology* 15 (4), pp. 216–221. DOI: 10.1016/j.tcb.2005.02.002.

Tan, Han L.; Chiu, Shu-Ling; Zhu, Qianwen; Huganir, Richard L. (2020): GRIP1 regulates synaptic plasticity and learning and memory. In *Proc Natl Acad Sci USA* 117 (40), pp. 25085–25091. DOI: 10.1073/pnas.2014827117.

Taylor, David R.; Hooper, Nigel M. (2006): The prion protein and lipid rafts. In *Molecular membrane biology* 23 (1), pp. 89–99. DOI: 10.1080/09687860500449994.

Taylor, David R.; Parkin, Edward T.; Cocklin, Sarah L.; Ault, James R.; Ashcroft, Alison E.; Turner, Anthony J.; Hooper, Nigel M. (2009): Role of ADAMs in the ectodomain shedding and conformational conversion of the prion protein. In *The Journal of biological chemistry* 284 (34), pp. 22590–22600. DOI: 10.1074/jbc.M109.032599.

Taylor, David R.; Watt, Nicole T.; Perera, W. Sumudhu S.; Hooper, Nigel M. (2005): Assigning functions to distinct regions of the N-terminus of the prion protein that are involved in its copper-stimulated, clathrin-dependent endocytosis. In *J Cell Sci* 118 (Pt 21), pp. 5141–5153. DOI: 10.1242/jcs.02627.

Thiagarajan, Tara C.; Lindskog, Maria; Tsien, Richard W. (2005): Adaptation to synaptic inactivity in hippocampal neurons. In *Neuron* 47 (5), pp. 725–737. DOI: 10.1016/j.neuron.2005.06.037.

Thiery, J. (2003): Cell adhesion in development: a complex signaling network. In *Current Opinion in Genetics & Development* 13 (4), pp. 365–371. DOI: 10.1016/S0959-437X(03)00088-1.

Togashi, Hideru; Sakisaka, Toshiaki; Takai, Yoshimi (2009): Cell adhesion molecules in the central nervous system. In *Cell Adhesion & Migration* 3 (1), pp. 29–35. DOI: 10.4161/cam.3.1.6773.

Trajkovic, Katarina; Hsu, Chieh; Chiantia, Salvatore; Rajendran, Lawrence; Wenzel, Dirk; Wieland, Felix et al. (2008): Ceramide triggers budding of exosome vesicles into multivesicular endosomes. In *Science (New York, N.Y.)* 319 (5867), pp. 1244–1247. DOI: 10.1126/science.1153124.

Tumbarello, David A.; Kendrick-Jones, John; Buss, Folma (2013): Myosin VI and its cargo adaptors - linking endocytosis and autophagy. In *J Cell Sci* 126 (Pt 12), pp. 2561–2570. DOI: 10.1242/jcs.095554.

Turrigiano, G. G.; Leslie, K. R.; Desai, N. S.; Rutherford, L. C.; Nelson, S. B. (1998): Activity-dependent scaling of quantal amplitude in neocortical neurons. In *Nature* 391 (6670), pp. 892–896. DOI: 10.1038/36103.

Turrigiano, Gina G. (2008): The self-tuning neuron: synaptic scaling of excitatory synapses. In *Cell* 135 (3), pp. 422–435. DOI: 10.1016/j.cell.2008.10.008.

Twelvetrees, Alison E.; Pernigo, Stefano; Sanger, Anneri; Guedes-Dias, Pedro; Schiavo, Giampietro; Steiner, Roberto A. et al. (2016): The Dynamic Localization of Cytoplasmic Dynein in Neurons Is Driven by Kinesin-1. In *Neuron* 90 (5), pp. 1000–1015. DOI: 10.1016/j.neuron.2016.04.046.

Um, J. W.; Kaufman, A. C.; Kostylev, M.; Heiss, J. K.; Stagi, M.; Takahashi, H. et al. (2013): Metabotropic glutamate receptor 5 is a coreceptor for Alzheimer abeta oligomer bound to cellular prion protein. In *Neuron* 79 (5), pp. 887–902. DOI: 10.1016/j.neuron.2013.06.036.

Um, J. W.; Nygaard, H. B.; Heiss, J. K.; Kostylev, M. A.; Stagi, M.; Vortmeyer, A. et al. (2012): Alzheimer amyloid-beta oligomer bound to postsynaptic prion protein activates Fyn to impair neurons. In *Nat Neurosci* 15 (9), pp. 1227–1235. DOI: 10.1038/nn.3178.

van Niel, Guillaume; Charrin, Stéphanie; Simoes, Sabrina; Romao, Maryse; Rochin, Leila; Saftig, Paul et al. (2011): The tetraspanin CD63 regulates ESCRT-independent and -dependent endosomal sorting during melanogenesis. In *Developmental cell* 21 (4), pp. 708–721. DOI: 10.1016/j.devcel.2011.08.019.

Varoqueaux, Frédérique; Jamain, Stéphane; Brose, Nils (2004): Neuroligin 2 is exclusively localized to inhibitory synapses. In *European journal of cell biology* 83 (9), pp. 449–456. DOI: 10.1078/0171-9335-00410.

Vassallo, Neville; Herms, Jochen (2003): Cellular prion protein function in copper homeostasis and redox signalling at the synapse. In *Journal of neurochemistry* 86 (3), pp. 538–544. DOI: 10.1046/j.1471-4159.2003.01882.x.

Vella, Laura J.; Greenwood, Deanne L. V.; Cappai, Roberto; Scheerlinck, Jean-Pierre Y.; Hill, Andrew F. (2008): Enrichment of prion protein in exosomes derived from ovine cerebral spinal fluid. In *Veterinary immunology and immunopathology* 124 (3-4), pp. 385–393. DOI: 10.1016/j.vetimm.2008.04.002.

Vella, Laura J.; Hill, Andrew F.; Cheng, Lesley (2016): Focus on Extracellular Vesicles: Exosomes and Their Role in Protein Trafficking and Biomarker Potential in Alzheimer's and Parkinson's Disease. In *International journal of molecular sciences* 17 (2), p. 173. DOI: 10.3390/ijms17020173.

Viles, J. H.; Cohen, F. E.; Prusiner, S. B.; Goodin, D. B.; Wright, P. E.; Dyson, H. J. (1999): Copper binding to the prion protein: structural implications of four identical cooperative binding sites. In *Proc Natl Acad Sci USA* 96 (5), pp. 2042–2047. DOI: 10.1073/pnas.96.5.2042.

Vorberg, Ina M. (2019): All the Same? The Secret Life of Prion Strains within Their Target Cells. In *Viruses* 11 (4). DOI: 10.3390/v11040334.

Wagner, Wolfgang; Brenowitz, Stephan D.; Hammer, John A. (2011): Myosin-Va transports the endoplasmic reticulum into the dendritic spines of Purkinje neurons. In *Nat Cell Biol* 13 (1), pp. 40–48. DOI: 10.1038/ncb2132.

Wang, Shiwei; Cesca, Fabrizia; Loers, Gabriele; Schweizer, Michaela; Buck, Friedrich; Benfenati, Fabio et al. (2011): Synapsin I is an oligomannose-carrying glycoprotein, acts as an oligomannose-binding lectin, and promotes neurite outgrowth and neuronal survival when released via glia-derived exosomes. In *J. Neurosci.* 31 (20), pp. 7275–7290. DOI: 10.1523/JNEUROSCI.6476-10.2011.

Wang, Zhiping; Edwards, Jeffrey G.; Riley, Nathan; Provance, D. William; Karcher, Ryan; Li, Xiang-Dong et al. (2008): Myosin Vb mobilizes recycling endosomes and AMPA receptors for postsynaptic plasticity. In *Cell* 135 (3), pp. 535–548. DOI: 10.1016/j.cell.2008.09.057.

Watt, N. T.; Taylor, D. R.; Kerrigan, T. L.; Griffiths, H. H.; Rushworth, J. V.; Whitehouse, I. J.; Hooper, N. M. (2012): Prion protein facilitates uptake of zinc into neuronal cells. In *Nat Commun* 3, p. 1134. DOI: 10.1038/ncomms2135.

Welte, Michael A. (2004): Bidirectional transport along microtubules. In *Current biology : CB* 14 (13), R525-37. DOI: 10.1016/j.cub.2004.06.045.

Westergard, Laura; Christensen, Heather M.; Harris, David A. (2007): The cellular prion protein (PrP(C)): its physiological function and role in disease. In *Biochimica et biophysica acta* 1772 (6), pp. 629–644. DOI: 10.1016/j.bbadis.2007.02.011.

White, Anthony R.; Collins, Steven J.; Maher, Fran; Jobling, Michael F.; Stewart, Leanne R.; Thyer, James M. et al. (1999): Prion Protein-Deficient Neurons Reveal Lower Glutathione Reductase Activity and Increased Susceptibility to Hydrogen Peroxide Toxicity. In *The American Journal of Pathology* 155 (5), pp. 1723–1730. DOI: 10.1016/S0002-9440(10)65487-9.

Whitechurch, Benjamin C.; Welton, Jeremy M.; Collins, Steven J.; Lawson, Victoria A. (2017): Prion Diseases. In : Neurodegenerative Diseases: Springer, Cham, pp. 335–364. Available online at https://link.springer.com/chapter/10.1007/978-3-319-57193-5_13.

Wiedenmann, Bertram; Franke, Werner W. (1985): Identification and localization of synaptophysin, an integral membrane glycoprotein of Mr 38,000 characteristic of presynaptic vesicles. In *Cell* 41 (3), pp. 1017–1028. DOI: 10.1016/S0092-8674(85)80082-9.

Wik, Lotta; Klingeborn, Mikael; Willander, Hanna; Linne, Tommy (2012): Separate mechanisms act concurrently to shed and release the prion protein from the cell. In *Prion* 6 (5), pp. 498–509. DOI: 10.4161/pri.22588.

Wilson, Nathan R.; Kang, Jiansheng; Hueske, Emily V.; Leung, Tony; Varoqui, Helene; Murnick, Jonathan G. et al. (2005): Presynaptic regulation of quantal size by the vesicular glutamate transporter VGLUT1. In *J. Neurosci.* 25 (26), pp. 6221–6234. DOI: 10.1523/JNEUROSCI.3003-04.2005.

Yáñez-Mó, María; Siljander, Pia R-M; Andreu, Zoraida; Zavec, Apolonija Bedina; Borràs, Francesc E.; Buzas, Edit I. et al. (2015): Biological properties of extracellular vesicles and their

physiological functions. In *Journal of extracellular vesicles* 4, p. 27066. DOI: 10.3402/jev.v4.27066.

Zhang, Nan; He, Fengling; Li, Ting; Chen, Jinzhi; Jiang, Liping; Ouyang, Xin-Ping; Zuo, Lielian (2021): Role of Exosomes in Brain Diseases. In *Front. Cell. Neurosci.* 15, p. 743353. DOI: 10.3389/fncel.2021.743353.

Zhang, Yuan; Zhao, Yanfang; Zhang, Lei; Yu, Wanpeng; Wang, Yu; Chang, Wenguang (2019): Cellular Prion Protein as a Receptor of Toxic Amyloid-β42 Oligomers Is Important for Alzheimer's Disease. In *Frontiers in cellular neuroscience* 13, p. 339. DOI: 10.3389/fncel.2019.00339.

Zhen, Yan; Stenmark, Harald (2015): Cellular functions of Rab GTPases at a glance. In *J Cell Sci* 128 (17), pp. 3171–3176. DOI: 10.1242/jcs.166074.

Zhu, Caihong; Aguzzi, Adriano (2021): Prion protein and prion disease at a glance. In *J Cell Sci* 134 (17). DOI: 10.1242/jcs.245605.

Zöller, Margot (2009): Tetraspanins: push and pull in suppressing and promoting metastasis. In *Nature reviews. Cancer* 9 (1), pp. 40–55. DOI: 10.1038/nrc2543.

5. Appendix

5.1 Hazardous substances

Chemical	Cat. No.	Supplier	GHS labelling	Hazard statements	Precautionary statements
Acrylamide/Bis-acrylamide	A2917	Sigma Aldrich, Germany	GHS06, GHS08	H301, H312, H332, H315, H317, H319, H340, H350, H361f, H372	P201, P280, P302, P352, P304, P340, P305, P351, P338, P308, P310
Ammonium persulfate (APS)	9592.1	Carl Roth GmbH and Co. KG, Germany	GHS03, GHS07, GHS08	H272, H302 H315, H317 H319, H334 H335	P261, P280 P302/352 P305/351/338 P332/313 P337/313
Ampicillin sodium salt	K029.1	Carl Roth GmbH and Co. KG, Germany	GHS08	H317, H334	P261, P280 P302/352 P342/311 P305/351/338 P310
Bicuculline (Bic)	0109	Tocris Bioscience, UK	GHS06, GHS09	H300, H311 H331, H400	P260, P264 P273, P280 P301/310 P302/352 P304/340
Calcium chloride	C4901	Sigma Aldrich, Germany	GHS07	H319	P280 P305/351/338 P337/313
1,4-Dithiothreit (DTT)	6908.2	Carl Roth GmbH and Co. KG, Germany	GHS07	H302, H315 H319, H335 H412	P260, P270 P305/351/338 P337/313
Ethanol	9065.4	Carl Roth GmbH and Co. KG, Germany	GHS02, GHS07	H225 H319	P210, P233 P305/351/338
Ethanol, denatured	2211-5L	Chemsolute	GHS02, GHS07	H225 H319	P210, P240 P241, P260 P280 P303/361/353 P305/351/338 P501
Forskolin	1099	Bio-Tech, UK	GHS07	H312	P280 P302/352/312 P362/364 P501

Hydrochloric acid	4625.1	Carl Roth GmbH and Co. KG, Germany	GHS05, GHS07	H290, H314, H318, H335	P280, P303, P361, P353, P305, P351, P338, P310
Isopropanol	6752.2	Carl Roth GmbH and Co. KG, Germany	GHS02, GHS07	H225, H319 H336	P210, P233 P305/351/338
Kanamycin A	T832.3	Carl Roth GmbH and Co. KG, Germany	GHS08	H360	P201, P202, P280, P308+P313
Methanol	P717.1	Carl Roth GmbH and Co. KG, Germany	GHS02, GHS06, GHS08	H225, H301, H311, H331, H370	P201, P233, P280, P301, P310, P303, P361, P353 P304, P340, P311
Paraformaldehyde (PFA)	0335.3	Carl Roth GmbH and Co. KG, Germany	GHS02, GHS05, GHS07, GHS08	H228, H302, H332, H315, H317, H318, H335, H350	P201, P210, P280, P302, P353, P305, P351, P338
Phenylmethylsulfonyl fluoride (PMSF)	6367.1	Carl Roth GmbH and Co. KG, Germany	GHS05, GHS06	H301, H314	P260, P280, P301, P310, P330, P303, P361, P353, P304, P340, P310, P305, P351, P338
Rolipram	0905	Bio-Tech	GHS07	H302, H315, H319. H335	P261, P264, P264+P265, P270, P271, P280, P301+P317, P302+P352, P304+P340, P305+P351+P338, P319, P321, P330, P332+P317, P337+P317, P362+P364, P403+P233, P405, and P501
Sodium dodecyl sulfate	L4509	Sigma Aldrich, Germany	GHS02, GHS05, GHS07	H228, H302, H332, H315, H318, H335, H412	P210, P261, P280, P301, P312, P330, P305, P351, P338, P310, P370, P378
Sodium hydroxide	6771.3	Carl Roth GmbH and Co. KG, Germany	GHS05	H290, H314	P280, P301, P330, P331, P305, P351, P338, P308, P310

N,N,N',N'-Tetramethyl ethylenediamine (TEMED)	T9821	Sigma Aldrich, Germany	GHS02, GHS05, GHS07	H225, H332, H302, H314	P210, P280, P301, P330, P331, P303, P361, P340, P304, P353, P312, P305, P351, P338
Tetrodotoxin citrate	120055	Abcam, UK	GHS06	H300, H310, H330, H319	P280, P330, P302, P352, P310, P304, P340
Triton X-100	3051.2	Carl Roth GmbH and Co. KG, Germany	GHS05, GHS07, GHS09	H302 H318 H410	P273 P280 P302/352 P305/351/338 P313

5.2 Velocity data

Table 9: Velocities of YFP-PrP^C transport vesicles moving inward in ctrl and cLTD conditions.

Conditions	v_{net} in µm/s	v_{mean} in µm/s	v_{max} in µm/s
Ctrl	0.564 ± 0.138	0.768 ± 0.131	1.123 ± 0.202
cLTD	0.404 ± 0.094	0.443 ± 0.089	0.651 ± 0.130

Table 10: Velocities of outward-moving YFP-PrP^C transport vesicles in ctrl and cLTD conditions.

Conditions	v_{net} in µm/s	v_{mean} in µm/s	v_{max} in µm/s
Ctrl	0.238 ± 0.161	0.530 ± 0.159	0.798 ± 0.209
cLTD	0.458 ± 0.141	0.698 ± 0.133	0.855 ± 0.183

Table 11: Velocities of YFP-PrP^C transport vesicles moving inward in ctrl and cLTP conditions.

Conditions	v_{net} in µm/s	v_{mean} in µm/s	v_{max} in µm/s
Ctrl	0.821 ± 0.159	0.981 ± 0.197	1.004 ± 0.250
cLTP	0.491 ± 0.074	0.685 ± 0.130	0.952 ± 0.336

Table 12: Velocities of outward-moving YFP-PrP^C transport vesicles in ctrl and cLTP conditions.

Conditions	v_{net} in µm/s	v_{mean} in µm/s	v_{max} in µm/s
Ctrl	0.602 ± 0.223	0.658 ± 0.230	1.197 ± 0.294
cLTP	0.537 ± 0.120	0.746 ± 0.118	0.834 ± 0.451

5.3 Publication List

Kneussel, Matthias; Sánchez-Rodríguez, Noelia; **Mischak, Michaela**; Heisler, Frank F. (2021): Dynein and muskelin control myosin VI delivery towards the neuronal nucleus. In *iScience* 24 (5), p. 102416. DOI: 10.1016/j.isci.2021.102416.

Acknowledgements

First, I would like to thank my supervisor Dr. Frank Heisler for the supervision of my doctoral thesis and the opportunity to work in his research group. My thanks also go to Prof. Matthias Kneussel, for letting me work in his lab and his input to the project. Thank you to the Dr. Hans Ritz und Lieselotte Ritz Stiftung for supporting this project.

It has been a challenge, so I am very happy that I had my great colleagues in the Institute of Molecular Neurogenetics and the Center for Molecular Neurobiology Hamburg. Although it was hard to get together and meet people during the corona pandemic, I still got to meet a lot of nice people and talk about science and other things. Thank you to the past and present technicians of the Institute of Molecular Neurogenetics, who were a big help! Thanks to the PhD students. It was great fun to work with you and I wish you all luck and success! I also want to thank Hannah Voß for her help with analyzing the exosomes.

Special thanks go to Yvonne and Noelia, who worked in the lab with me and were always kind and supportive when I needed it. I will miss you!

I also want to thank Kira, Felix, Noelia, Jenni, my mom, and Dr. Penelope Kay-Fedororv for the proof reading.

I want to thank Prof. Schlüter for agreeing to be the examiner of my thesis.

Thank you to my mom and dad for giving me all the opportunities that led me here and for always supporting me. Thank you to my sister and all my friends for the moral support. And finally, I want to thank Philipp for his never-ending support and patience.

Eidesstattliche Erklärung

Hiermit versichere ich an Eides statt, die vorliegende Dissertation selbst verfasst und keine anderen als die angegebenen Hilfsmittel benutzt zu haben. Die eingereichte schriftliche Fassung entspricht der auf dem elektronischen Speichermedium. Ich versichere, dass diese Dissertation nicht in einem früheren Promotionsverfahren eingereicht wurde.

_____	_____
Datum, Ort	Unterschrift

Eidesstattliche Erklärung

Hiermit versichere ich an Eides statt, die vorliegende Dissertation selbst verfasst und keine anderen als die angegebenen Hilfsmittel benutzt zu haben. Die eingereichte schriftliche Fassung entspricht der auf dem elektronischen Speichermedium. Ich versichere, dass diese Dissertation nicht in einem früheren Promotionsverfahren eingereicht wurde.

22.9.2022, Hamburg

Datum, Ort

Unterschrift

Michaela Auschak